Evaluation of Future Meteorological and Hydrological Drought in the Rufiji Basin

Dwayne Liam Fernandes

Dissertation presented for the degree of
MASTER OF SCIENCE
In the Department of Environmental and Geographical Science
University of Cape Town

Supervisor: Dr. Piotr Wolski

February 2024

PLAGIARISM DECLARATION

I acknowledge and understand the concept of plagiarism and hereby declare that the entirety of this thesis, barring properly cited work, is solely my own. I am well-informed about the University of Cape Town's stance on plagiarism. I affirm that this dissertation represents original efforts undertaken by me for my university project, and all materials not originating from me have been accurately referenced according to the university's guidelines.

Signed by candidate

Dwayne Liam Fernandes

10th February 2024

ACKNOWLEDGEMENTS

First and foremost, I extend my deepest gratitude to my supervisor, Dr. Piotr Wolski, whose invaluable guidance, patience, and expertise have been the cornerstone of this journey. Without his dedicated mentorship and unwavering support, this thesis would not have been conceivable. His commitment to excellence and his generosity in sharing his vast knowledge have profoundly shaped my academic and personal growth.

I am also immensely thankful to the National Research Fund and the Post Graduate Funding Office (PGFO), whose financial support made my Master's studies and this research project possible. Their investment in my education has been instrumental in paving the path to achieving my academic goals.

A special word of thanks goes to Dr. Emmanuel Likoya, who played a pivotal role during the initial stages of my work. Dr. Likoya's expertise in the SWAT model and his ability to elucidate its complexities have been invaluable. His willingness to impart his knowledge and insights has significantly contributed to my understanding of the subject matter.

I am grateful to Mr. Phillip Mukwenha for his indispensable IT support throughout my studies. His technical assistance and problem-solving skills have been crucial in overcoming the numerous challenges encountered along the way.

My heartfelt appreciation extends to the Boonzaaier family, whose love and support have been a source of comfort and encouragement during my time in South Africa. Their kindness and hospitality have made my Master's journey a memorable experience.

To my family - Mum, Dad, sister, aunts, uncles, and cousins - your unwavering support, whether emotional or financial, has been my backbone. Your belief in my abilities and your constant encouragement have been sources of strength and motivation, for which I am eternally grateful.

A special thank you to Odille, my support system and rock. Your presence and steadfast support have been my refuge in challenging times. Your belief in me and your unwavering support have made all the difference, and I deeply appreciate everything you have done for me.

Finally, I dedicate this work to my late Aunty Marina, whose memory and spirit have been a guiding light throughout this journey. I know she would have been immensely proud to see me complete my Master’s and witness the person I have become. Her legacy continues to inspire me, and this achievement is a tribute to her enduring influence in my life.

Thank you all for being part of my journey and for contributing in countless ways to the completion of this thesis. Your support and encouragement have been the pillars of my success.

ABSTRACT

This research is driven by the critical need to understand the dynamics of drought patterns in the Rufiji Basin, Tanzania, under both current and future climatic scenarios. Droughts, with their profound impact on the socio-economic fabric and environmental sustainability of the region, represent a significant challenge in the Rufiji Basin, where both meteorological and hydrological droughts are prevalent. To tackle this issue, the study applies three key drought indices—the Standardized Precipitation Index (SPI), the Standardized Precipitation-Evapotranspiration Index (SPEI), and the Streamflow Drought Index (SDI)—to analyze 12-month drought events within the basin. This approach allows for a examination of drought characteristics, including their frequency, intensity, as well as its spatial distribution by the use of hydrological flux variables such as precipitation, evapotranspiration, lateral flow, and soil moisture.

This research distinguished itself by segmenting the Rufiji River Basin, which encompasses four primary basins—the Great Ruaha, Kilombero, Luwegu, and Lower Rufiji—into six parts. Specifically, the Great Ruaha Basin was further divided into the Upper Great Ruaha, Lower Great Ruaha, and Little Ruaha, allowing for a more nuanced analysis of hydrological dynamics within the region.The study's goal was to ascertain the unique drought characteristics of each sub-basin.

Historical climate data was sourced and downscaled from ERA5 Land, and future climate scenarios were based on simulations from 13 CORDEX Regional Climate Models (RCMs). The analyses of the SPI and SPEI utilized the CORDEX climate data in its calculation. The historical time period selected for this study was 1991-2020, aligning with the guidelines of the World Meteorological Organization (WMO). The periods designated for the near future and far future analyses were 2031-2060 and 2071-2100, respectively.

The study employed the SWAT+ hydrological model, calibrated at Stiegler’s Gorge on a monthly base. The model achieved a Nash-Sutcliffe Efficiency (NSE) of 0.7 which was used to simulate historical and future streamflow projections. This calibration refined the model's peak and base flows for better simulation accuracy. Following the SWAT+ analysis, the Streamflow Drought Index (SDI) analysis was conducted to further investigate hydrological drought characteristics. The SWAT+ model also facilitated the creation of the maps to investigate predicted changes in hydrological fluxes such as precipitation, evapotranspiration, lateral flow and soil moisture.

Findings from the study reveal that under both RCP 4.5 and RCP 8.5 scenarios, there is a projected increase in the intensity and frequency of meteorological droughts within some sub-basins in both the near and distant future, with a significant exacerbation during the latter period. All CORDEX models indicated an increase in temperature, especially under the RCP 8.5 scenario, with little variability of

future precipitation trends. Despite common beliefs that global warming would universally increase intensity and magnitude of drought through increased evapotranspiration, modelling output suggests this trend may not hold true for all sub-basins. Regions such as the Kilombero and Lower Rufiji sub-basins, along with the vicinity of the Mtera Reservoir, are anticipated to see a rise in wetting predominantly due to future increases in precipitation. However, these areas could also encounter issues like diminished soil moisture and lateral flow if the least optimistic model projections come to pass. On the other hand, the Luwegu and Little Ruaha sub-basins emerge as particularly sensitive to increases in potential evapotranspiration and temperature and could be more likely to face heightened frequencies and intensities of droughts.

These shifts hold critical implications for the ecological systems and human endeavours within these sub-basins. For example, in the Luwegu, where the Nyerere National Park is situated, changes in drought conditions could have a marked impact on wildlife and the broader ecosystem. In the Little Ruaha, critical for its wetlands, the anticipated reduction in soil moisture and lateral flow poses risks to dependent agricultural and forestry operations. This research highlights the urgent need for comprehensive water resource management and adaptive measures to counteract the negative impacts of evolving drought patterns in the Rufiji Basin, thereby protecting its natural environments and the livelihoods dependent on them

TABLE OF CONTENTS

PLAGIARISM DECLARATION ii

ACKNOWLEDGEMENTS iii

ABSTRACT iv

LIST OF FIGURES ii

LIST OF TABLES iv

LIST OF ACRONYMS AND ABBERVIATIONS v

CHAPTER 1: INTRODUCTION 1

1.1 Background 1

1.2 Climate of Eastern Africa 2

1.2.1 Historical and Projected Precipitation Changes for the Region 3

1.2.2 Historical and Projected Temperature Changes for the Region 5

1.3 Research Statement 5

1.4 Aims and Objectives 6

1.5 Thesis Outline 6

CHAPTER 2: STUDY AREA 8

2.1 Physiography and Geomorphology 9

2.2 Climate and Hydrology 11

2.3 Socio-Economic Factors 14

2.3.1 Demographics and Ethnic Composition 15

2.3.2 Fishing, Crop Cultivation & Livestock Keeping 16

2.3.3 Irrigation and Hydropower 18

CHAPTER 3: LITERATURE REVIEW 20

3.1 What is Drought? 20

3.2 Types of droughts 20

3.2.1 Meteorological drought 21

3.2.2 Agricultural Drought 22

3.2.3 Hydrological Drought 22

3.2.4 Socio-Economic Drought 22

3.3 Drought Quantification 24

3.3.1 Meteorological Drought Indices 24

3.3.2 Hydrological Drought Indices 30

3.4 Climate and Hydrological Modelling Frameworks and tools 32

3.4.1 Climate Modelling 32

3.4.3 Hydrological Modelling 36

CHAPTER 4: DATA AND METHODS 39
4.1 General analytical framework 39
4.2 Data 40
4.2.1 GIS Data 40
4.2.2 Hydrological Data 41
4.2.3 Historical Climate Data (ERA5-Land) 43
4.2.4 CORDEX Data 43
4.3 Methods 47
4.3.1 Drought Indices 47
4.3.2 Development and implementation of SWAT+ over the Rufiji Basin 52
4.3.3 Preparation of climate input files for setting up model calibration and simulations 58
4.3.4 SWAT+ Calibration and Validation 59
4.3.5 Spatial Analysis of projected changes in hydrological fluxes 60
CHAPTER 5: RESULTS & ANALYSIS 62
5.1 Results of hydrological model calibration 62
5.2 Historical drought 64
5.3 Projected changes in LSU-level hydrological fluxes 66
5.3.1 Historical Period 66
5.3.2 Hydrological fluxes under RCP 4.5 projections 69
5.3.3 Hydrological fluxes under RCP 8.5 projections 70
5.4 Future meteorological and hydrological drought 73
5.4.1 Projected changes in frequency of meteorological and hydrological Drought 73
5.4.2 Projected changes in intensity of meteorological and hydrological Drought 78
CHAPTER 6: DISCUSSION 83
6.1 Summary 89
6.2 Limitations 90
CHAPTER 7: SUMMARY AND CONCLUSIONS 91
REFERENCES 95

LIST OF FIGURES

Figure 1.1: The maximum positioning of the ITCZ during the northern hemisphere summer (July ITCZ) and the southern hemisphere summer (January ITCZ) (Source: Nguvava, 2020)……..3

Figure 2.1: Rufiji Basin with the Main Sub-Basins, River Drainage Network and Principal Rivers. Data source: Global Multi-Resolution Terrain Elevation Data (GMTED) 2010 (estimated 200 meters of horizontal resolution and 30 meters of vertical accuracy), retrieved from https://lta.cr.usgs.gov/GMTED2010.....8

Figure 2.2: Slope of Rufiji Basin, with Longitudinal Profiles for Rivers within Four Main Sub-Basins……9

Figure 2.3: Distribution of Eight Landscape Elements in Rufiji Basin According to the Eight Classes (Source: Smith et al., 2016)……10

Figure 2.4: Mean Monthly Precipitation over Rufiji Sub-Basins (Derived from FAO Local Climate Estimator (FAO2005))……12

Figure 2.5: Annual Average Runoff (P-ET) and Actual Evaporation (ET) as Percentages of Total Precipitation (P) in the Four Sub-Basins of Rufiji (Extracted from Smith et al. (2015))……12

Figure 2.6: Average Monthly Discharges for Lower Rufiji, Great Ruaha, and Kilombero Rivers (Source: Global Runoff Data Center 2015)……14

Figure 2.7: Sub-basin Share of Total Basin Population of 3.6 million in 2012 (Source: WREM International 2015; Adapted from Smith et al., 2016)……15

Figure 3.1: Relationship between meteorological, agricultural, hydrological & socio-economic drought……21

Figure 3.2: (a) proportion of drought occurrence by continent 1970-2008; (b) proportion of people affected by each disaster type per continent 1970-2008……23

Figure 3.3: (a) number of reported droughts by country 1970-2008, (b) number of persons affected by drought 1970-2008, (c) map of Africa showing drought vulnerability 1970-2004. Source: (UNDRR, 2009; Haile, 2005)……24

Figure 3.4: Classification and Sample SPI graph……28

Figure 4.1: General Study Framework……39

Figure 4.2: Monthly Mean Streamflow Hydrograph at Stiegler Gorge. No data record for 1963……42

Figure 4.3: Bias-Corrected CORDEX data – Monthly Average Precipitation ((a)RCP 4.5, (c) RCP8.5) and Monthly Average Temperature ((b)RCP 4.5, (d) RCP 8.5)) for the 1991-2020 period……45

Figure 4.4: Figure 4.4: Top panel: Annual average precipitation from the CORDEX models and ERA5-Land for the (a) RCP 4.5 and (b) RCP 8.5 scenarios over the Rufiji Basin. Bottom panel: Annual average maximum and minimum temperatures from the CORDEX models and ERA5-Land for the (c) RCP 4.5 and (d) RCP 8.5 scenarios over the Rufiji Basin ……46

Figure 4.5: Geospatial arrangement of input and output datasets used in the implementation of the SWAT+ model over the Rufiji Basin: (a) SWAT+ sub-basin structure and river network structure. (b) Digital Elevation Map (90m x 90m, SRTM), (c) Land Use Map (ESA, 300m), (d) Soil map (FAO Soil, 450m), (e) SWAT+ LSU shapefile, (f) Gridded climate stations.……55

Figure 4.6: Map delineating the sub-basins used in the study, the Kilombero wetland, lakes, and the calibration and gauging points within the Rufiji Basin……58

Figure 5.1: (a) Hydrograph of Stiegler Gorge (Observed flow – orange) vs SWAT+ simulation before calibration (green), (b) Simulated hydrograph after calibration (blue) vs Observed flow at Stiegler Gorge (orange) (shows validation and calibration periods)……63

Figure 5.2: Comparative Analysis of Drought Frequency (a), (b), (c) and Drought Intensity (d), (e), (f) Across Different Indices Using ERA5-Land Data (1991-2020) for severe droughts (<-1.5) ……64

Figure 5.3: Historical LSU maps showing the (a) Annual Average Precipitation, (b) Annual Average Evapotranspiration, (c) Annual Average Lateral flow, (d) Annual Average Soil Moisture in mm for the 1991-2020 period over the Rufiji Basin, derived from SWAT+ and ERA5-Land climate data……68

Figure 5.4: Spatial Maps displaying the Minimum, Maximum, and Ensemble Mean changes in values for Precipitation, Evapotranspiration, Lateral Flow, and Soil Moisture under RCP 4.5 scenario for the two time periods: 2031-2060 and 2071-2100, compared to 1991-2020……69

Figure 5.5: Spatial Maps displaying the Minimum, Maximum, and Ensemble Mean changes in values for Precipitation, Evapotranspiration, Lateral Flow, and Soil Moisture under RCP 4.5 scenario for the two time periods: 2031-2060 and 2071-2100, compared to 1991-2020……70

Figure 5.6: Boxplots of Frequencies of Drought Months with SPI/SPEI/SDI < -1.5 over various time periods for the RCP 4.5 scenario……74

Figure 5.7: Boxplots of Frequencies of Drought Months with SPI/SPEI/SDI < -1.5 over various time periods for the RCP 8.5 scenario……76

Figure 5.8: Boxplots of Intensities of Drought Months with SPI/SPEI/SDI < -1.5 over various time periods for the RCP 4.5 scenario……79

Figure 5.9: Boxplots of Intensities of Drought Months with SPI/SPEI/SDI < -1.5 over various time periods for the RCP 8.5 scenario……81

LIST OF TABLES

Table 2.1: Characteristics of Rufiji Sub-Basins. (Source: WREM, 2012)……13

Table 3.1: Advantages and Disadvantages of various SPI timescales……26

Table 3.2: Summarization of Empirical, Conceptual and Physically Based Models……38

Table 4.1: Comparison of ESA and SWAT+ Land Use Codes used in the study……40

Table 4.2: List of GCM and downscaling RCM pairs utilized in the study……44

Table 4.3: SDI classification……51

Table 5.1: SWAT+ Parameters used for Calibration……62

LIST OF ACRONYMS AND ABBERVIATIONS

BCM	Billion Cubic Meters
BMI	Bhalmey-Mooley Index
CGIAR-CSI	Consultative Group on International Agricultural Research – Consortium for Spatial Information
CMIP	Coupled Model Intercomparison Project
CMIP5	Coupled Model Intercomparison Project 5
CMIP6	Coupled Model Intercomparison Project 6
CORDEX	Coordinated Regional Climate Downscaling Experiment
CSAG	Climate Science Analysis Group
CSV	Comma Separated Values
DEM	Digital Elevation Map
DJFM	December-January-February-March
ECMWF	European Centre for Medium-Range Weather Forecasts
ENSO	El Nino Southern Oscillation
ERA5	ECMWF Re-Analysis Fifth Generation
ESA	European Space Agency
FAO	Food and Agriculture Association
GCMs	Global Circulation Models
GDP	Gross Domestic Product
GRDC	Global Runoff Data Centre
GWL	Global Warming Level
HRU	Hydrological Response Unit
IOD	Indian Ocean Dipole
IPCC	Intergovernmental Panel on Climate Change
ITCZ	Inter-Tropical Convergence Zone
IUSS	International Union of Soil Sciences
JNHPP	Julius Nyerere Hydropower Plant

LSU	Landscape Unit
m.a.s.l.	Meters Above Sea Level
MIKE-SHE	Mike System Hydrologique European
MW	Mega Watts
NSE	Nash-Sutcliffe Efficiency
PET	Potential Evapotranspiration
PDSI	Palmer Drought Severity Index
PRCP	Precipitation
QDM	Quantile Delta Mapping
QGIS	Quantum Geographical Information System
QSWAT	Quantum/ QGIS Soil and Water Assessment Tool
RCMs	Regional Climate Models
RCP	Representative Concentration Pathway
SAGCOT	Southern Agricultural Growth Corridor of Tanzania
SDI	Streamflow Drought Index
sEA	Southeastern Africa
SPI	Standardized Precipitation Index
SPEI	Standardized Precipitation Evapotranspiration Index
SRTM	Shuttle Radar Topography Mission
SSA	Sub-Saharan Africa
SSPs	Shared Socio-economic Pathways
SWAT	Soil and Water Assessment Tool
TMAX	Maximum Temperature
TMIN	Minimum Temperature
TOPMODEL	Topography Based Hydrological Model
UN	United Nations
UNCCD	United Nations Convention to Combat Desertification
UNDRR	United Nations Office for Disaster Risk Reduction
UNEP	United Nations Environmental Programme
UNESCO	United Nations Educational, Scientific and Cultural Organization
USDA-ARS	United States Department of Agriculture – Agricultural Research Service

WCRP World Climate Research Programme

WMO World Meteorological Association

CHAPTER 1: INTRODUCTION

1.1 Background

Accessibility and availability to water is a fundamental resource in bolstering socio-economic opportunities and attenuating poverty in many developing nations. Water resources give the ability to expand the economy through agricultural development, hydropower generation and water supply for domestic, urban and industrial use. However, the impacts of climate change as well as an increased demand on water from growing populations, industrial growth and hydropower generation have put major stresses on existing water resources. According to the UN Convention to Combat Desertification (UNCCD), it was estimated that by 2030, water stress will affect about 2.7 billion people in sub- tropical regions, endangering food production systems of over 2.6 billion smallholder farmers (UNCCD, 2013).

It has become unanimously accepted in the last few decades, that climate change and global warming are becoming a worldwide phenomenon. These changes are projected to impact water resources through increasingly unpredictable precipitation, higher temperatures leading to higher rates of evaporation and a higher frequency of natural disasters such as floods and droughts. Of all the major continents on Earth, Sub-Saharan Africa is projected to be most at risk to climate disasters and vulnerability to climate risks (IPCC, 2022). Having one of the largest population growth rates worldwide, river basins in these parts of the world are under high risk. Growing economies and limited government intervention to adaptation and mitigative measures to combat climate change exacerbate the predicted effects of climate change in these regions (IPCC, 2022)

Climate risk exposure and vulnerability are considerable across critical economic sectors in Sub-Saharan Africa (SSA) (Richardson, 2007; Jury, 2002, Conway et al., 2017, Barrios et al., 2010; Brown et al., 2011). Recent extreme droughts & flooding events demonstrate the scale of disruption (Siderius, 2018; Gannon et al., 2018; Watkiss et al., 2011).Southern Africa's drought from 2015 to 2016 emphasized the cascading nature of effects related to power outages, water shortages and food instability, which disproportionately affected small and medium sized businesses (Siderius, 2021)

In the late 1980's the United Nations Environmental Programme (UNEP) in conjunction with the World Meteorological Organization (WMO), developed the International Panel on Climate Change (IPCC) with the objective to provide governments at various levels with scientific information that they can utilize to create climate policies. The organization is a collective of governments and researchers from member states of the United Nations (UN) or the WMO. Researchers volunteer their time to evaluate thousands of scientific papers to provide a comprehensive summary about what is known about the drivers of climate change, its impacts and future risks, and how adaptation and mitigation can reduce those risks. Every few years, the IPCC release assessment reports detailing these factors for every sub-

region in the world, as well as historical and future trends in temperature and precipitation for that region (IPCC, 2022).

The sixth and long-awaited latest assessment report was released in 2022, and outlines some of the historical, prevailing and predicted trends in it. The next few chapters will focus on condensing some of the information regarding climate change, especially temperature and precipitation, in the Southern East African Region where the Rufiji Basin is located, with information sourced from the chapter on Africa within the assessment.

Building on insights from prior assessments, several key conclusions have surfaced. Statistics show that there has been a reduction in food security due to climate change through losses in crop yields, rangelands, livestock and fisheries, declining food nutritional quality, access and distribution of food leading to price spikes. The risk to crop yields are significantly less at a global warming increase of 1.5^{o}C of future global warming compared to a 2^{o}C increase, leading to a large reductions in maize cropping and reduced fishery catches (IPCC, 2022).

The greatest reduction in economic growth for a temperature increase from 1.5^{o}C to 2^{o}C of global warming are projected to impact low- and middle-income countries, with Africa bearing an increasing proportion of exposure globally. The IPCC forecasts increased deaths from undernutrition, malaria, diarrhoea, heat stress and illnesses related to fire, which will be exacerbated due to poverty and limited financing impacting on an already struggling capacity to adapt (IPCC, 2022).

1.2 Climate of Eastern Africa

Eastern Africa's climate is complicated, mostly as a result of the interplay between the marine and terrestrial environments it lays in close proximity to (Lyon, 2017; Yang et al., 2015). Generally, the region has a semi-arid climate and exhibits small variations in temperature throughout the year, with rainfall showing significant spatial-temporal variability (Yuan et al., 2013).

Eastern Africa's climate is shaped by a combination of large-scale atmospheric systems and local geographical features, each influencing temperature and precipitation patterns across the region. Key drivers include the seasonal movement of the Inter-Tropical Convergence Zone (ITCZ), the Hadley Cell circulation, and the African Rain Belt, which collectively regulate the timing and amount of rainfall (Siderius et al., 2021). The movement of the ITCZ, for example, impacts both temperature and precipitation, bringing seasonal rains as it shifts northward in the northern hemisphere summer and southward in the southern hemisphere summer (Nguvava, 2020; Anyah & Qui, 2012). This movement not only brings variability to rainfall but also affects temperature, with cooler temperatures during rainy periods and warmer, drier conditions when the ITCZ is distant (Hastenrath, 2001).

Local topography further shapes these patterns by influencing low-level air circulation and moisture transfer, creating short-distance variations in rainfall and temperature due to the orographic effect (Kinuthia, 1992; Nicholson, 1996). For instance, mountainous areas can intercept moist air, leading to increased precipitation on windward slopes and creating rain shadows in leeward areas, thus producing distinct microclimates.

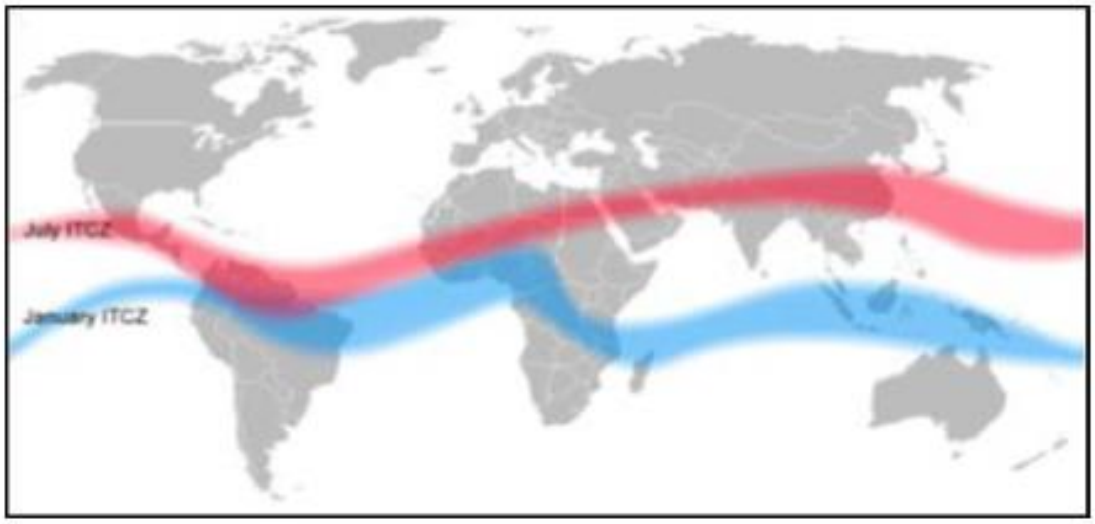

Figure 1.1: The maximum positioning of the ITCZ during the northern hemisphere summer (July ITCZ) and the southern hemisphere summer (January ITCZ) (Source: Nguvava, 2020).

1.2.1 Historical and Projected Precipitation Changes for the Region

The Southeastern Africa (sEA) region is considered a 'climate transition zone'. In terms of rainfall variability, sEA is situated in a complex transition zone that responds to dominant global and regional climate variability modes, such as the El Niño-Southern Oscillation (ENSO) and the Indian Ocean Dipole (IOD). The sEA marks the geographical transition from the bimodal rainfall regimes of equatorial East Africa to the north, to the unimodal southern African regime to the south (Siderius et al., 2021).

Years with above-average rainfall in Eastern Africa are often associated with El Niño events, particularly from October to December, while La Niña years typically bring drier conditions. Additionally, Siderius et al. (2021) report that positive phases of the Indian Ocean Dipole (IOD) are linked to higher-than-average rainfall, whereas negative IOD phases generally result in drier conditions. For instance, during the positive IOD phases in 1961-62 and 1967-68, Eastern Africa experienced increased rainfall independently of the El Niño-Southern Oscillation (ENSO). In contrast, the 1997-98 period saw intensified rainfall due to the combined influence of El Niño and a positive IOD.

Rainfall patterns in Eastern Africa are predominantly categorized into two distinct regimes: the bimodal and unimodal patterns. The bimodal regime, which is prevalent in most upper parts of Eastern Africa, has been observed to demonstrate a long-term wetting trend, particularly in the short rains occurring during October, November, and December. This trend, evident from the 1960s to the present, is linked to a warming of the western Indian Ocean and a consistent intensification of the Indian Ocean Walker Cell, as reported by Manatsa & Behera (2018), Nicholson (2015, 2017), and Liebmann et al. (2014).

Conversely, southern regions of Tanzania, particularly within the latitudes of 8 to 12 degrees south, display a unimodal rainfall regime that is similar to that of Southern Africa, as documented in studies by Bouimetarhan (2015) and Siderius et al. (2021). Encompassed within this area, the Rufiji catchment experiences a tropical summer rainfall pattern. Here, a well-defined single rainy season is observed, spanning from November to April, as detailed by Palmer et al. (2023), Temple and Sundborg (1972) and Kijazi and Reason (2005).

Beginning in the year 2000, a marked shift has been observed in the correlation between the ENSO and drought occurrences, as noted by Park et al. (2020). This period has seen several droughts closely associated with La-Nina Events, contrasting with earlier decades when drought years did not demonstrate a significant connection to these events. This trend is further evidenced in the findings of Siderius et al. (2021), highlighting the evolving nature of this relationship within the Rufiji Basin.

From 2005, the frequency of drought within the East African region has doubled from one every six years to one every three years and has now shown a greater severity during the long rainfall months (Ayana et al., 2016; Haile et al., 2019) with the most prominent ones in arid and semi-arid parts of the region (Nicholson, 2017).

Projected precipitation shows higher mean annual rainfall at Global Warming Levels (GWL) of 1.5^{o}C & 2^{o}C from 25 CORDEX models (Nikulin et al., 2018; Osima et al., 2018). The 0.5^{o}C increment change from 1.5^{o}C shows an increased dry spell duration of between 2 and 4 days (Hoegh-Guldberg et al., 2018; Nikulin et al., 2018; Osima et al., 2018; Weber et al., 2018). There is however a low confidence of this increased projected mean rainfall (Gutierrez et al., 2021). Even though some studies project an increase of end of century rainfall (Otieno & Anyah, 2013; Kent et al., 2015) the mechanics governing these are not well understood. Projected wetting conflicts with the observed drying trends, bringing about the term ‘the East African rainfall paradox’ (Rowell et al., 2015, Wainwright et al., 2018). In some regions of East Africa, no significant predicted trend is observable in modelled outputs across efforts, with CMIP5 and CORDEX data showing opposite signs of change (Lyon et al., 2017; Lyon and Vigaud, 2017; Osima et al., 2018; Kendon et al., 2019; Ogega et al., 2020)

Ponderous rainfall events are projected to increase over the region at a GWL of 2^{o}C & higher (high confidence) (Nikulin et al., 2018; Finney et al., 2020; Ogega et al., 2020; Li et al., 2021). Frequency of

drought events, duration and magnitude are projected to increase in Sudan, South Sudan, Somalia and Tanzania (Liu et al., 2018; Nguvava et al., 2019; Haile et al., 2020; Spinoni et al., 2020).

1.2.2 Historical and Projected Temperature Changes for the Region

Historical observations for the East African region have shown that the mean temperature has increased by 0.7ºC – 1ºC for the 1973- 2013 period, with trends showing an increase in number of warm nights, warm days and warm spells (Ayugi & Tan, 2018; Camberlin, 2018; Russo et al., 2016; Gebrechorkos et al., 2019; Nashwan & Shahid, 2019). The northern region of Southern Africa has experienced a comparable increase in mean annual temperature, ranging from 1.04°C to 1.44°C between 1961 and 2015 (Gutiérrez et al., 2021). Like in Eastern Africa, this warming has been accompanied by a rise in the frequency of hot days and heightened heat stress, with considerable impacts on agriculture and human health (Ceccherini et al., 2017; Kruger & Nxumalo, 2017a, 2017b).

Projected temperatures for Eastern Africa indicate mean annual increases of approximately 0.6°C, 1.1°C, and 2.1°C above the 1994–2005 average under global warming levels (GWLs) of 1.5°C, 2°C, and 3°C above pre-industrial levels, respectively. In contrast, parts of Southern Africa are expected to experience slightly higher warming rates, with mean annual temperatures projected to rise by about 1.2°C, 2.3°C, and 3.3°C above the 1995–2004 average under the same GWLs. These trends suggest that both regions will likely face significant temperature increases, with implications for ecosystems, agriculture, and water resources (IPCC, 2022).

The projected annual frequency of heat waves is expected to rise significantly, with increases of 2 to 4 heat waves under a global warming level (GWL) of 1.5°C, 4 to 8 under a GWL of 2°C, and 8 to 12 under a GWL of 3°C (Engelbrecht et al., 2015; Russo et al., 2016; Dosio, 2017; Weber et al., 2018; Seneviratne et al., 2021). Moreover, children born in 2020 within a scenario aligned with a 1.5°C increase are projected to experience 3 to 4 times more heat waves throughout their lifetimes compared to individuals born in 1960 (Thiery et al., 2021).

1.3 Research Statement

The objective of this study is: "To investigate the potential future impacts of climate change on the characteristics of meteorological and hydrological droughts within the Rufiji River Basin"

1.4 Aims and Objectives

The focus of this research is to assess the influence of climate change on the future characteristics of meteorological and hydrological drought in the Rufiji Basin, utilizing simulations from regional climate models as well as a hydrological model – SWAT+. The specific goals of this analysis include:

Segmenting and comprehending the Rufiji Basin for a detailed assessment at the sub-basin level.

Implementing and calibrating the SWAT+ hydrological model to simulate the historical as well as future streamflow patterns and assess the impact on hydrology under various climate change scenarios.

Evaluating future climate projections and examining the likelihood of changes in drought frequency and severity under the RCP 4.5 and RCP 8.5 scenarios, both in the near-term (2031-2060) and long-term future (2071-2100), relative to historical records (1991-2020)

Employing diverse indices to analyze meteorological and hydrological droughts, with a focus on detailing the characteristics of future drought conditions across the sub-basins

Assess the spatial susceptibility of the basin to future droughts and evaluate the magnitude of changes in meteorological and hydrological variable fluxes, including precipitation, evapotranspiration, lateral flow, and soil moisture, under projected future climate.

1.5 Thesis Outline

This thesis is organized into 7 chapters:

- **Chapter 1**: Introduction to the context of climate change, including IPCC's historical and projected climate scenarios. The chapter offers an overview of the prevailing climate in East Africa.
- **Chapter 2**: Description of the study area, encompassing climate and hydrology, physiography and geomorphology, and socio-economic aspects such as demographics, ethnic groups, agriculture, irrigation, and hydropower in the basin.
- **Chapter 3**: A literature review focusing on drought classification and quantification, introduction to drought indices, and an overview of climate and hydrological modelling frameworks, including a description of hydrological models.
- **Chapter 4**: Outline of the methodologies used in this research, information on climate data sources and hydrological data, methods for applying various indices, and details of the SWAT+ model set up and calibration.
- **Chapter 5**: Presentation of results and analysis, including frequency and intensity boxplots for different RCP pathways and model outcomes. Also included is a spatial representation of future

fluxes in meteorological and hydrological variables within the basin under both RCP scenarios for comparisons of the near and far future to the historical period.

- **Chapter 6**: Discussion of the results, concluding with a summary.
- **Chapter 7**: Conclusion of the thesis, summarizing key findings and offering recommendations.

CHAPTER 2: STUDY AREA

The Rufiji River Basin (RRB), one of a total of nine river basins in Tanzania, is the largest, covering roughly 20% of the country's land mass and providing about 20% of the nation's renewable water resources (Smith, 2016; Mwalyosi, 1988). The basin lies entirely within Tanzania with a catchment area of about 177,429 km^2 and is situated between the latitudes of 5.7^{o}S and 10.5^{o}S and longitudes of 33.5^{o}E and 39^{o}E. The main trunk of the Rufiji river is fed by three main tributaries, the Great Ruaha, Kilombero and the Luwegu. The lower reaches of the river are generally referred to as the Lower Rufiji River (Mwalyosi, 1990; Nguvava, 2020).

The Great Ruaha, Kilombero, Luwegu and the Lower Rufiji are the four main sub-basins that make up the Rufiji River Basin, and account for 47%, 23%, 14% and 17% of its area respectively (Smith, 2016, Mwalyosi, 1990). The main source of water is the Kilombero sub-basin which supplies more than 60% of the total water in the basin (Mwalyosi, 1990; Nguvuva, 2020) and provides water even in drier months due to the wetland encompassed within its sub-basin. The main Rufiji River dicharges into the Indian Ocean in a place known as Mafia Island (Nguvuva, 2020).

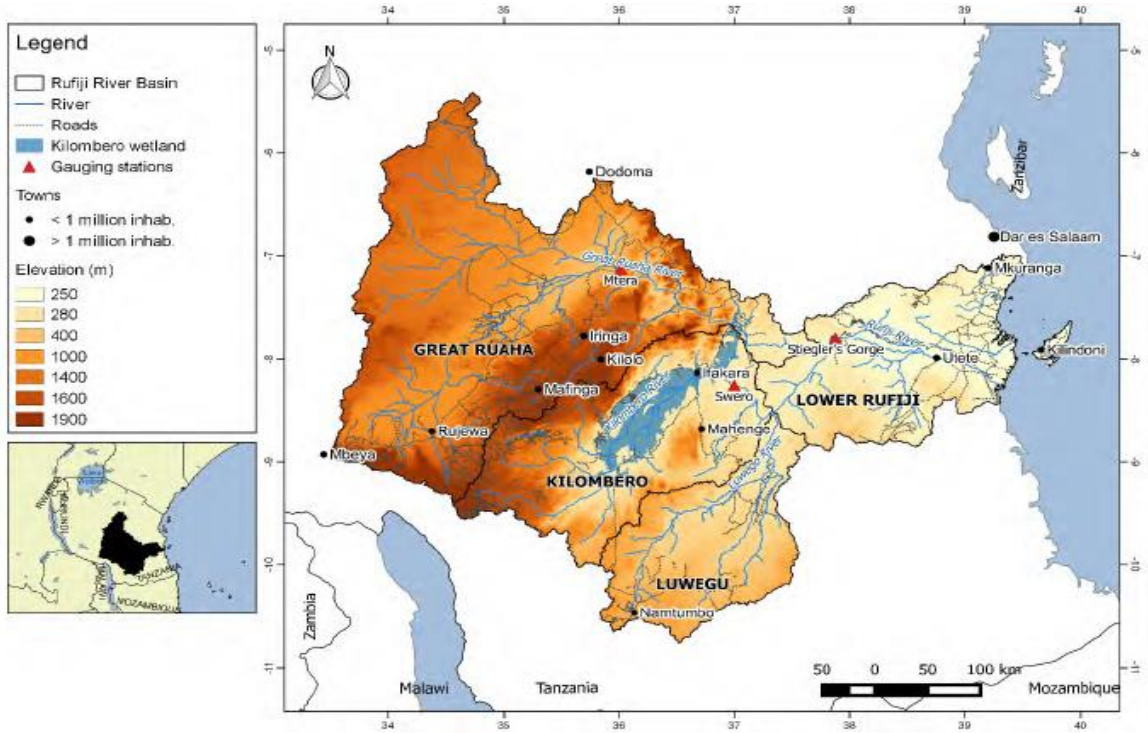

Figure 2.1: Rufiji Basin with its main sub-basins, River Drainage Network and Principal Rivers.(Data source: Global Multi-Resolution Terrain Elevation Data (GMTED) 2010 (estimated 200 meters of horizontal resolution and 30 meters of vertical accuracy), retrieved from https://lta.cr.usgs.gov/GMTED2010)

2.1 Physiography and Geomorphology

The geography of the Rufiji River Basin spans from relatively flat land downstream in the East to mountainous regions up to 3000m above sea level in the West (Smith, 2016; Nguvuva, 2020). Around 60% of the basin and the majority of the Great Ruaha sub-basin are located between 500 and 1500 meters above sea level (m.a.s.l.) elevation. Elevations greater than 1,500 m.a.s.l. are concentrated in the divide between the Kilombero and Great Ruaha sub-basins and on the boundary of the Rufiji River Basin with the Lake Nyasa and Rukwa Basins.

The Kilombero floodplain, half of the Luwegu basin and a small section of the Great Ruaha between the Kidatu dam and the confluence with the Rufiji River all fall within the 200-500 m.a.s.l. range, and account for about 20% of the basin's area (Smith, 2016). These flat areas also include parts of the Kilombero floodplain. Only about 9% of the basin's surface lies below 200 m.a.s.l. and is restricted to the Lower Rufiji basin.

In the basin the flattest river is the Lower Rufiji, with an average slope of 1.4^{o} and a maximum slope of 34^{o} whereas the Luwegu has the steepest decline with an average slope of 2.4^{o} and a maximum of 48^{o} (see Figure 2.2). Over an altitude of 350 m.a.s.l., the Kilombero river contains the longest and steepest section in the whole basin (Smith, 2016).

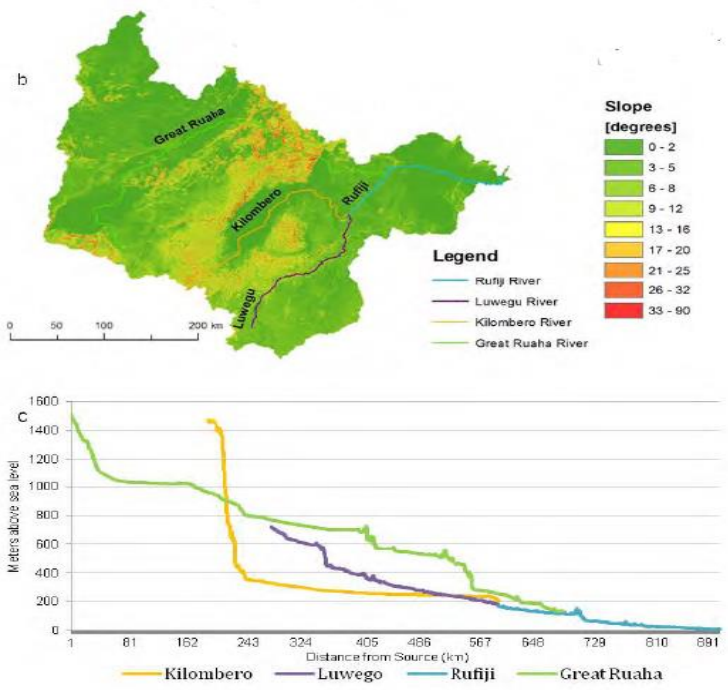

Figure 2.2: Slope of Rufiji Basin, with Longitudinal Profiles for Rivers within Four Main Sub-Basins (Data source: Smith, 2016)

There are 3 major floodplains along the Great Ruaha river, located at elevations of 1,025 m.a.s.l. (about 100km along the river's axis), 700 m.a.s.l. (also about 100km along the river's axis) and 575 m.a.s.l. (about 70km along the river's axis) as well as a smaller floodplain at about 500 m.a.s.l. just downstream of the Kidatu dam (extending for about 30km).

At a height of 200-300 m.a.s.l., the Kilombero has a long and broad floodplain that stretches for nearly 250km to the confluence of the Luwegu and Great Ruaha. Downstream of Stiegler's Gorge, the Lower Rufiji features a sizable floodplain that stretches for roughly half of its length before flowing out into the Indian Ocean (Smith, 2016).

Smith et al. (2016) divide the basin into 8 different groups of landscapes, with a mix of characteristics determined by the (1) slope gradient of steepness; (2) local convexity or positive curvature (longitudinal curvature of slopes) and (3) surface texture or roughness (frequency of ridges and valleys). The classes represented in the basin are:

1. Dissected plateau or mountain tops; steep terrains with a complex drainage system
2. Elevated plateaus without a dense drainage network
3. Mountain slopes and isolated basins; slopes connecting mountain tops to lower landforms
4. Confined valleys – steep valleys with the drainage only in the main valley floor
5. Lower slopes; lower parts of the mountain slopes connecting the mountain front with the lower terrains
6. Alluvial fans and piedmonts; alluvial fans of deposited fluvial sediment where a valley enters a plain and are the place for avulsion of the main rivers.
7. Confined valleys and smooth hills
8. Floodplains and river valleys; flattest landforms, where the drainage can take a braided pattern

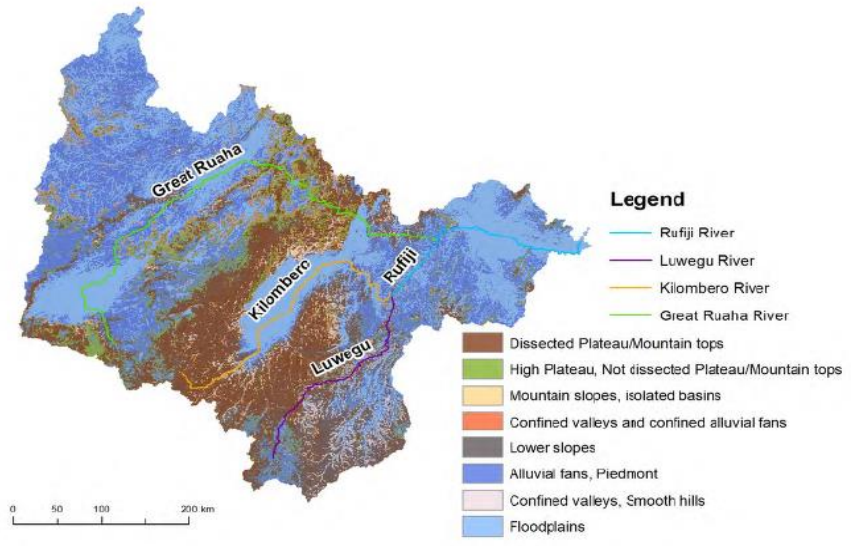

Figure 2.3: Distribution of Eight Landscape Elements in Rufiji Basin According to the Eight Classes (Data source: Smith et al., 2016)

Dissected plateaus (mostly found in the basin's centre) reflect the geological and tectonic structure of the basin). These plateaus are dominated by gneiss. Large portions of the Great Ruaha, Kilombero and the Lower Rufiji sub-basins are occupied by floodplains, while the steeper Luwegu has a narrow one. A large proportion of the basin also comprises of alluvial fans and piedmont and hills at varying elevations, including in the highlands of the Great Ruaha sub-basin.

2.2 Climate and Hydrology

The Rufiji basin, representative of the climatic patterns in the southern regions of Eastern Africa, is characterized by a distinct tropical summer rainfall regime, with a big proportion exhibiting a single and well-defined rainy season that extends from November to April, as described by Temple and Sundborg (1972) and Kijazi and Reason (2005). In certain areas of the region, the rainy season exhibits a bimodal pattern, characterized by rainfall peaks in December and January, a drier period in February, followed by another peak in April. In contrast, the dry season, which extends from May to October, is primarily influenced by the southeasterly trade winds (Bouimetarhan, 2015; Walter and Lieth, 1960; Nicholson et al., 1988).

The estimated mean annual precipitation of the entire basin is estimated to be between 800 - 1,100 mm/y (Smith, 2016; Temple and Sundborg 1972). There are however large variations of mean annual rainfall across the four sub-basins, ranging from 0-250 mm/y in the Great Ruaha, to 1,600 mm/y within the Kilombero sub-basin (Nguvava, 2020; Temple and Sundborg 1972). The mean annual precipitation over the Lower Rufiji and the Luwegu sub-basins is between 650 -1,000 mm/y (Nguvava, 2020; Temple and Sundborg 1972). The Figure below shows mean monthly rainfall over the sub-catchments:

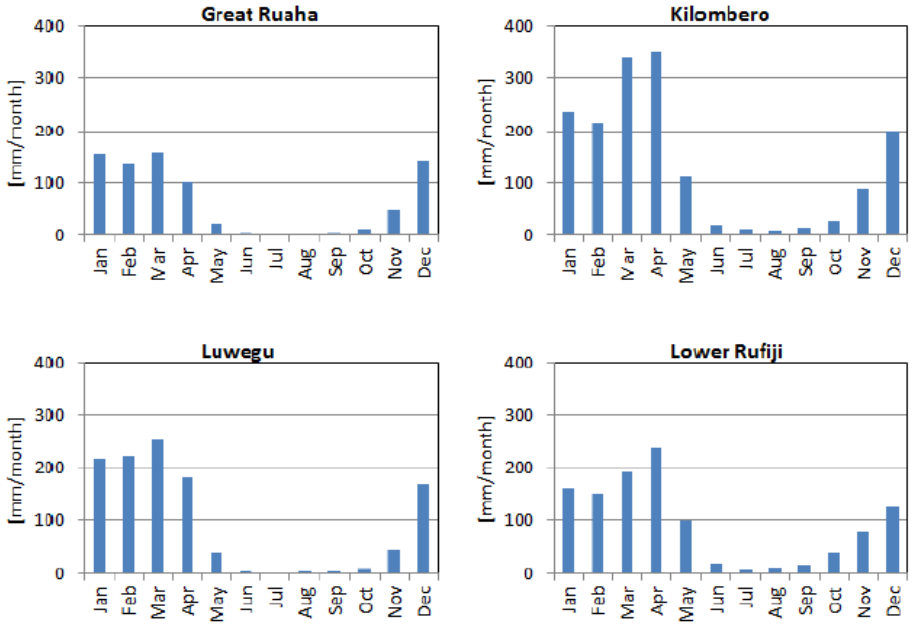

Figure 2.4: Mean Monthly Precipitation over Rufiji Sub-Basins (Derived from FAO Local Climate Estimator (FAO 2005)).

In the entirety of the sub-basins, the majority of the precipitation that occurs as rainfall is reintroduced into the atmosphere through processes such as evaporation and plant transpiration (Smith, 2016; World Evaporation Web Viewer, 2015). This ratio of evaporation to rainfall is highest in the Great Ruaha sub – Basin where just 10% of rainfall is estimated to enter the river as surface water and replenish ground water aquifers (Figure 2.5).

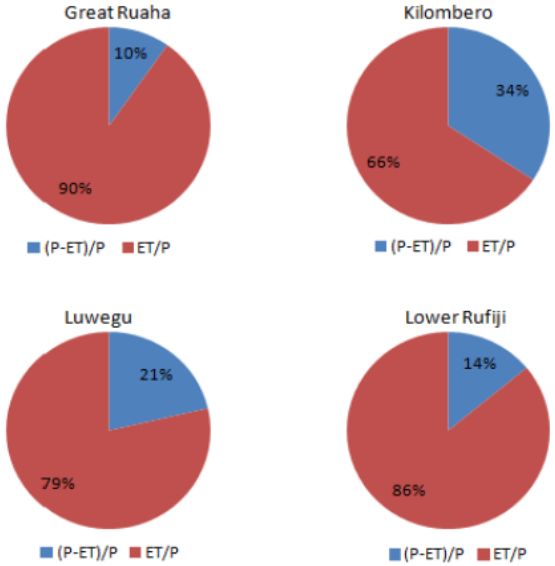

Figure 2.5: Annual Average Run-off (P-ET) and Actual Evaporation (AET) as Percentages of Total Precipitation (P) in the Four Sub-Basins of Rufiji (Extracted from Smith et al. (2016))

The Kilombero sub-basin has the largest percentage of annual average runoff in the basin (62%), with the Luwegu and Lower Rufiji exhibiting intermediate runoff rates with 18% and 15% respectively. The Great Ruaha (5%) exhibits the lowest percentage of runoff rates (Table 2.1). The data demonstrates that the Kilombero sub-basin followed by the Luwegu have the greatest potential for water resources and are within the same range as reported by WREM International (2015) (Smith, 2016).

Table 2.1: Characteristics of Rufiji Sub-Basins.
(Source: Smith, 2016; WREM, 2012)

Sub-Basin	Catchment Area (km^2)	% of Drainage Area	Mean Annual Precipitation ($mm\ y^{-1}$)	Mean Annual Runoff ($bcm\ y^{-1}$)	% of Annual Runoff
Great Ruaha	85,554	47	400-1,200	3.3	15
Kilombero	40,330	22	1,000-2,000	13.8	62
Luwegu	25,288	14	800-1,000	4	18
Lower Rufiji	32,619	18	650-110	1.1	5
Rufiji Total	183,791	100		22.2	100
Tanzania	**945,203**			**89**	

The Rufiji Basin experiences a range of temperatures, with highs reaching 30°C or more during the dry season closer to the coast, and cooler temperatures between 10°C and 20°C further inland, particularly near highland areas. Since the 1960s, average temperatures in Tanzania have risen by approximately 0.23°C per decade, while annual rainfall has decreased at an average rate of 3.3% per decade (McSweeney et al., 2010). This increase in temperature and subsequent rise in evaporation could heighten the frequency of droughts in the region, leading to reduced stream flows and land degradation (Siderius, 2021).

Looking ahead, climate projections suggest an overall increase in annual precipitation, though with moderate confidence. This precipitation is likely to be unevenly distributed throughout the year, with an increased likelihood of intense rainfall events (Smith et al., 2016).

In the Rufiji Basin, river discharge patterns align closely with precipitation patterns, exhibiting a lag of approximately one month between the onset and conclusion of the high-flow season. Compared to the Kilombero and downstream sub-basins, the Great Ruaha sub-basin displays a more pronounced range of seasonal variability in discharge values, as expected due to its smaller proportion of runoff within the basin. During the dry season, the Great Ruaha's monthly average flow is less than 10% of its average flow in the wet season, whereas in the Kilombero, this figure is closer to 25%. The monthly dry season flow in the Luwegu sub-basin is intermediate, falling between the Great Ruaha and Kilombero values. Similarly, discharge values in the Lower Rufiji are moderated due to the confluence of multiple upstream sources.

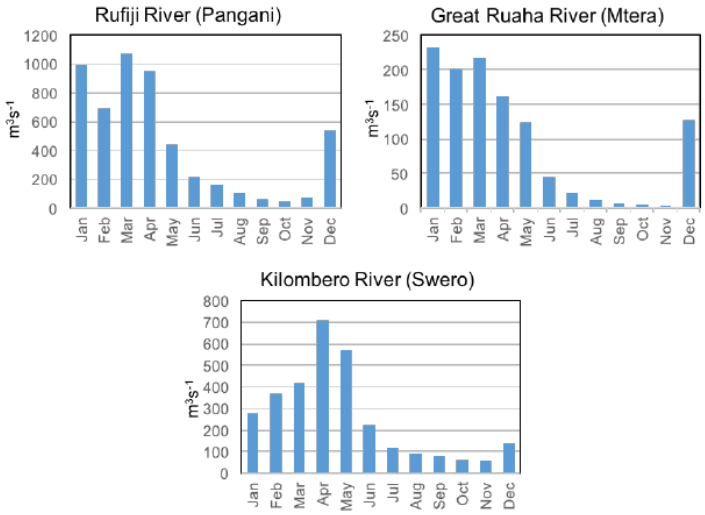

Figure 2.6: Average Monthly Discharges for Lower Rufiji, Great Ruaha, and Kilombero Rivers
(Source: Smith, 2016, Global Runoff Data Center 2015)

In their study, Duvail and Hamerlynek (2007) examined the perceptions of flooding within the socio-economic contexts of agriculture and dam construction. According to their analysis of the available reliable flow data from 1957 to 1984, the average annual discharge of the river at Stiegler's Gorge (Lower Rufiji, Figure 2.1) is estimated at approximately 800 cubic meters per second (m^3/s). The river flow demonstrates significant seasonal variation, with average monthly discharge fluctuating from around 200 m^3/s in October/November, coinciding with the onset of the short rains, to over 3000 m^3/s in April. During El-Nino events, peak flows have been recorded at about 10,300 m3/s, as observed in mid-February 1998, based on reports by JBG Gauff Ingenieure (2000) and Erftemeijer & Hammerlynck (2005). During such high-flow periods, the water level in Stiegler Gorge is estimated to rise to 14 meters above the levels typically seen in the dry season.

2.3 Socio-Economic Factors

In his findings, Hamisi (2013) identifies the Rufiji Basin as one of Tanzania's most vulnerable regions, largely due to increasing human pressures and climate variability. According to Hamisi, climate fluctuations have altered river runoff and sedimentation, while human activities, including deforestation and overgrazing, have exacerbated environmental stress. This has led to a decline in the operational efficiency of upstream hydropower plants, impacting energy output. Specifically, Hamisi attributes increased flooding, droughts, soil salinity, and delayed rainfall to climate variability. Rainfall patterns in the basin are marked by unpredictable seasonal anomalies and highly variable event frequency and intensity; when it does rain, it is typically intense and brief. Such variability has also resulted in the

displacement of local communities and the destruction of crops, reducing living standards and further challenging the resilience of affected populations.

Moreover, temperature increases have led to higher evaporation rate, soil droughts, and salinity intrusion. Fish catches and spawning have been impacted by climate change, which have damaging consequences on communities fishing practices and nutrition levels. Extreme land degradation is a result of unsustainable land use including deforestation and overgrazing. The sum of these impacts has led to changes in the water balance and farming uncertainty especially for small farming stakeholders (Hamisi, 2013).

2.3.1 Demographics and Ethnic Composition

According to a 2012 census, the Rufiji Basin's population is estimated to be around 3.6 million, accounting for about 8.3% of the population of mainland Tanzania. Around 54% of this population lives in the Great Ruaha sub-basin, 29% in Kilombero, and 15% in the lower Rufiji. Covering about 14% of the total area of the Rufiji Basin, the Luwegu sub-basin is home to only about 2% of the Rufiji's entire population, as it is encompassed mainly by the Selous Game Reserve, now the Julius Nyerere National Park, established in 1922 (Smith et al., 2016).

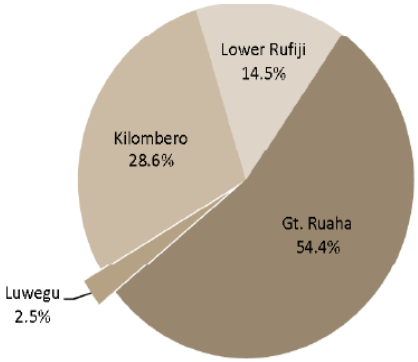

Figure 2.7: Sub-basin Share of Total Basin Population of 3.6 million in 2012 (Source: WREM International 2015; Adapted from Smith et al., 2016)

In contrast to the rest of the country, the Basin's population has been expanding at a moderate rate. In 2012, the annual average population growth was at about 2%. The sub-basins growth rates differ due to variances in, for example, rural-urban migration, adult outmigration, and/or the creation of protected areas such as the Kitulo National Park (Smith, 2016). Because of these disparities in growth rates, the Great Ruaha and Kilombero sub-basins shares of the Rufiji Basin's total population is likely to rise in the future while the Luwegu and Lower Rufiji sub-basins proportion of total population are projected to fall (WREM International, 2015). It is estimated that half of the population living in the Rufiji basin are under the age of 20, with 75% being under the age of 40. The female to male ratio is about equal

while the average household consists of four to five people. Only 28% of the Basin's population reside in urban areas, with the rest living in rural areas (Smith, 2016).

The Rufiji sub-basins are ethnically diverse, with the local tribes comprising of the Hehe, Nyakyusa, Gogo, Pogoro, Wasangu, Wanji, Ndamba, Bena and other small communities. These groups bring traditions and worldviews that have a strong influence on the interaction with rivers and natural resources within their surroundings. The communities within the Rufiji Basin make the most of local resources, focusing primarily on land for agriculture while also utilizing water resources, including fishing and gathering various materials for additional uses when available. However, this intensive resource use can sometimes result in overexploitation, especially as demand grows. In the Lower Rufiji sub-basin, ethnic groups maintain stronger cultural ties with Swahili traditions, reflecting the influence of the delta and coastal regions on their livelihoods and social practices.

2.3.2 Fishing, Crop Cultivation & Livestock Keeping

Historically, the Rufiji is known as 'the land of plenty' (Elton, 1879; cited in Hoag, 2003; Duvail, 2007). The Kilombero valley, the Lower Rufiji freshwater floodplain and the estuarine marine systems of the Rufiji Delta are particularly valuable fishing areas. Fishing is also carried out on the Mtera Reservoir in the Great Ruaha sub-basin.

Small scale fishermen, who frequently utilize sub-par fishing equipment and/or poisoning in some cases, dominate the fishing industry. The estimated 21,000 metric tonnes of fish produced annually in the Basin is about 8% of Tanzania's yearly fish production (Smith et al., 2016). A thriving shrimp, prawn, finfish, crab and gastropod fishing sector is supported by the Rufiji mangrove-estuarine system. The Rufiji delta provides more than 80% of the prawns captured in Tanzania, most of which is exported. In estuary locations, sea grass farming is also conducted (Smith et al., 2016).

The basin provides surpluses that are marketed to surrounding towns including Dar es Salaam, Morogoro and Dodoma. The region serves as a regional food basket for agricultural produce. Rice, maize, round potatoes, beans, groundnuts, cowpeas, sunflower, sesame, pigeon peas, sorghum, millet, wheat, sweet potato, cassava, cashew, tomatoes, onions among other vegetables are some of the major crops farmed in the region. Small-holder farmers dominate agriculture, which is characterized by low inputs and low productivity (Smith et al., 2016).

The Great Ruaha is extensively used for irrigation upstream of the Mtera and Kidatu hydroelectric stations. The Usangu Plains are the primary area for the basin. Maize, beans, rice and vegetables among other crops are grown here, the first two being rain-fed with the latter relying on irrigation methods. The rice paddies are usually grown over an area of 15,000-20,000 hectares (ha) and can be maximized

to an area of about 40,000-55,000 ha, depending on availability of water (Mtahiko et al., 2006; Mwakalila, 2011, SAGCOT, 2013).

Within the Kilombero sub-basin, farming is primarily done in the lower and some higher parts of the flood plain. Although rice and maize are the two major crops grown, a wide variety of plants such as sesame, potatoes, cassava and fruits like bananas, mangoes and oranges are also cultivated. This is done for both food subsistence and for commercially (generally for basic needs i.e., School fees, medication and transportation) (Smith et al., 2016).

Significant agricultural activity is supported by the Lower Rufiji sub-basin, primarily in the Rufiji floodplains and delta. According to recent estimates, 58,500 acres or about 10% of the terrestrial area are used for agricultural purposes (Smith et al., 2016). The most significant crop grown is rice (the staple) and is grown by around 76% of households. The majority of agricultural production is for subsistence, with excesses being sold (Smith et al., 2016).

Historically, there hasn't been much animal production in the Rufiji Basin. Just 10% of the average household's income comes from raising animals (Smith et al., 2016). However, since the 1970's, livestock rearing (especially nomadic pastoralism) has been one of the key issues of natural resources management in the basin. Presently, areas with quite high stocking rates can be found, mainly in the arid central belt, in some areas of Kilombero and more and more in the coastal zones (SAGCOT, 2013). Traditional pastoralist groups that have migrated from other regions of Tanzania raise a substantial share of the cattle in the Basin. The number of indigenous cattle, goats and sheep in the basin is estimated to be around 1.4 million, 670,000, and 420,000 respectively (SAGCOT, 2013)).

With cattle numbers in the hundreds of thousands and numbers of goats, sheep and donkeys in the tens of thousands, the Usanga Plains in the Great Ruaha sub-basin are a significant livestock pastoral area. Water is scarce in the central Usangu Plains during the dry season and pastoralists migrate their herds to the sole permanent water source, the Utengule - Ihefu wetland, further depleting the area's available water resources (SAGCOT, 2013).

Because they are unable to graze their animals in Northern regions of Tanzania, the Barabaig pastoralists, like the Maasai of the Pangani Basin, have pushed away from their original territories that they inhabited since colonial and post-colonial periods, moving into the Lower-Rufiji floodplain in search of grazing lands, a practice occurring since the 1990's. About 4,500 acres of arable farmland have been affected and the antagonism between settled farmers and animal owners in the area has gotten worse (Rufiji District Commission, 2012). The situation was made worse by the preceding five-year drought (2007-2012), which had a negative impact on the traditional pastoralists grazing sites and led to migration into the Lower Rufiji (Smith et al., 2016).

2.3.3 Irrigation and Hydropower

Higher levels of institutional and infrastructural investment are required in areas where rainfall is clearly seasonal and characterized by considerable interannual variability to ensure fundamental water security (Grey & Sadoff, 2007; Siderius et al., 2021). Infrastructure investments for irrigation and hydropower are frequently viewed as essential for socioeconomic development and control of water resources (Hall et al., 2014; Siderius et al., 2021).

Yet in Sub-Saharan Africa such unpredictability is occasionally disregarded in plans for development of surface and groundwater developments, including in commitments made in policy to boost irrigation. In addition, the region also exhibits poor policy coherence when it comes to taking climate change into account in the highly interrelated water, energy and agricultural sectors (Pardoe et al., 2018; England et al., 2018; Siderius et al., 2021).

The largest basin in Tanzania, the Rufiji, provides water to around 4.5million people and produces 80% of Tanzania's hydropower. A majority of the basin is targeted for socioeconomic growth by the government over the next two decades as part of the Southern Agricultural Growth Corridor of Tanzania (SAGCOT) (Paul & Steinbrecher, 2013; Geressu et al., 2020). To promote economic growth, the SAGCOT, which consists of many clusters of focused activity, seeks to increase the domestic and foreign investment in agricultural value chains (Issac & Guyver, 2011; Milder et al., 2021; Geressu et al., 2020). The effort includes greater agricultural productivity, especially through increased irrigation and sustainable water resource management and is seen as essential to its success.

Furthermore, the expansion of energy supply is a critical is a critical component of economic development (Government of Tanzania, 2016), especially in a region where half the population still lacks direct access to electricity (World Bank, 2018; Siderius et al., 2021) and is heavily reliant on hydropower, where hydropower generation produces 40% of Tanzania's electricity (Government of Tanzania, 2016; Hoag, 2013; Siderius et al., 2021)

One of the megaprojects planned in the Basin is the construction of a dam and a hydroelectric plant at Stiegler's Gorge dubbed the Julius Nyerere Hydropower Plant (JNHPP) after Tanzania's founding father. The dam's inception stretches back to colonial times at the beginning of the 20th Century and has become a flagship development project for Tanzania. The Gorge's ravine is projected to house a dam that is 131 meters high and 700 meters wide (Dye, 2019; Odebrecht, 2013). The Rufiji's waters would thus be held back by the dam, creating a reservoir that is projected to be the sixth largest in Africa (Dye, 2019). According to the most recent design, the hydropower plant will be able to generate a maximum output of 2,115 MW, thus making it Africa's largest dam by installed hydropower, alongside Egypt's Aswan High Dam (2100MW), narrowly surpassing Mozambique's Cahora Bassa Dam (2075MW) and

Angola's Lauca Dam (2069MW); or second largest if Ethiopia's Grand Renaissance Dam is finished (Dye, 2019).

The location of the hydropower dam at Stiegler's Gorge within the Selous Game Reserve, now known as Nyerere National Park—a UNESCO World Heritage Site—makes this ambitious engineering project highly contentious. The park is celebrated for its exceptional ecological importance as a region with high biodiversity, distinctive landforms, wildlife and flora and fauna. It boasts a vast flat expanse with fluctuating riverbeds, marshlands and lakes, that extend beyond the reserve to the Rufiji river's delta. The delta is also protected by the Ramsar Convention, a group with the highest international protocol for wetlands. Only two of the Rufiji's tributaries have been dammed as of yet, making this river the last significant river in East Africa that is virtually free flowing (Dye, 2019; 2021).

CHAPTER 3: LITERATURE REVIEW

3.1 What is Drought?

Droughts are natural hazards that can occur anywhere around the world and are not bound to just semi-arid regions. In contrast to aridity, which is characterized by a persistently dry climate and little yearly or seasonal precipitation, drought is a temporary condition. Therefore, with a drought it is anticipated that long term "normal" circumstances will return.

Although many societies around the world recognize and accept the term "drought", no universally agreed quantitative definition of the term exists. A general definition accepted by the United Nation's Convention to Combat Drought and Desertification (UNCCD) states that "A drought is a naturally occurring phenomenon that exists when precipitation has been significantly below normal recorded levels, causing serious hydrological imbalances that adversely affect land resource production systems" (General, U.S., 1994). Other well-known organizations like the FAO describe it as "the percentage of years when crops fail from the lack of moisture" (FAO, 1983), while the IPCC defines it as "a lack of rainfall resulting in water shortages for a particular activity or group" (IPCC, 2007). Perhaps the most straightforward way to define drought is to think of it as a severe lack of precipitation, over an extended period where rain was projected, over a substantial area, affecting soils, the hydrology of the area as well as people's livelihoods.

3.2 Types of droughts

As stated in Wang et al. (2016), a drought results from a lack of precipitation over a lengthy period, which causes a shortage of water for a particular activity, population, or area of the environment. This results in a complex interaction between (1) natural precipitation deficiencies or excessive evaporation over different spatial and temporal extents and (2) the water needs of humans and the environment, which may be made worse by ineffective water management, planning and delivery.

Depending on the many aspects of the hydrological cycle that are impacted by a drought occurrence, numerous operational drought concepts are put into practice. Operational drought definitions attempt to pinpoint the onset, duration and impact of a drought as well as the afflicted sector, procedure or social group (Wilhite, 2000; Wang et al. 2016). Droughts are therefore categorized into 4 main classes, (1) meteorological, (2) agricultural, (3) hydrological and (4) socio-economical (Mishra & Singh, 2010; Wilhite & Glantz, 1985; Wang et al., 2016). Generally, all droughts start off with a deficiency in precipitation, usually accompanied by high temperatures, leading to increased rates of evaporation, strong winds and less cloud cover. This in-turn leads to reduced infiltration and therefore the propagation of other types of droughts as explained in Figure 3.1 below:

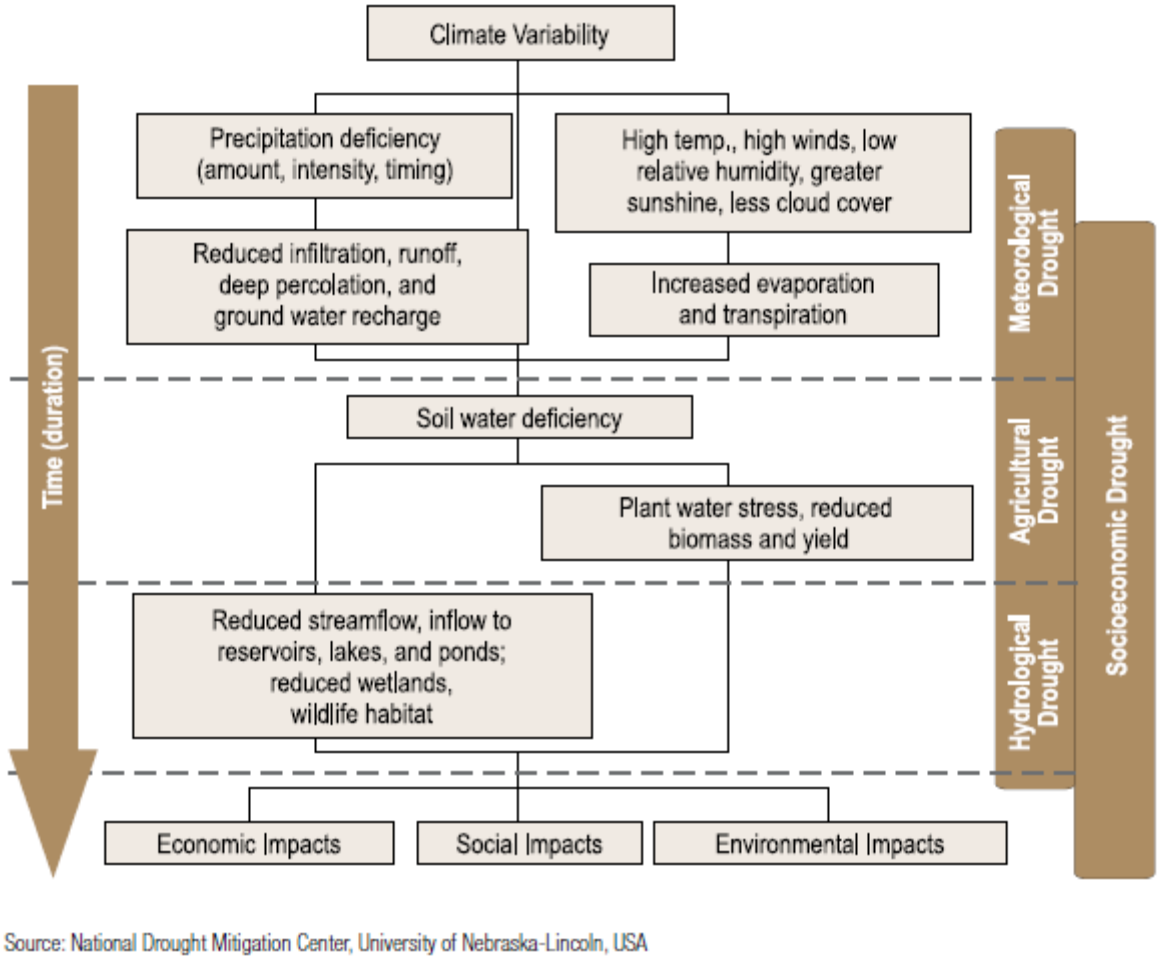

Figure 3.1: Relationship between meteorological, agricultural, hydrological & socio-economic drought

3.2.1 Meteorological drought

A meteorological drought is the degree of precipitation deficit from a pre-determined threshold which is generally a long-term average (Gibbs, 1975; Dai, 2011). Meteorological drought analysis makes use of precipitation patterns within the given area for comparison (Pinkeye, 1966; Chang 199; Mishra et al, 2010). However, there could be varying atmospheric circulations within a study area, therefore precipitation thresholds should be region specific (Nguvava, 2020). Generally, precipitation is the main predictor of water availability. A fall in precipitation levels is normally accompanied by decreased cloudiness and relative humidity levels, leading to increased temperatures and evaporation levels resulting in reduced infiltration, percolation, runoff and ground-water recharge.

Changes in large scale atmospheric circulation patterns are the primary causes of meteorological dryness, which are frequently induced by variations in tropical sea surface temperatures (SST) or other remote factors (Giannini et al., 2003; Hoerling et al., 2006).

3.2.2 Agricultural Drought

A period of soil moisture deficit is known as Agricultural Drought and is brought on by below average precipitation, above normal evapotranspiration, elevated temperatures and continuous wind (Mishra & Singh, 2010). The drought can be exacerbated by the impacts humans have on the quality of the soil, where factors such as erosion and slope can affect infiltration rates (Wilhite & Glantz, 1985). Plant growth is affected as a result and agricultural output is diminished. Due to the variability in demands for water in different plants, each plant has varying water requirements. This can result in massive crop failures and subsequent livestock losses leading to impacts such as famine and malnutrition (Rojas et al., 2011). This type of drought typically comes before a hydrological drought (Nguvava et al., 2019).

3.2.3 Hydrological Drought

When water shortages in rivers, lakes, reservoirs and aquifers fall below long-term average levels, a hydrological drought occurs (Wilhite, 2005). Hydrological droughts often follow meteorological and agriculture droughts because the effects of precipitation shortages take longer to manifest. It usually has a direct impact on hydropower generation leading to power outages, loadshedding and dam operation problems (Calzi, 2013).

Water borne diseases such as cholera, diarrhoea and tuberculosis could result from this type of drought, directly impacting the quality and availability of water for home and industrial use (Jain et al., 2015). Hydrological droughts are frequently brought on by changes in climatic conditions but can be worsened by other elements such as poor water management, changing land uses and land degradation. For example, during the Great Ruaha's dry season, overgrazing and increased agricultural activity in the Rufiji's Ihefu basin jeopardized the environment of Ruaha National Park (Mwakalila, 2011).

3.2.4 Socio-Economic Drought

A socio-economic drought is one that continues during and that can last long after a meteorological, agricultural and hydrological drought has ended and has an impact on people and the economy. This usually occurs when there is a surplus demand for economic resources and outweighs the weather-related deficit in the supply of water (Dracup et al., 1980; Mishra & Singh, 2010). Drought is the most

widespread natural disaster in Africa. However, less than 20% of the disasters on the continent involve drought, yet more than 80% its population is affected by it (See Figure 3.2).

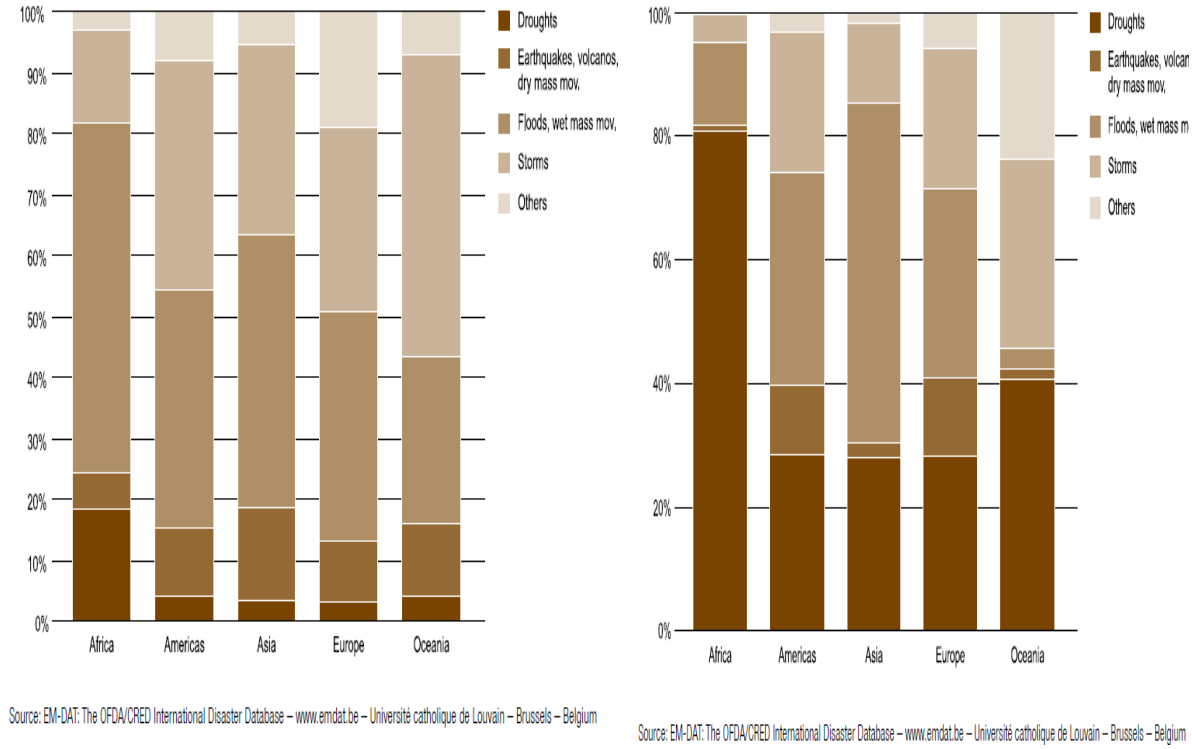

Figure 3.2: Proportion of natural disaster occurrence by continent 1970-2008 (left); Proportion of people affected by each disaster type per continent 1970-2008 (right) (Source: UNISDR, 2019)

More than 300 million people have been impacted by 291 drought events that have occurred in Africa between 1900 and 2013 (Masih et al., 2014). Disasters caused by drought are more common in some regions than other, and each country's capacity to cope with their repercussions differ. Despite suffering significant economic losses, first world countries have the ability to reduce the effects of drought on human mortality. This is not the case for many developing and impoverished African nations where drought seriously impedes a nation's economic development leading to emigration, famine and death (Makhanya, 2021). From the Figure below you can see that Tanzania is affected by drought events and has a high vulnerability to future droughts.

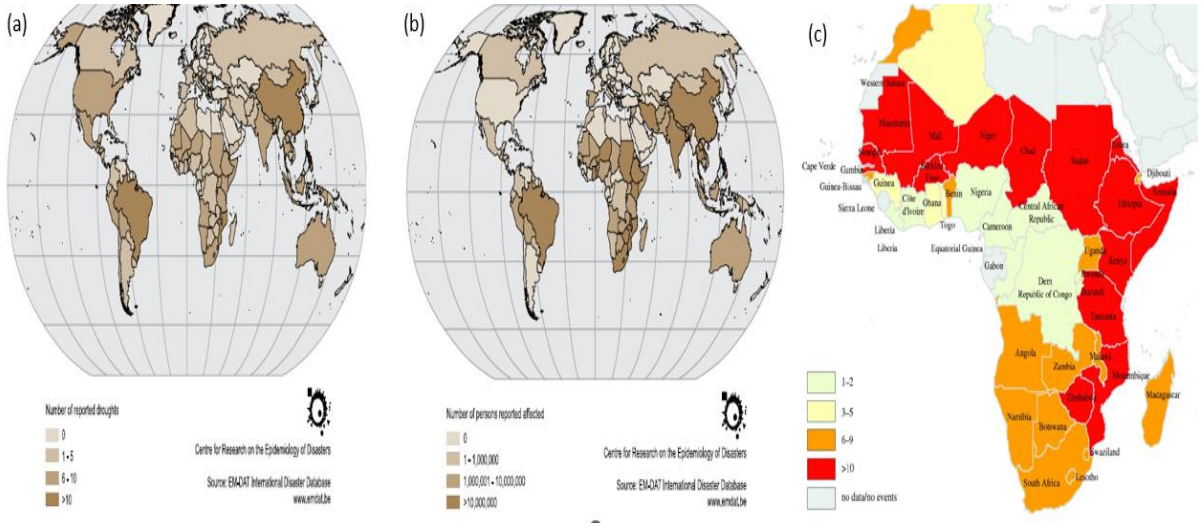

Figure 3.3: (a) number of reported droughts by country 1970-2008, (b) number of persons affected by drought 1970-2008, (c) map of Africa showing drought vulnerability 1970-2004. Source: (UNISDR, 2009; Haile, 2005)

In 2011, drought led to a significant reduction in Tanzania's energy supply, primarily due to decreased hydroelectric generation caused by lower precipitation levels. This shortfall placed increased strain on industrial operations requiring a steady power supply, thereby affecting multiple sectors of the economy (Nguvava, 2020).

3.3 Drought Quantification

Research on drought monitoring faces a significant problem in determining the best index to describe or measure droughts (Ujeneza & Abiodun, 2014). Drought severity must be assessed using an index or indices that (a) are easily understood, (b) carry physical meaning, (c) are responsive to a wide range of drought conditions, (d) are unaffected by the area of application, (e) reveal drought with a short lag after its onset, and (f) are based on readily available data.

To characterize the many types of droughts (such as meteorological, agricultural, and hydrological), various drought indicators have been developed, however their effectiveness varies across different geographic regions (Heim, 2002; Mishra & Singh, 2010).

3.3.1 Meteorological Drought Indices

Many drought indices exist that aim to explain drought events such as the Palmer Drought Severity index (PDSI) (Palmer, 1965), the Standard Precipitation Index (SPI) (McKee et al., 1993), the Bhalme-Mooley Index (BMI) (Bhalme & Mooley, 1979), and the Standardized Precipitation Evapotranspiration Index (SPEI) (Vicente-Serrano et al., 2010a). While none of the drought indices are inherently better than the others, some are more appropriate for describing drought under particular circumstances.

One of the first attempts to identify droughts using information other than precipitation data was made by Palmer (1965), who created the PDSI. A soil water balance equation is used to generate this drought index, which also includes information on temperature, precipitation, and soil moisture to determine the supply and demand for moisture (Mishra & Singh, 2010; Vicente-Serrano et al., 2010a). As a result, PDSI serves as an effective tool in studies of climate change because it considers sensitivities to both precipitation and temperature (Mishra & Singh, 2010).

Despite this fact, PDSI is complex in its equations and variables used (Ntale & Gan, 2003) and several studies (Alley, 1984; Guttman, 1991; Guttman et al., 1992; McKee et al., 1995) documented the limitations of PDSI, which prompted the creation of substitute indices. Palmer (1965) created the crop moisture index (CMI) (Palmer, 1968), the hydrological drought index (PHDI), and the soil moisture drought index (Z-index) to overcome some of the PDSI's inadequacies. However over recent years the index is not used as frequently owing to its complexity and lacking multi-timescale capabilities. Below is a concise description of the utilized indices within this study:

3.3.1.1 Standardized Precipitation Index (SPI)

Due to its ability to categorize various types of droughts, the SPI (multi-scale drought index; developed by McKee et al., 1993) has grown in popularity among researchers. The WMO has recommended it as the best approach to characterise meteorological droughts (Hayes et al., 2011; Keyantash, 2022). SPI can track both rainy and dry events at various timescales and is solely dependent on precipitation amounts. The Standardized Precipitation Index (SPI) works by standardizing precipitation data over specified timescales, which allows for the monitoring of both wet and dry periods. By using different timescales (e.g., 3, 6, 12, or 24 months), SPI captures various drought impacts across multiple sectors; shorter timescales (e.g., 3 months) reflect meteorological drought conditions, while longer timescales (e.g., 12 or 24 months) can provide insights into hydrological drought impacts on streamflow and groundwater levels (Belayneh et al., 2014; Bernard et al., 2013; Degefu & Bewket, 2014; Vicente-Serrano et al., 2012b). SPI works by fitting these accumulating precipitation data to a parametric statistical distribution, from which non-exceedence probability are translated to the conventional normal distribution (mean= 0, standard dev. = 1).

At a 3-month timestep, SPI has been useful in illustrating meteorological droughts, SPI-6 is highly associated with an agricultural drought indicator (as a decline in precipitation would eventually lead to decreasing soil moistures), whereas SPI-12 and SPI-24 can detect hydrological droughts as the decrease in available water would most likely manifest declines in streamflow, reservoir storages and groundwater levels.

The SPI addresses the severity of meteorological drought, or shortfall of precipitation. A simple, obvious indicator for drought—possibly the most basic definition conceivable—is the lack of precipitation. Interpreting the severity of the precipitation deficit can be difficult though, due to the wide variations in precipitation climatology across geographic regions and temporal scales. For instance, should a month be classified as drought if it occurs during a prolonged stretch of extremely dry weather? Additionally, the magnitude of the precipitation deficiency or excess should be assessed in relation to a local climatological norm. Therefore, the difficulty in defining a drought is not in the direct measurement of hydrometeorological data, but rather in the objective evaluation of the findings.

An established timescale serves as an indication of the prevailing conditions within the specified period compared to all previous years. Consequently, users of the index have the flexibility to set the timescale based on their preferences and the specific time of year they are examining. The SPI can be calculated for periods ranging from 1 month to 72 months. According to Guttmann (1999), the optimal practical application window is between 1 and 24 months. Based on Guttman's suggestion to have about 50–60 years of running data accessible to calculate SPI, this 24-month limit was established. As the sample size gets smaller, the statistical confidence of the probability estimated on the tails (both wet and dry extremes) weakens, especially after 24 months, unless one has 80–100 years of data. The WMO recommends utilizing a reference period of at least 30 years of precipitation totals when calculating the Standardized Precipitation Index (SPI) to ensure accurate and meaningful results.

Table 3.1: Advantages and Disadvantages of various SPI timescales

TIMEFRAME	**ADVANTAGES**	**DISADVANTAGES**
SPI-1	- Can be related closely to meteorological types of droughts along with short-term soil moisture and crop stress, especially during the growing season.	- In regions where rainfall is normally low during a month, large negative or positive SPIs may result even though the departure from the mean is relatively small
SPI-3	- Can act a better indicator of available moisture conditions than the sluggish Palmer Index or other hydrological indices available, especially at the start of growing seasons	- It's crucial to evaluate the 3-month SPI against longer timeframes, as it may lead to a misinterpretation, for example one may assume a drought is over just because of a temporary wet period - May be misleading in regions where very little rain falls or is projected over distinct periods of the year, thereby giving large negative or positive SPIs with precipitation totals not very different from the mean

SPI-6	- Can be very effective in showing the precipitation over distinct season eg: a 6-month SPI over the Rufiji Basin from November to April would give a fairly accurate representation of the amount of precipitation that has fallen during the crucial rainy season	- Might not be very suitable for portraying short events such as flash floods as drier months in the period may level out the mean. - Does not consider yearly variability in a basin.
SPI-9	- SPI values below -1.5 for these durations are often indicative of major effects of dryness on agriculture and maybe other sectors - This time span begins to bridge the gap between short-term seasonal droughts and longer-term droughts that may become hydrological, or multi-year, in nature	- Same as for SPI-6
SPI-12 & ABOVE	- A 12-month SPI is a useful tool for comparing precipitation over 12 consecutive months to precipitation over the same 12 consecutive months in all previously available data years - SPIs for these periods are typically linked to streamflows, reservoir levels, and even groundwater levels at longer timescales.	- Because lengthy durations represent the sum of shorter periods that may be above or below normal, the longer SPIs tend to lean toward zero unless there is a strong wet or dry trend.
OVERALL SPI	- It can be computed over a variety of timescales - Shorter period SPIs, such as 1-, 2-, or 3-month SPIs, can provide early warning of drought and aid in determining drought severity. - It is spatially consistent, allowing comparisons between different locations with various climatic conditions - Given that it is probabilistic, it has historical context, which is ideal for decision-making	- It solely takes precipitation into account - The SPI is merely a measure of water supply, therefore its capacity to reflect the impact of rising temperatures (related with climate change) on moisture demand and availability is constrained - Sensitive to the volume and dependability of the data used to fit the distribution; optimal age range is 30–50 years - Does not consider intensity of precipitation or how it might affect the system of interest's runoff, streamflow, and availability of water.

To calculate the SPI, a probability density function must be fitted to a frequency distribution of the total amount of precipitation for a station or grid point over an accumulation period. The frequency distribution statistics are computed ideally using a reference period of at least 30 years. The WMO strongly advises choosing the period from 1991 to 2020 as the SPI Reference Period as it reflects the prevailing climatic conditions of any area. The parameters of the probability density function are then

used to calculate the cumulative probability of observed precipitation for the given month and time period. The cumulative probability is then transformed to a standardised normal distribution with mean zero and variance one, yielding the SPI value.

McKee et al., (1993) defined drought intensities based on the SPI using the classification scheme presented in the SPI value table below (Figure 3.5). They also proposed SPI-based definitions for drought occurrences at any timeline. A drought event occurs when the SPI is constantly negative and reaches -1.0 or less. When the SPI reaches positive values, the drought event comes to an end. As a result, each drought event has a duration defined by its commencement and termination, as well as an intensity (-1, -2... etc) for every month within the specified calculation. The "magnitude" of a drought event is defined as the positive total of the SPI for all the months during the drought episode.

2.0+	extremely wet
1.5 to 1.99	very wet
1.0 to 1.49	moderately wet
-.99 to .99	near normal
-1.0 to -1.49	moderately dry
-1.5 to -1.99	severely dry
-2 and less	extremely dry

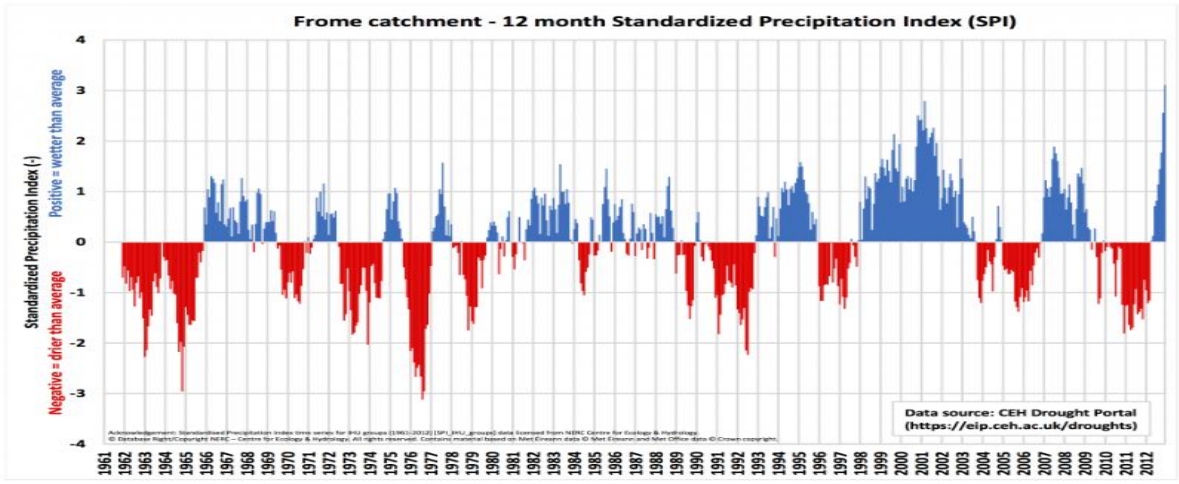

Figure 3.4: Classification and Sample SPI graph

In Eastern Africa and Rufiji Basin, SPI has been used in several studies. Ntale & Gan (2003) made use of various drought indices (improved versions of the PDSI & SPI, as well as BMI) to monitor droughts over Eastern Africa. Among the three indices used they found that the SPI was better suited to monitoring East African droughts as it more easily adapted to local climate, had low data requirements,

could be computed at almost any time scale, had no theoretical upper or lower bounds and was simple to interpret.

Pauline & Grab (2017) investigated the onset of rainy days and Standardized Precipitation Index (SPI) trends from 1960 to 2014 at three meteorological stations— Igawa, Iringa, and Mtera—located in the Great Ruaha sub-basin, the most extensive of the Rufiji River Basin's four sub-basins. Their research revealed a progressive delay in the rainfall onset in Igawa and Mtera, aligning with findings from similar studies in southern Africa that observed delays in the rainy season's start, extended drought periods, and shortened rainy seasons (Twomlow et al., 2008; Shongwe et al., 2011). In contrast, the Iringa station recorded an earlier onset of rainfall, differing from the patterns observed at the other two stations. This discrepancy suggests that while Igawa and Mtera are becoming increasingly susceptible to delayed rainfall and drought conditions, Iringa may experience a more favorable hydrological regime (Pauline & Grab, 2017). The analysis showed significant interannual and decadal rainfall variability, with a consistent drying trend post-2000, particularly at the Mtera station, which experienced numerous drought years. While the Igawa station recorded three drought occurrences in the 2000s, with some exceeding a -2 SPI level and one surpassing -2.5, the Iringa station documented two drought years between 2009 and 2011 that exceeded a -3 SPI level, reaching -5, indicating an exacerbation of drought conditions in recent decades.

3.3.1.2 Standardized Precipitation Evaporation Index (SPEI)

The Standardized Precipitation Evaporation Index (SPEI) was created by Vicente-Serrano et al. (2010) and serves as an extension of the WMO's recommended SPI and because it employs a more comprehensive estimate of water availability, thus has tremendous potential as a meteorological drought index (Stagge et al., 2014). Unlike the SPI which assumes that droughts are primarily governed by the temporal variability of precipitation and that this variation is much more important than other climatic variables (such as evaporative demand of the atmosphere), the SPEI integrates evapotranspiration rates which allows drought situations to be analyzed based on fluctuations in the water balance (Vicente-Serrano et al., 2010). The SPEI is an improved alternative to the SPI given that global temperatures have been on the rise over the last 150 years and climate change models predicting a significant increase over the twenty-first century, it is reasonable to believe that temperature rise will have major effects on drought conditions.

SPEI quantifies the dry and wet conditions at various time frames, much like SPI on the same timescales such as the 1-,3-,6-,9-, 12- and 24- month periods. The scale used to quantify the drought and wet events is also similar with positive values indicating wet events and negative values indicating drier periods. The intensity, frequency and magnitude of events have the same calculation as the SPI. Where the SPEI differs is in its calculation of the climatic water balance, which is the difference between precipitation

and Potential Evaporation (PET) (Vicente-Serrano et al., 2010). SPEI is more complicated than SPI since it considers a variety of other factors, including temperature, sun radiation, relative humidity, and wind speed depending on the PET calculation used (Stagge et al., 2014).

The inclusion of PET (McMahon et al., 2013) can be implemented using various equations, depending on data availability. Some of the PET methods that can be employed, in order of increasing complexity, include Thornthwaite (Thornthwaite, 1948), Hargreaves (Hargreaves & Samani, 1985), Penman-Montieth with the Hargreaves radiation term (Allen et al., 1998), Priestley-Taylor (Priestley & Taylor, 1972), and FAO-56 Penman-Montieth (Allen et al., 1998). In the original calculations of the SPEI, Vicente Serrano et al. (2010) utilized the Hargreaves method for calculating PET due to its reduced data input requirements and simplicity. The Hargreaves equation only requires the site's latitude and mean daily temperature on a monthly scale. However, employing a specific equation to estimate PET is not essential for calculating SPEI, as alternative equations can also be used depending on data availability. If comprehensive data are accessible (such as relative humidity, temperature, wind speed, and solar radiation), the FAO-56 Penman-Monteith equation (Allen et al., 1998) is recommended (Vicente Serrano, 2014). If the data required for PET computation are limited, the Hargreaves equation (preferred) or the Thornthwaite equation (alternative) are suggested. In some parts of the world, differences between the SPEI series derived using the various ETo equations can be substantial. According to Beguera et al. (2014), these disparities were often greater in semi-arid to mesic zones and smaller in humid ones.

In general, the SPEI's low data requirements, ease of use, flexibility, and consideration of the two primary factors that affect drought severity (precipitation and atmospheric evaporative demand) are strong arguments for advising using it in place of other drought indices. Beyond the context of global warming, the SPEI can consider the potential effects of temperature variability and temperature extremes. Its few shortcomings are the extra data requirements compared to the SPI; sensitivity of the method used to calculate PET as well as the long base period (30-50 years) for data inputs.

3.3.2 Hydrological Drought Indices

The term "hydrological drought" refers to a considerable decline in the availability of water resources in all of its forms in the terrestrial phase of the hydrological cycle. Various hydrological variables, such as streamflow (including snowmelt and springflow), lake and reservoir level, and groundwater level, reflect these forms. Streamflow is by far the most important variable in terms of quantity of water among these variables. It is the primary variable used to express surface water resources.

There are several different indices for describing hydrological drought, however most of the older methods required much data and processing power. On the other hand, straightforward and useful

indices, alike to the Standardized Precipitation Index (SPI), have been employed to measure meteorological droughts. According to earlier studies, hydrological droughts can be analyzed using the runs method (Yevjevich, 1967) or through a standardized indices approach. Yevjevich (1967) used the threshold technique to define a drought event as a time period in which the hydrological variable (such as streamflow, groundwater flow, or reservoir storage) is below the predefined truncation level. However, Yevjevich's method did not standardize flows which lead to it not being able to be used to show magnitudes of droughts (Van Loon, 2015). To eliminate major discrepancies among climate types and compare global drought studies, standardization is essential (Van Loon, 2015). Using standardized indices, drought intensity can be evaluated over time and geography, including comparisons between basins with differing regime characteristics, flow variability, and flow amplitude (Vicente- Serrano et al., 2012a).

The Standardized Runoff Index (SRI) (Shukla & Wood, 2008) and the Standardized Streamflow Index (SSFI) (Moddares, 2007) are both hydrological indicators that employ McKee's (1993) SPI concept. The SSFI measures monthly normalized anomalies in observed or simulated streamflow, whereas the SRI measures anomalies in modelled runoff per unit area.The Surface Water Supply Index (SWSI) (Shafer & Dezman, 1982) and the Palmer Hydrological Drought Index (PHDI) (Palmer, 1965), are two existing indices for describing a hydrological drought, but are often data and computationally intensive.

All in all, a hydrological drought episode is associated with a decrease in streamflow relative to normal conditions. Each drought event is distinguished by four characteristics: (1) its level of severity as measured by a drought index, (2) its beginnings and length, (3) its geographical extent, and (4) its regularity of occurrence.

3.3.2.1 Streamflow Drought Index (SDI)

Nalbantis &Tsakiris (2009) formulated the Streamflow Drought index (SDI), to assess and evaluate hydrological droughts. The reason for coming up with the index was to circumvent the use of existing hydrological drought indices that were data and computationally intensive. Like the SRI and SSFI, the SDI is built on the same principal of the SPI index, albeit considering monthly streamflow means rather than precipitation. Nablantis & Tsakaris (2009) showed the index has a close correlation to SPI in the longer term over 6 months when applied to a river basin located in the West Sterea Hellas Water District in central Greece and can be used in conjunction with SPI as a predictor of hydrological droughts.

Like the SPI and SPEI indices, the SDI can be used on diverse timescales of 1-, 3-, 6-, 9-, 12-, 24- and 48 months to assess drought conditions over a specific location. The start of the calculation of the index should coincide with the start of the hydrological year in the basin. Therefore, for measurements on the Rufiji, the index would start in November, when the short rains begin to fall over the basin. For

assessment of short-lived droughts and to assess reduced flow in rainier months, a 3- month SDI is prescribed. To comprehensively evaluate and understand the hydrological variability of a basin, it is advisable to extend the analysis to include a 12-month Standardized Drought Index (SDI) calculation. This is because it considers both the wetter and drier months and can therefore show annual variability of the basin.

Like the SPI and the SPEI, the SDI uses the same methodology of calculation of the index, using streamflow values over the calculation and time-period, whereas the SPI and SPEI would use precipitation and PET as inputs. The index uses the same technique as the SPI/SPEI where a probability density function must be fitted to a frequency distribution of the total amount of precipitation for a station over an accumulation period. The frequency distribution statistics are computed using a reference period of at least 30 years. SDI employs the same scale as the SPI to assess drought conditions, with Figures in the negative exhibiting drier episodes whereas wetter months are denoted by positive values (Nablantis & Tsakaris, 2009).

3.4 Climate and Hydrological Modelling Frameworks and tools

3.4.1 Climate Modelling

3.4.1.1 Reanalysis models

Climate data reanalysis is a scientific method used to create a comprehensive picture of the climate system's past state. This is achieved by combining past observations with modern weather forecast models. The process involves assimilating data from various sources, such as satellites, weather balloons, buoys, and surface weather stations, into a consistent, gridded dataset that represents the state of the Earth's atmosphere, land surface, and oceans over time. Reanalysis projects use advanced data assimilation techniques and computational resources to blend historical data with models, aiming to produce a more accurate and complete representation of past weather and climate conditions (Thejll & Gleisner, 2015; ECMWF, 2023).

The availability of reanalysis datasets, while currently limited in scope, is gradually expanding. These datasets, which are widely utilized within the scientific community, predominantly encompass global atmospheric data. However, the range of reanalysis extends beyond the atmosphere, with specialized datasets also existing for oceanic and terrestrial surface analyses. This diversification reflects the growing interest and technological advancement in comprehensively understanding different components of the Earth's climate system (Gleixner et al., 2020).

Two notable reanalysis models are the ERA-Interim and ERA5, both of which are among the latest reanalysis products developed by the European Centre for Medium-Range Weather Forecasts (ECMWF). These products are created by integrating a numerical weather prediction model with observational data gathered from satellites and ground observations. Introduced in 2007, ERA-interim delivered daily climate information until August 2019. It was then succeeded by ERA5, which has been providing hourly meteorological conditions dating back to 1979 and is anticipated to extend its coverage back to 1950 (Gleixner et al., 2020).

3.4.1.2 Climate projections

Global climate models (GCM) and regional climate models (RCM) are the most often utilized dynamic models for climate studies across the scientific community (IPCC, 2007; IPCC, 2014). GCMs have been proven to be effective in furthering our understanding of the dynamic mechanisms regulating climatic variability, and several studies have shown that GCMs can mimic observed or projected drought patterns with great precision (Cook & Vizy, 2012; Shongwe et al., 2011). However, certain studies have assessed that General Circulation Models (GCMs) with coarse resolutions (grid cells of 200-300 km) may lack the capability to capture the influences of local forcing, including terrain and vegetation effects, as well as the land-sea boundary. These aspects are better represented at finer scales (Wang et al., 2004). Additionally, extreme events, such as heavy precipitation, are often not adequately captured or their intensity is unrealistically low at coarse resolutions, as indicated by various studies (e.g., Endris et al., 2015). However, this limitation can be addressed by downscaling GCM models to finer resolutions using Regional Climate Models (RCMs) (Nguvava, 2020).

The GCMs (Global Climate Models) used in the study were part of the Coupled Model Intercomparison Project Phase 5 (CMIP5), an international initiative coordinated by the World Climate Research Programme. CMIP5 serves as a platform for comparing different climate models to understand their strengths and weaknesses, thereby improving their accuracy and reliability. It involves a set of standardized experiments conducted by climate modelling groups worldwide, focusing on both historical climate assessment and future climate projections. The historical simulations enable researchers to test the models against observed climate data, while future projections are based on Representative Concentration Pathways (RCPs) that outline various scenarios of greenhouse gas concentrations and radiative forcing (Taylor et al., 2012).

CMIP5 models has been instrumental in advancing climate science, contributing significantly to research and policy-making, especially in the context of the Intergovernmental Panel on Climate Change (IPCC) reports. The project fosters global collaboration, bringing together a multitude of scientists and research institutes to pool expertise and resources. The publicly available data from CMIP5 simulations is extensively used for various studies, including analyzing regional climate

impacts, extreme events, and long-term climate changes. This collaborative effort and data availability make CMIP5 a cornerstone in understanding and addressing global climate dynamics (Taylor et al., 2012).

CMIP5 includes four Representative Concentration Pathways (RCPs) that are differentiated by their radiative forcing levels by the year 2100: RCP2.6, RCP4.5, RCP6.0, and RCP8.5. These range from low (RCP2.6) to high (RCP8.5) greenhouse gas concentration scenarios. While CMIP5 provided critical insights into potential climate futures, it was limited by its reliance on radiative forcing metrics alone, which did not fully account for the socioeconomic contexts influencing emissions trajectories (Eyring et al., 2016; Hausfather, 2019).

In contrast, the sixth phase of the project, CMIP6, launched in 2019, marked a significant evolution in climate scenario development. CMIP6 introduced Shared Socioeconomic Pathways (SSPs) that integrate greenhouse gas emissions pathways with socioeconomic narratives, allowing for a richer and more nuanced exploration of potential climate futures. This innovative approach not only addresses the limitations of the RCPs from CMIP5 but also enhances the realism of "business-as-usual" scenarios by considering diverse socioeconomic factors, such as population growth, economic development, and technological advancements. By combining SSPs with traditional RCPs, CMIP6 offers a more comprehensive framework for understanding the multifaceted interactions between climate change and human systems, thereby improving the relevance of climate projections for policymakers and stakeholders (Eyring et al., 2016; CMIP6, 2019).

However, CMIP6 data was not used as part of this study as it has not yet been downscaled by the Coordinated Regional Climate Downscaling Experiment (CORDEX). Moreover, in their study, Ayugi et al., 2021, highlight that CMIP6 models have not been utilized in the East African region. They note that these latest GCM models, like their predecessors, have challenges in accurately simulating extreme events and tend to overestimate OND (October-November-December) rainfall peaks within the region. This persistent uncertainty affects stakeholders, including policymakers and climate information users, as it limits reliable future climate projections for OND rainfall. The study emphasizes the need for further research to understand and address these systematic biases and calls for careful assessment studies to identify models that can more accurately simulate observed patterns in East Africa.

Downscaling of GCM projections can be done via two methods: Statistically and Dynamically (Hewitson, 2013). The link between regional and/or local physiographic traits, such as land-sea distribution and topography, and the large-scale climatic state is the foundation of statistical downscaling. GCMs provide the large-scale features while the small-scale features are taken from specific grid points or meteorological stations. The first strategy is to develop a statistical model that explains the relationship between global-scale climatic variables (also known as "predictors") and regional or local variables (also known as "predictands"). The output is then passed into established

statistical models and the estimation of local/regional climatic variables is made. Due to their relative simplicity and lower processing cost compared to dynamical downscaling approaches, statistical downscaling methods are widely used. However, this method's primary flaw is that the statistical associations of the past climate will remain unchanged for the predicted future climate (Nguvava, 2020).

Dynamical downscaling involves the nesting of high-resolution RCMs within a coarse GCM simulation (Giorgi & Mearns, 1999). Small-scale characteristics like topography and land use that may have an impact on climatological variables like precipitation and wind can be incorporated because of the high horizontal resolution of RCMs (usually less than 50 km) (Nguvava, 2020). Herrmann and Mohr (2011) stated that higher resolution simulations are the optimum method for any future projection over the region due to the intricacy of the geography over eastern Africa.

The World Climate Research Program (WRCP) initiated the CORDEX program to provide low-scale climate modelling products for historical and future decades (Jones, 2011). The CORDEX-Africa project was established to generate high-quality multi-model climate change simulations, specifically for researching the impacts and adaptation to climate change in Africa (Haensler et al., 2013; Kim et al., 2014; Dosio & Panitz, 2016; Dosio, 2017). Regional Climate Models (RCMs) with a spatial resolution of about 10 - 50 km^2 have facilitated downscaled analyses of changing temperatures and droughts, aligning with the scale at which water resources are managed (Nikulin et al., 2012).

The CORDEX ensemble has been extensively applied in various studies in Eastern Africa to assess the models' ability to capture both geographical and temporal climate variability and to predict future climatic conditions in the region. For example, Endris et al. (2013) demonstrated that the majority of CORDEX Regional Climate Models (RCMs) accurately simulate eastern African rainfall characteristics. While most observed regional response to ENSO and Indian Ocean Dipole (IOD) forcings were reproduced, they noted biases in some models depending on the region and thus recommended using the ensemble mean.

On a regional level, Nguvava (2020) integrated outputs from the Coordinated Regional Climate Downscaling Experiment (CORDEX) into the Soil and Water Assessment Tool (SWAT) to analyse the potential impacts of climate and land use changes on water availability in the Rufiji Basin, with a focus on hydrological droughts within the basin. At the sub-basin level, Naschen et al. (2018) also used the SWAT model and CORDEX output to study the water balance and land use change in the Kilombero basin. Their study revealed that the basin is significantly influenced by land use change, with potential exacerbation by future climate change.

Mutaboya et al. (2018) employed high-resolution CORDEX climate simulations to assess the potentia effects of climate change on water resources in the Mbarali River sub-catchment within the Great Ruaha sub-basin of the Rufiji River Basin. The findings indicated that the four main factors determining

changes in the catchment water balance—rainfall, groundwater recharge, evaporation, and surface runoff—are projected to increase in the future under both RCP 4.5 and RCP 8.5 emission scenarios. While stream flows are projected to decrease by 13.33% under RCP 4.5 and 13.67% under RCP 8.5 emission scenarios, it is noteworthy that modelled surface runoff under RCP 8.5 is higher than predicted under RCP 4.5.

To project future hydro-meteorological droughts, various studies have utilized Global Climate Models (GCMs) downscaled outputs, hydrological models, and drought indices as key tools (Wanders et al., 2015; Tan et al., 2020). These investigations convert hydro-meteorological variables into drought indices to assess drought characteristics, including frequency, magnitude, and intensity.

3.4.3 Hydrological Modelling

The hydrological cycle comprises several interconnected components, and runoff plays a crucial role in linking precipitation to streamflow. Surface runoff modelling is employed to enhance the understanding of watershed yields and responses, evaluate water availability, and project changes over time (Vaze, 2012). A model, as defined by Sorooshian et al. (2008), serves as a simplified representation of a real-world system. The effectiveness of a model is determined by its ability to produce outcomes close to reality while utilizing the fewest parameters and maintaining model simplicity. Key inputs for all models include rainfall data and drainage area. Additionally, watershed factors such as soil characteristics, plant cover, terrain, soil moisture levels, and subsurface aquifer characteristics are often considered. Hydrological models are increasingly recognized as essential and vital tools for the effective management of water and environmental resources (Devia et al., 2015).

Previous global studies underscore the importance of evaluating hydro-climatic extremes, such as drought, in order to better understand the risks related to water resource management (Tan et al., 2020). Long-term observational data serve as the most reliable source for understanding the hydro-climate system and are crucial for monitoring drought (Tan et al., 2020). However, in poorly assessed regions like Eastern Africa, the precision and accessibility of observational data are limited. Additionally, certain hydrological variables may not be recorded, exhibit poor data consistency, or have observations influenced by human activity.

Hydrological models offer a valuable means to extend data series, fill data gaps, and restore interrupted time series to their natural state (Van Loon, 2015). The use of models is essential in compensating for the limitations of observational data. Given their capacity to forecast system behaviour, employing hydrological models to understand the connection between hydrological processes and environmental challenges has become common practice. The adaptability of models to a wide range of basin sizes and environmental factors further enhances their utility (Tan et al., 2020). Therefore, hydrological

modelling proves to be a useful technique for assessing how climate change may impact the availability of water resources.

Various theories have been proposed for categorizing hydrological models, with some focusing on how watershed processes are modelled (deterministic or stochastic) while other models may focus on the spatial distribution of input parameters (Refsgaard, 1996). Models can be further classified into empirical, conceptual, or physically based models.

1. **Empirical Models:**
    - *Description:* Empirical models are simple "black box" models that prioritize input precision over catchment dynamics. They rely solely on available data without considering the characteristics of the hydrological system.
    - *Use:* Limited to observation-oriented tasks and not suitable for modelling flow variations in a catchment.
    - *Example:* Unit hydrograph.
2. **Conceptual Models:**
    - *Description:* Conceptual models describe all constituent hydrological processes using interconnected reservoirs. These models represent the physical components of a watershed, with parameters evaluated through calibration and field data.
    - *Use:* Semi-empirical equations, calibration requires a large amount of meteorological and hydrological records.
    - *Examples:* TOPMODEL (Beven & Kirkby, 1979), HBV (Bergström, 1992).
3. **Physical Models (Dynamical Models or Mechanistic Models):**
    - *Description:* Physical models are idealized mathematical representations of actual phenomena, incorporating the fundamentals of physical processes. They employ measurable state variables that are both time- and space-dependent.
    - *Use:* Requires less hydrological and meteorological data for calibration, but a comprehensive assessment of catchment physical characteristics is needed.
    - *Examples:* MIKE SHE (Abbott et al., 1986), SWAT (Arnold et al., 1998a).

It should be noted that the Soil and Water Assessment Tool (SWAT) occupies a unique position between conceptual and physical modelling. While it incorporates physical processes in its simulations, many of

its internal algorithms, such as the SCS-Curve Number method, are empirically derived and conceptual in nature. Curve numbers serve as calibration parameters rather than directly measurable physical properties, highlighting the model's reliance on empirical relationships. This blend of conceptual and physical approaches means that SWAT does not fit neatly into rigid categories; instead, it should be understood as part of a continuum that captures the complexities of hydrological modelling.

The table below summarizes the properties of these models:

Table 3.2: Summarization of Empirical, Conceptual and Physically Based Models. Source: Devia et al., 2015)

Empirical model	Conceptual model	Physically based model
Data based or metric or black box model	Parametric or grey box model	Mechanistic or white box model
Involve mathematical equations , derive value from available time series	Based on modeling of reservoirs and Include semi empirical equations with a physical basis.	Based on spatial distribution, Evaluation of parameters describing physical characteristics
Little consideration of features and processes of system	Parameters are derived from field data and calibration.	Require data about initial state of model and morphology of catchment
High predictive power, low explanatory depth	Simple and can be easily implemented in computer code.	Complex model. Require human expertise and computation capability.
Cannot be generated to other catchments	Require large hydrological and meteorological data	Suffer from scale related problems
ANN, unit hydrograph	HBV model, TOPMODEL	SHE or MIKESHE model, SWAT
Valid within the boundary of given domain	Calibration involves curve fitting make difficult physical interpretation	Valid for wide range of situations.

This study has employed the Soil and Water Assessment Tool (SWAT+), a version of SWAT, as a physically and conceptually based model to evaluate hydrological changes in the Rufiji Basin under historical and future climate scenarios. Further details about the SWAT model and its operations will be provided in the next chapter.

CHAPTER 4: DATA AND METHODS

4.1 General analytical framework

This analysis employed a comprehensive approach to assess future drought characteristics in comparison to historical patterns, offering critical insights into water resource availability. The Standardized Precipitation Index (SPI) and Standardized Precipitation Evapotranspiration Index (SPEI) were used as key indicators of drought severity and duration. These indices enabled an examination of drought patterns across various timeframes. Additionally, the Streamflow Drought Index (SDI) was applied to assess hydrological drought, using the Soil and Water Assessment Tool (SWAT) model to evaluate streamflow variations and gain insights into water flow trends and potential impacts on water resources. SWAT+ further supported spatial comparisons of various climatic and hydrological variables. This integrated approach allowed for a thorough assessment of drought and streamflow characteristics across both temporal and spatial scales.

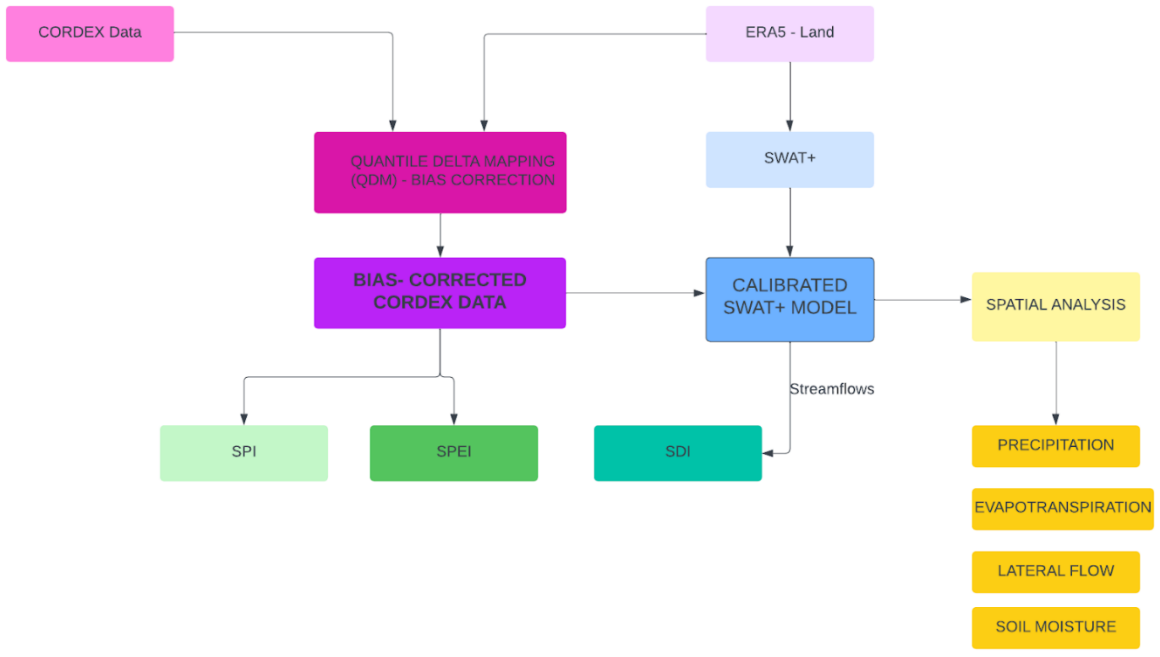

Figure 4.1: General Study Framework

4.2 Data

4.2.1 GIS Data

SWAT+ requires spatial elevation, soil and land use maps to delineate and simulate hydrological responses of the watershed. The Digital Elevation Model (DEM) utilized in this study was obtained from a 90 m × 90 m resolution Shuttle Radar Topography Mission (SRTM). This topographic data was sourced through the International Consultative Group on Agricultural Research (CGIAR-CSI) from the Space Information Consortium, as detailed by Jarvis et al. (2008).

Land cover and land use data for the basin in question was sourced from the European Space Agency (ESA)- Climate Change Initiative (CCI) (source: https://maps.elie.ucl.ac.be/CCI/viewer/) . That data is based on reanalysis data (chapter 3.4.1.1) and have a spatial resolution of 300 meters (ESA, 2017). The choice of the 1992 land use map for this analysis stems from the necessity to calibrate the model using streamflow data available only from 1955 to 1978. As the earliest accessible dataset, the 1992 land use map (Figure 4.5(d)) was deemed suitable for aligning with the temporal scope of the available streamflow data during the calibration period. The SWAT model employs land cover/use and soil data to parameterize processes such as runoff, infiltration, and evaporation. These data need to be formatted specifically for SWAT, typically represented in pre-defined SWAT categories or through lookup tables with parameters for custom classes. To adapt the land cover/use data from the ERA5 Land Classes a CSV lookup table was utilized. This translation process included categorizing various land classes like Agricultural (AGRL), Forests (FRSD), Shrubland (SHRB), and Urban areas (URBN) into the format required by SWAT (source: https://swat.tamu.edu/media/69419/Appendix-A.pdf).

Table 4.1: Comparison of ESA and SWAT+ Land Use Codes used in the study

ESA Land use Code	ESA Description	SWAT+ Land use Code	SWAT+ Description
10	Cropland, rainfed	**AGRL**	Agricultural Land
20	Cropland, irrigated/post flood	**AGRL**	Agricultural Land
30	Mosaic cropland (>50%)/Natural vegetation (<50%)	**AGRL**	Agricultural Land
40	Mosaic natural vegetation (>50%)/Cropland (<50%)	**AGRL**	Agricultural Land
50	Tree cover, broadleaved, evergreen, closed to open (>15%)	**FRSD**	Forests
60	Tree cover, broadleaved, evergreen, closed to open (>15%)	**FRSD**	Forests

70	Tree cover, needle-leaved, evergreen	**FRSD**	Forests
80	Tree cover, needle-leaved, deciduous	**FRSD**	Forests
90	Tree cover, mixed leaf type	**FRSD**	Forests
100	Mosaic tree and shrub (>50%)/ herbaceous cover (<50%)	**FRSD**	Forests
110	Mosaic tree and shrub (>50%)/ Tree and shrub (<50%)	**FRSD**	Forests
120	Shrubland	**SHRB**	Shrubland
130	Grassland	**RNGE**	Grassland
150	Sparse vegetation	**RNGE**	Grassland
160	Tree cover, flooded, fresh or brackish water	**FRSD**	Forests
170	Tree cover, flooded, saline water	**FRSD**	Forests
180	Shrub or herbaceous cover, flooded, fresh/saline	**SHRB**	Shrubland
190	Urban areas	**URBN**	Urban
200	Bare areas	**BSVG**	Sparse Vegetation
210	Water bodies	**WATR**	Water

The soil data, acquired from the FAO Soils (website), features a resolution of 450 meters and encompasses fundamental physical properties, providing insights into key parameters such as the percentage composition of texture components (sand, silt, and clay), bulk density, porosity, and the water saturation content (IUSS Working Group WRB, 2015). There were 32 distinct soil groups present within the Rufiji Basin (Figure 4.5(d)). These classes were entered into SWAT+ in the "Create HRU" step of delineating the river basin by selecting "global soils" for the raster used (link: https://swat.tamu.edu/media/116333/swatplus-training-manual-v1-locked.pdf)

4.2.2 Hydrological Data

Acquiring hydrological data post-1978 proved to be difficult, as this data is not readily available online and often entangled in bureaucratic red tape. Similarly, obtaining climatic data prior to the 1980s was challenging due to the absence of satellite data from that era. Hydrological data for the 1955-1978 period was therefore sourced from the Global Runoff Data Centre (GRDC), which serves as an international repository for hydrological data spanning up to 200 years. Founded in the early nineties, the primary objective of the GRDC is to support earth scientists in analysing global climate trends and evaluating environmental impacts and risks through facilitating multinational and global long-term hydrological studies (GRDC). Monthly streamflow data for a total of 32 gauging points from within the

Rufiji Basin were extracted from its online repository and examined for availability of quality data The analysis revealed that the majority of the stations were situated on smaller tributaries characterized by irregular flows and inconsistencies in the data.

Consequently, it was determined that the gauge at 'Stiegler Gorge' (7.8°S, 37.92°E), located along the Rufiji River within the Lower Rufiji Basin, in proximity to the site of the proposed JNHPP, would be used for calibrating the SWAT+ model in this study. However, due to minor gaps in the 'Stiegler Gorge' streamflow data, it was decided that the 'Pangani' (7.8°S, 37.87°E) gauging station would be employed to infill the missing values. Additionally, linear interpolation was applied where no data existed for both gauging stations. In total, data gaps for a 24-month period from 1955 to 1978 were addressed through interpolation and infilling, resulting in a continuous hydrograph. Notably, data for the year 1963 was entirely absent and thus excluded from the analysis. Stiegler Gorge, being the furthest downstream gauging station and acting as the critical point connecting the sub-basin's rivers, as well as its proximity to the site of the new JNHPP and reliable post-processing data, was ultimately selected for calibration of the SWAT+ model. Although a dam for the JNHPP currently exists at the site, it was not incorporated into the SWAT+ model delineation due to its non-operation at the time of model calibration, its early stages of development, and the lack of available data on outflows from the dam.

The hydrograph for Stiegler Gorge is presented below:

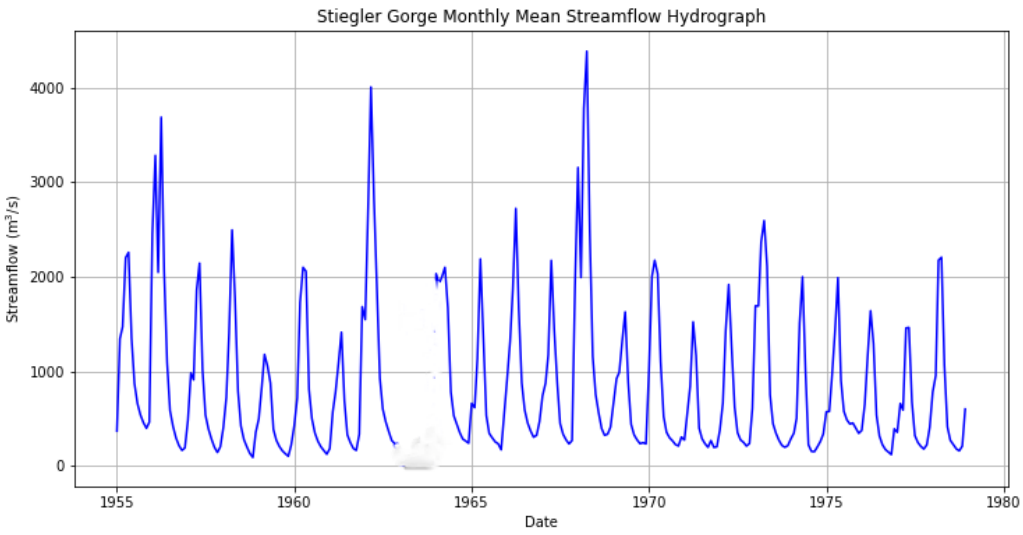

Figure 4.2: Monthly Mean Streamflow Hydrograph at Stiegler Gorge. No data record for 1963.

4.2.3 Historical Climate Data (ERA5-Land)

Due to the unavailability of reliable observed climate data before the 1980s and the lack of post-1978 streamflow records, as well as the need for essential variables such as wind speed, solar radiation, and humidity, alongside temperature and rainfall, to obtain optimal outputs from the SWAT+ model, the decision was made to use reanalysis ERA5-Land data to implement and calibrate the SWAT+ model as well as bias-correcting CORDEX data. This approach was preferred to avoid relying on generic SWAT+ data for the basin. The ERA5-Land dataset provided a comprehensive set of climate variables that were necessary for the accurate calibration of the hydrological model.

ERA5-Land is a reanalysis dataset that presents a consistent portrayal of the evolution of climate/weather variables near land surface spanning several decades, showcasing an enhanced resolution in comparison to ERA5. This dataset is derived by re-running the land surface model component of the ECMWF ERA5 climate reanalysis model. Reanalysis is the process of integrating model-generated data with global observations, resulting in a globally comprehensive and coherent dataset established through the application of physical principles (Muñoz-Sabater, 2021). The ERA5 and ERA5-Land dataset covers the period from 1950 to within 2-3 months of the present, featuring a native resolution of 9km. For this research, data encompassing precipitation, temperature, humidity, wind speed, and solar radiation was employed and down sampled to a resolution of 0.5^{o} by 0.5^{o} across the basin area (Figure 4.6(f)) to be compatible with the 0.44^{o} by 0.44^{o} CORDEX grid used for future climate projections.

This climate data was utilized within the SWAT+ Editor for both model running and calibration purposes. Each grid point served as a SWAT+ climate station, and climate data from the 1970-1980 period was used to calibrate the model, as it aligned with the available hydrological data. While ERA5-Land is available at a higher resolution, this dataset was selected for its compatibility with: (i) the CORDEX data resolution, (ii) other datasets used in the development of the hydrological model, and (iii) the broader objectives of this study.

4.2.4 CORDEX Data

This research undertook an analysis of 13 RCM-GCM pairs under both the RCP 4.5 and RCP 8.5 scenarios, yielding a total of 26 simulations. While the CORDEX ensemble includes a broader range of models, these specific RCM-GCM pairs were selected for their comprehensive inclusion of all necessary climate variables required for SWAT+ and their reliability in terms of data accuracy. A total of four Regional Climate Models (RCMs) were employed to downscale nine Global Climate Models (GCMs). Data from the CORDEX Africa initiative was sourced from the CSAG Repository (CSAG website).

The CORDEX modelling experiment, which downscales Global Circulation Model (GCM) climate projections generated under the CMIP5 framework, presents data at a grid resolution of 0.44° x 0.44° for both its historical (1950-2005) and future (2006-2100) climate periods. This study relies on CORDEX data derived from CMIP5 projections, as the downscaling of CMIP6 data by CORDEX had not been completed as of 2023. This choice reflects the reliance on available, downscaled data for regional climate analysis, despite the advancement of global climate models in the CMIP6 framework. For clarity, the nomenclature used in this work presents the GCM followed by the corresponding downscaling RCM. The table below outlines the thirteen models utilized in this analysis:

Table 4.2: List of GCM and downscaling RCM pairs utilized in the study

No.	GCM	Downscaling RCM	Acronym utilized in study
1	**CCCma-Canadian Centre for Climate Modelling and Analysis** *CCCma-CanESM2*	**CCCma-Canadian Centre for Climate Modelling and Analysis** *CCCma-CanRCM4*	CCCMA-RCM
2	**CCCma-Canadian Centre for Climate Modelling and Analysis** *CCCma-CanESM2*	**SMHI-Swedish Meteorological and Hydrological Institute** RCA4- Rossby Centre Regional Atmospheric Model, version 4 *SMHI-RCA4.v1*	CCCMA-SMHI
3	**CNRM-National Centre for Meteorological Research (France)** *CNRM-CERFACS-CNRM-CM5*	**SMHI-Swedish Meteorological and Hydrological Institute** *SMHI-RCA4.v1*	CNRM-SMHI
4	**CSIRO-Commonwealth Scientific and Industrial Research Organisation** *CSIRO-QCCCE-CSIRO-Mk3-6-0*	**SMHI-Swedish Meteorological and Hydrological Institute** *SMHI-RCA4.v1*	CSIRO-SMHI
5	**ICHEC-Irish Centre for High-End Computing** *ICHEC-EC-EARTH*	**KNMI-Royal Netherlands Meteorological Institute** *KNMI-RACMO22T.v1*	ICHEC-KNMI
6	**ICHEC-Irish Centre for High-End Computing** *ICHEC-EC-EARTH*	**MPI-Max Planck Institute for Meteorology (Germany)** *MPI-CSC-REMO2009.v1*	ICHEC-MPI
7	**ICHEC-Irish Centre for High-End Computing** *ICHEC-EC-EARTH*	**SMHI-Swedish Meteorological and Hydrological Institute** *SMHI-RCA4.v1*	ICHEC-SMHI
8	**IPSL-Institut Pierre-Simon Laplace (France)** *IPSL-IPSL-CM5A-MR*	**SMHI-Swedish Meteorological and Hydrological Institute** *SMHI-RCA4.v1*	IPSL-SMHI
9	**Model for Interdisciplinary Research on Climate (Japan)** *MIROC-MIROC5*	**SMHI-Swedish Meteorological and Hydrological Institute** *SMHI-RCA4.v1*	MIROC-SMHI
10	**MPI-Max Planck Institute for Meteorology (Germany)** MPI-M-MPI-ESM-LR	**MPI-Max Planck Institute for Meteorology (Germany)** *MPI-CSC-REMO2009.v1*	MPI-MPI
11	**MPI-Max Planck Institute for Meteorology (Germany)** MPI-M-MPI-ESM-LR	**SMHI-Swedish Meteorological and Hydrological Institute** *SMHI-RCA4.v1*	MPI-SMHI
12	**NCC-National Capital Commission (Canada)** *NCC-NorESM1-M*	**SMHI-Swedish Meteorological and Hydrological Institute** *SMHI-RCA4.v1*	NCC-SMHI
13	**NOAA- National Oceanic and Atmospheric Administration** *NOAA-GFDL-GFDL-ESM2M*	**SMHI-Swedish Meteorological and Hydrological Institute** *SMHI-RCA4.v1*	NOAA-SMHI

Although CORDEX data are downscaled, they are not free from bias, as systematic discrepancies exist between the model outputs and observed data. To enable the use of CORDEX data for driving the SWAT model, a bias correction process was applied using the Quantile Delta Mapping (QDM) technique (Cannon et al., 2015). QDM is a statistical method designed to adjust model biases by aligning the distribution of climate variables from a GCM with that of observational data. This correction is essential when using climate model data to drive hydrological models, as it ensures the model simulates a realistic hydrological regime, thereby producing reliable datasets crucial for understanding climate impacts. Furthermore, QDM is an open-source methodology, with its code publicly accessible for widespread application within the scientific community. The CORDEX data, sourced from the CSAG archive were therefore bias corrected to the ERA5-Land dataset, with a reference period of 1991-2020, at a resolution of 0.5°.

Figure 4.3 below shows the comparison of bias corrected mean monthly precipitation and temperature values for the historical/present period (1991-2020) used in this study for all the CORDEX models under the RCP 4.5 and RCP 8.5 scenarios against ERA5-Land:

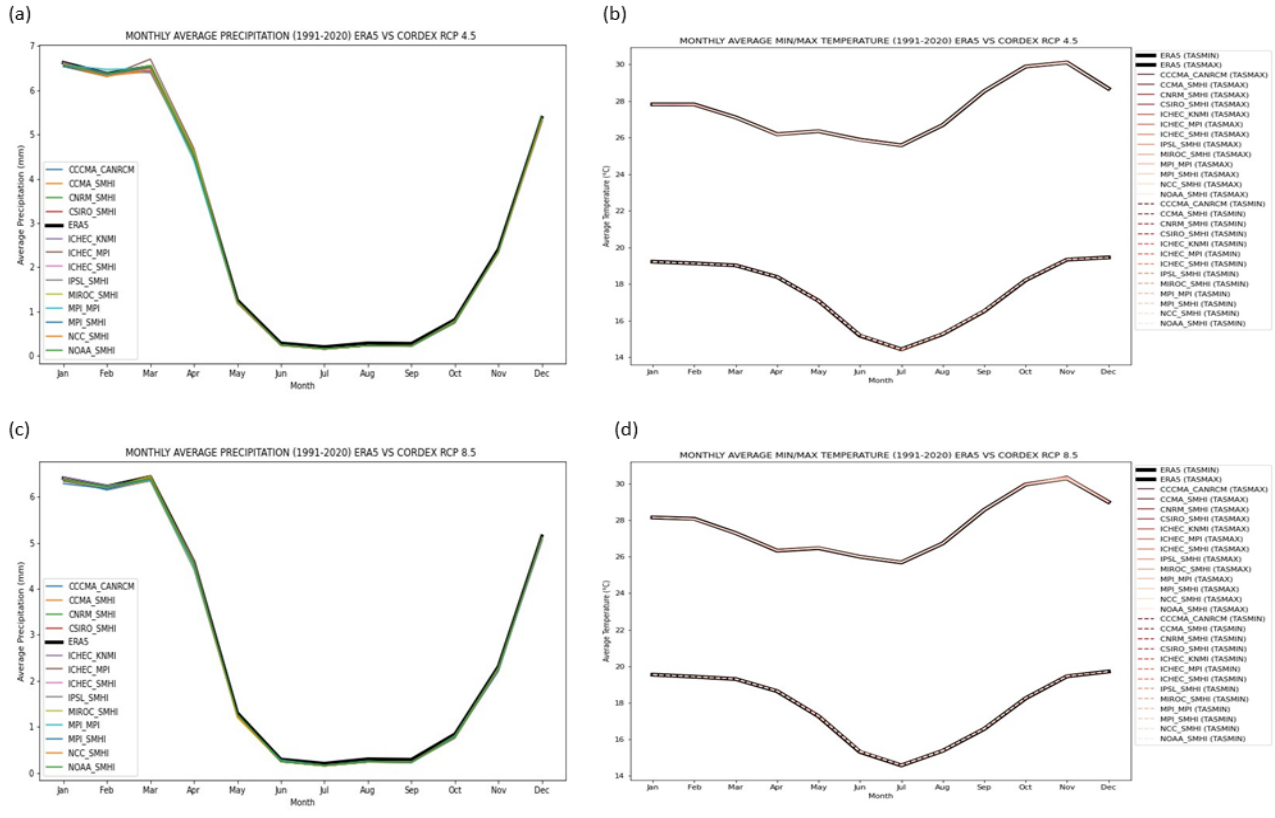

Figure 4.3: Bias-Corrected CORDEX data – Monthly Average Precipitation ((a)RCP 4.5, (c) RCP8.5) and Monthly Average Temperature ((b)RCP 4.5, (d) RCP 8.5)) for the 1991-2020 period.

The selected time frame for historical bias correction was the 30-year period from 1991-2020, in order to keep with the WMO guidelines on setting reference periods (WMO, 2017).

The impact of global warming was assessed over three distinct 30-year periods, representing the historical/present, near future, and far future. The selected timeframes for analysis were 1991-2020 for the historical/present period, 2031-2060 for the near future, and 2071-2100 for the far future. The CORDEX dataset provided key climate variables—precipitation, maximum temperature (TMAX), and minimum temperature (TMIN)—which were critical for both the implementation of the SWAT+ model and the calculation of the Standardized Precipitation Evapotranspiration Index (SPEI). The following graphs illustrate the annual average precipitation and temperature across all CORDEX projections (1970-2100), alongside the ERA5-Land data (1970-2020), providing a comparison of historical and projected trends.

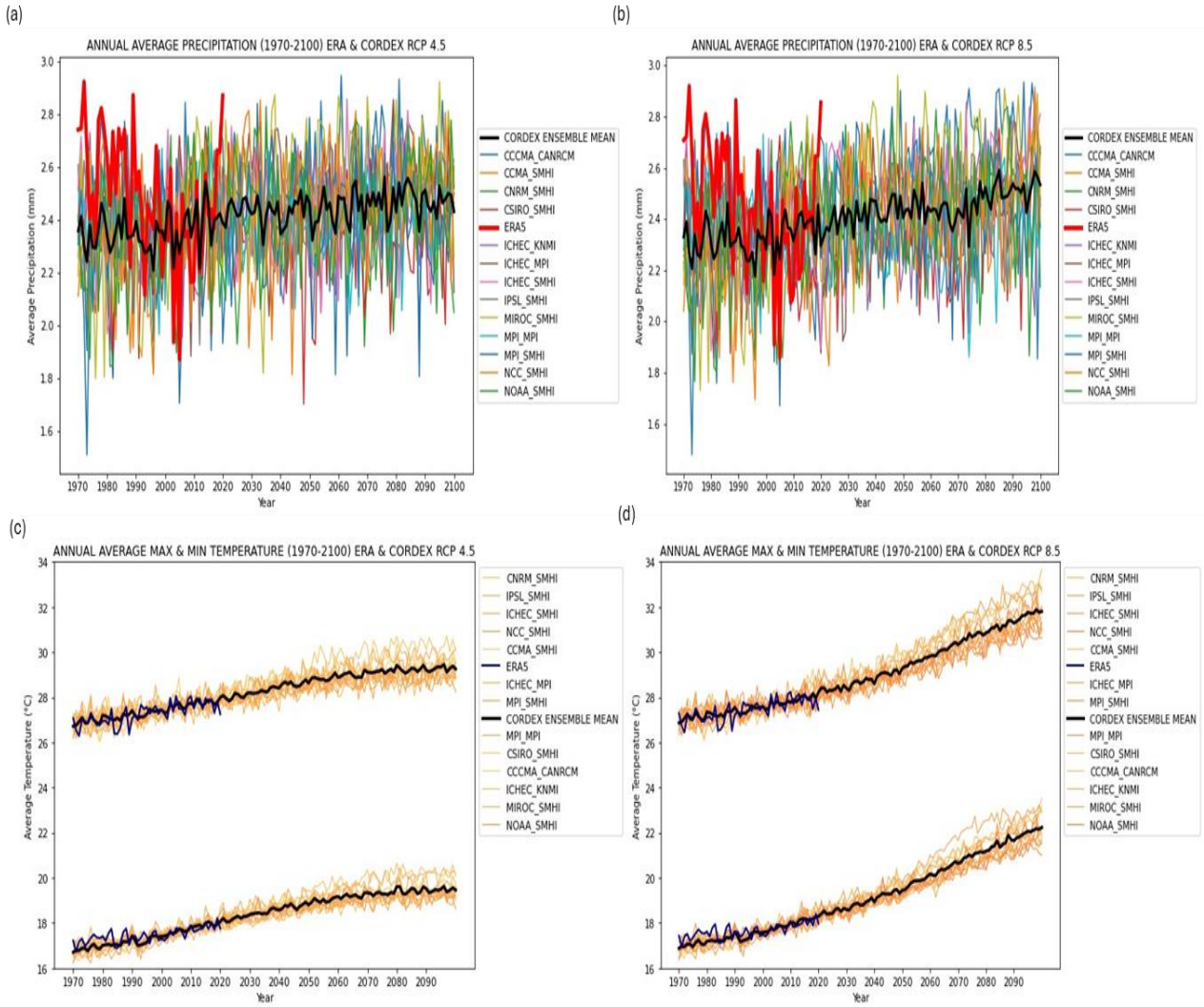

Figure 4.4: Top panel: Annual average precipitation from the CORDEX models and ERA5-Land for the (a) RCP 4.5 and (b) RCP 8.5 scenarios over the Rufiji Basin. Bottom panel: Annual average maximum and minimum temperatures from the CORDEX models and ERA5-Land for the (c) RCP 4.5 and (d) RCP 8.5 scenarios over the Rufiji Basin

Precipitation projections exhibit considerable variability, with magnitudes comparable to those observed during the historical period. A slight tendency towards increased rainfall is evident towards the end of the 21st century, with minimal distinction between the two scenarios considered. Temperature projections, on the other hand, show an upward trend. Under the RCP4.5 scenario, this trend begins to level off toward the end of the century, whereas under RCP8.5, it continues unabated. Observed temperature data, however, indicate a weaker trend during the historical period, while the projections from the climate models show more discernible warming trends in the future.

4.3 Methods

4.3.1 Drought Indices

4.3.1.1 SPI

To fulfil one of the principal objectives of this study, the Standardized Precipitation Index (SPI) was employed to evaluate meteorological droughts and forecast potential drought conditions within specific segments of the basin. The SPI was calculated using the SPEI package in RStudio, developed by Beguería and Vicente-Serrano (2017), enabling standardized analysis of precipitation deficits across various time scales.

The SPI calculation follows:

$$\mathbf{SPI} = \frac{\mathbf{P}-\mathbf{P}^*}{\sigma_\mathbf{p}}$$

where:

- P represents observed precipitation,
- P^* is the mean precipitation for the selected period, and
- σ_p denotes the standard deviation of precipitation.

To assess different drought types, SPI calculations can be applied to time scales from 1 to 48 months. These time frames refine SPI estimations for both short and prolonged drought events, represented as:

$$\mathbf{SPI_{i,k}} = \frac{\mathbf{P_{i,k}}-\mathbf{P_k^*}}{\sigma_{\mathbf{p,k}}}$$

where:

- i represents the year of calculation, and
- k denotes the time scale (e.g., $k = 1$ for a 3-month SPI).

For this study, a 12-month time scale was chosen. This period is a good measure for longer-lived droughts, as it tracks annual hydrological years and provides a solid basis for comparing meteorological droughts with hydrological droughts. By applying this time scale, the SPI analysis can capture drought events that span across seasons and provide more robust insights into longer-term precipitation deficits.

A Gamma distribution is fitted to the precipitation data and then transformed into a standard Gaussian distribution, ensuring that SPI values are normally distributed with a mean of zero. This standardization supports consistent cross-comparisons and fulfils the objective of accurately capturing drought variability within the basin.

The SPI was calculated for the historical period using ERA5-Land data, while projections were made using the CORDEX Ensemble models. Each sub-basin's daily precipitation (PRCP) data for each climate station or grid point (as shown in Figure 4.7(f)) were aggregated to obtain monthly mean values for precipitation. These monthly values were then averaged across all the grid points within the sub-basin to calculate a final average monthly precipitation for the entire sub-basin, which was subsequently used in the SPI calculations.

4.3.1.2 Standard Precipitation Evaporation Index (SPEI)

The Standardized Precipitation Evapotranspiration Index (SPEI) is a modified version of the Standardized Precipitation Index (SPI), which incorporates the effects of potential evapotranspiration (PET) in addition to precipitation. SPEI utilizes the same RStudio package (SPEI package, Beguería and Vicente-Serrano, 2017) but includes potential evapotranspiration (PET) in its calculation, providing a more comprehensive assessment of drought by accounting for both precipitation and atmospheric demand for water.

The SPEI calculation follows these steps:

1. **Calculate the climatic water balance (D)** by subtracting potential evapotranspiration (PET) from precipitation (P)

$$\mathbf{D = P - PET}$$

where:

- D represents the climatic water balance (or drought index),
- P is precipitation, and
- PET is potential evapotranspiration.

2. **Fit the water balance (D) to a probability distribution**, typically a log-logistic distribution, and transform it to a standard normal distribution:

$$\mathbf{SPEI} = \mathbf{F}(\mathbf{D})$$

where:

- F(D) is the function used to transform the cumulative probability of D into a standard normal distribution score (Z-score), standardizing D for consistent comparison across different time periods and regions.

Like SPI, the SPEI values are calculated for different time scales to reflect short- and long-term droughts. For this study, both indices were computed at a 12-month time scale, allowing for the assessment of longer-lived droughts.

The SPEI was calculated for the historical period using ERA5-Land data, while projections were made using the CORDEX Ensemble models. For each calculation, daily climate data from each grid point "climate station" within a sub-basin (refer to Figure 4.6(f)) were aggregated to compute monthly mean values for the required variables, including precipitation (PRCP), maximum temperature (TMAX), and minimum temperature (TMIN). This monthly dataset for each grid point within a sub-basin was subsequently aggregated across all grid points within the sub-basin to generate a monthly average for the entire basin.

The indices were computed at a 12-month time scale (i.e., SPI/SPEI-12), spanning from January 1990 to December 2100. The mid-latitude point of each sub-basin was used as the reference latitude for SPEI calculations within the RStudio package, and the Hargreaves method was applied to compute PET. The base reference period for the calculation of SPI and SPEI was set from 1991 to 2020.

4.3.1.3 Streamflow Drought Index (SDI)

The Streamflow Drought Index (SDI) was utilized to assess the likelihood of hydrological droughts at generic stream gauging points across the catchment area (Figure 4.5). This analysis was carried out using the Drought Indices Calculator (DRINC) application, developed by the National Technical University of Athens (Tigkas et al., 2015).

For the Rufiji Basin, where the hydrological year starts in November, a time series of monthly streamflow volumes $\mathbf{Q_{i,j}}$ is needed. Here:

- **i** represents the hydrological year.

- j represents the month within the hydrological year, where j=1 for November and j=12 for October.

For each hydrological year i, cumulative streamflow volumes **Vi,k** are computed for different reference periods k. These reference periods correspond to different durations (in months) over which drought conditions are assessed:

- k=1 for the 3-month period (November–January).
- k=2 for the 6-month period (November–April).
- k=3 for the 9-month period (November–July).
- k=4k for the 12-month period (November–October, corresponding to the entire hydrological year).

The cumulative streamflow volume for each reference period k of the i^{th} hydrological year is given by:

$$\mathbf{V_{i,k}} = \sum_{j-1}^{k} \mathbf{Q_{i,j}}$$

where $\mathbf{V_{i,k}}$ is the cumulative streamflow volume for the i^{th} hydrological year and the k^{th} reference period.

To normalize the distribution of the cumulative streamflow data, the natural logarithm of the streamflow volumes is applied. This transformation ensures that the data approximates a normal distribution, which is needed for subsequent calculations of the SDI.

The log-transformed cumulative streamflow volumes $\mathbf{ln(V_{i,k})}$ are computed as:

$$\ln(\mathbf{V_{i,k}})$$

This transformation results in data that can be modelled using a log-normal distribution.

For each reference period **k**, the mean **yk**_and standard deviation $\mathbf{s_{y,k}}$ of the log-transformed cumulative streamflow volumes $\mathbf{ln(V_{i,k})}$ are calculated over a long period of time (e.g., 30 years). These statistics are used to standardize the data.

- The mean $\mathbf{y_k}$ is calculated as:

$$y_k = \frac{1}{N} \sum_{i-1}^{N} \ln(V_{i,k})$$

- The standard deviation $\mathbf{s_{y,k}}$ is calculated as:

$$s_{y,k} = \sqrt{\frac{1}{N}\sum_{i-1}^{N}(\ln(V_{i,k}) - y_k)^2}$$

Where **N** is the number of years used to calculate the long-term mean and standard deviation (e.g., 30 years).

After transforming the streamflow data to a log-normal distribution, the SDI is calculated for each reference period k of the **ith** hydrological year using the following formula:

$$SDI_{i,k} = \frac{\ln(V_{i,k}) - y_k}{s_{y,k}}$$

Where:

- **ln($V_{i,k}$)** is the natural logarithm of the cumulative streamflow volume for the **ith** hydrological year and **kth** reference period.
- **y_k** is the long-term mean of the log-transformed cumulative streamflow volumes for the **kth** reference period, calculated over 30 years.
- **$s_{y,k}$** is the standard deviation of the log-transformed cumulative streamflow volumes for the **kth** reference period, calculated over the same 30-year period.

The SDI is a standardized index that quantifies the deviation of the log-transformed cumulative streamflow from the long-term mean for each reference period. A negative value of **SDIi,k** indicates a drought condition, with more negative values signifying more severe droughts. The criteria in Table 4.3 are used to define the five drought states that are taken into consideration, each of which is represented by an integer number ranging from 0 (no drought) to 4 (severe drought).

Table 4.3: SDI classification

State	Description	Criterion	Probability (%)
0	Non-drought	SDI $\geq$ 0.0	50.0
1	Mild drought	$-1.0 \leq$ SDI $<$ 0.0	34.1
2	Moderate drought	$-1.5 \leq$ SDI < -1.0	9.2
3	Severe drought	$-2.0 \leq$ SDI < -1.5	4.4
4	Extreme drought	SDI < -2.0	2.3

The SDI satisfies the general conditions (a) to (e) listed in the introduction of hydrological drought indices (see section 3.3) since it is comparable to the well-known index SPI, which satisfies these characteristics. In many instances where streamflow data is accessible through contemporary monitoring systems, requirement f is also satisfied. However, a weakness of the SDI is that it only requires one input (streamflow), which may not consider management decisions and could lead to results being skewed by periods of low flow (Nablantis & Tsakaris, 2009).

Calculation of the SDI was done using SWAT+ streamflow data and calculated at the outflow points of each sub-basin, with the exception of the Lower Rufiji, which utilized the Steigler Gorge as a gauging point (Figure 4.6). Steigler Gorge also served as the calibration point for the SWAT+ model. The SDI was calculated at a 12-month timescale (SDI-12) for the 1990-2100 period, with output being given at the monthly timestep. The reference period for calculation of SDI was set as 1991-2020.

4.3.2 Development and implementation of SWAT+ over the Rufiji Basin

4.3.2.1 General framework

In this research, the SWAT+ model was applied to the Rufiji catchment area in Tanzania, utilizing the data from the sources previously mentioned. The model was implemented with a daily time step. Given the availability of hydrological data, the model was calibrated for the period from 1975 to 1978 and validated for the period from 1971 to 1974, with a 3-year warm-up period applied to both calibration and validation phases. Climate data variables were inputted from the ERA-5 Land dataset created for each climate station within the SWAT+ sub-basins (see chapter 4.2.3 and Figure 4.5(f))

Once calibrated, the model was set up for simulations using CORDEX climate data (Figure 4.4) covering the period from 1988 to 2100, including a 3-year warm-up period. This period was then divided into three segments: historical (1991-2020), near future (2031-2060), and far future (2071-2100). The streamflow outputs from the SWAT model were compared across these periods to assess potential changes in hydrological drought characteristics within the Rufiji basin (chapter 5.4). Visual assessments of hydrological fluxes were also illustrated utilizing output from the SWAT+ model (chapter 5.3).

4.3.2.2 SWAT+

The Soil and Water Assessment Tool (SWAT+) is as a hydrological model developed by the United States Department of Agriculture-Agricultural Research Service (USDA-ARS). This model, as elucidated by Arnold et al. (1998) and Arnold et al. (2012), is characterized by its physical/conceptual

basis, semi-distributed nature, and continuous-time framework. Offering a versatile solution, SWAT+ proves instrumental in simulating various watershed-scale applications over extended timeframes, as noted by Neitsch et al. (2009).

SWAT+'s applicability can extend to ungauged river basins, as highlighted by Gassman et al. (2007). This feature proves particularly advantageous when examining watersheds characterized by limited data, such as the Rufiji River Basin. Notably, the model's computational efficiency enables the execution of simulations over expansive basins or those featuring intricate management practices. This efficiency is particularly beneficial, ensuring that the model can operate without requiring extensive time resources, thereby enhancing its feasibility for large-scale applications.

The integral components of the SWAT+ model encompass weather, hydrology, soil characteristics, plant growth, nutrients, pesticides, and land management, as detailed by Arnold et al. (2012). The model's applicability extends to the simulation of the impacts of land use and management practices on hydrological processes, encompassing surface and subsurface flow, as well as evapotranspiration. Additionally, SWAT+ is adept at modelling sediment yields of agricultural chemicals, including nutrients (Arnold et al., 1998; Neitsch et al., 2009).

In the simulation phase of SWAT+, the watershed undergoes division into sub-basins. The sub-basins are further stratified into hydrological response units (HRUs) or Landscape Units (LSUs), constituting regions characterized by homogeneous soil, land usage, and slope combinations. The simulation of both the land and water routing phases in SWAT+ relies on daily meteorological data as well as spatial data. Output results are available for daily, monthly, and annual timescales. SWAT+ ‘s hydrological cycle is modelled using the following water balance equation, as outlined by Neitsch et al. (2005):

$$SW_t = SW_0 + \sum_{i=1}^{t} (R_{day} - Q_{surf} - E_a - W_{seep} - Q_{gw})$$

For each day represented by time (t) in days, the final soil water content (SWt) is determined by considering the initial soil water content (SW_0) on day i, along with the daily amounts (in millimetres) of rainfall ($Rday$), surface runoff ($Qsurf$), evapotranspiration (Ea), water transferred inro the soil profile ($Wseep$), as well as deeper seepages into groundwater/aquifers (Qgw). A daily water balance is then calculated to simulate fluxes of variables within the various parts of a hydrological system.

4.3.2.3 Data pre-processing

Before implementation of the SWAT+ model, the required spatial datasets, needed for running the model (DEM, soils and land use maps) were reprojected to the Universe Transverse Mercator (UTM) Zone 37S Southern Hemisphere for the Rufiji Basin.

4.3.2.4 SWAT+ delineation of the Rufiji River Basin

The SWAT+ model was developed in QGIS version 3.22.11 using the SWAT+ plugin tool. Watershed delineation, channel network routing, and basin segmentation were based on DEM data input (Figure 4.6(a)). Initially, the Rufiji catchment was divided into 30 sub-basins through automated channel network delineation (Figure 4.6(a)). Additionally, part of the Kilombero wetland, specifically Kibasira Swamp, was designated as a reservoir to simulate delayed flow effects within the basin (Figure 4.6(a)). This reservoir acts as an impoundment, similar to techniques applied in studies by Jalowska and Yuan (2019) and Mishra et al. (2007), aimed at capturing delayed streamflow in sub-basins containing wetlands. This approach enhances the model's ability to predict hydrological behavior in complex watershed systems with wetland features.

Figure 4.6(b) shows the DEM elevation profile of the sub-basin, revealing an elevation range from 0 to 3000 m.a.s.l. The highest elevations are observed in the Kilombero and lower sections of the Great Ruaha sub-basin, while the lowest areas are situated in the Lower Rufiji sub-basin.

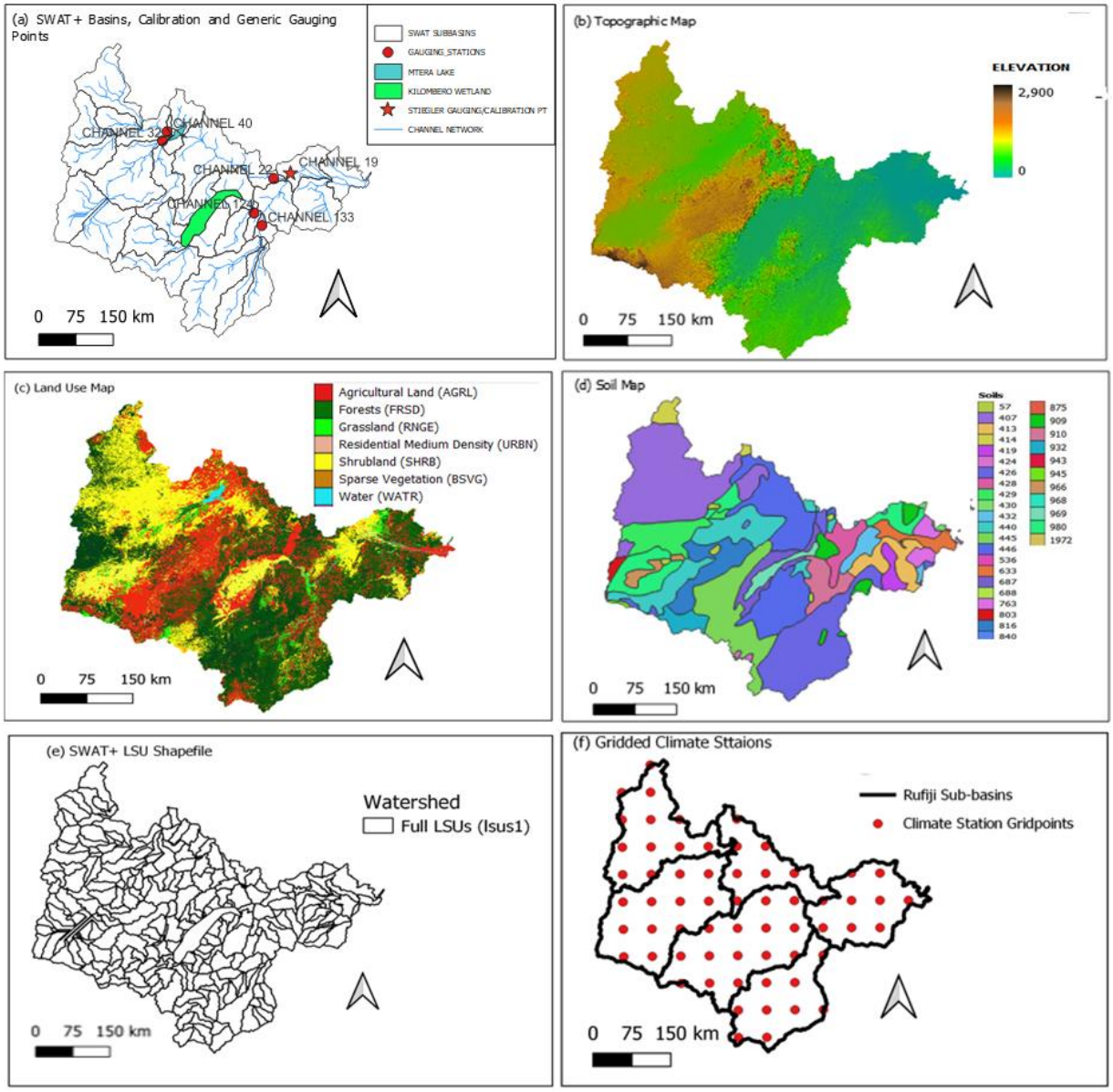

Figure 4.5: Geospatial arrangement of input and output datasets used in the implementation of the SWAT+ model over the Rufiji Basin: (a) SWAT+ sub-basin structure and river network structure. (b) Digital Elevation Map (90m x 90m, SRTM), (c) Land Use Map (ESA, 300m), (d) Soil map (FAO Soil, 450m), (e) SWAT+ LSU shapefile, (f) Gridded climate stations.

4.3.2.5 Parameterization of land surface hydrological processes

SWAT+ also required the input of land use and soil maps for the simulating the Rufiji Basin. The Land Use Map, Figure 4.5(c) indicates that predominant land uses in the basin include Forests, Agriculture, and Shrubland (45%, 25%, 25% respectively). Most agricultural practices are found within the Little Ruaha catchment, on the slopes of the highlands. Forests are prominent in the Kilombero and Luwegu basins, with coastal forests present in the Lower Rufiji sub-basin. The Kilombero sub-basin is predominantly made up of a wetland. Shrublands are a distinctive part of the Upper Great Ruaha

catchment while the Lower Great Ruaha has mountainous regions where the Great Ruaha snakes through. Urban Settlements make up less than 0.1% of the total land area.

The Land Use Map, Figure 4.5(c) indicates that predominant land uses in the basin include Forests, Agriculture, and Shrubland (45%, 25%, 25% respectively). Most agricultural practices are found within the Little Ruaha catchment, on the slopes of the highlands. Forests are prominent in the Kilombero and Luwegu basins, with coastal forests present in the Lower Rufiji sub-basin. The Kilombero sub-basin is predominantly made up of a wetland. Shrublands are a distinctive part of the Upper Great Ruaha catchment while the Lower Great Ruaha has mountainous regions where the Great Ruaha snakes through. Urban Settlements make up less than 0.1% of the total land area.

The Soil Map, Figure 4.5(d) shows 32 different soil types which can be looked up at FAO (IUSS Working Group WRB, 2015).

Figure 4.5(e) shows the Landscape Unit (LSU) locations over the Rufiji Basin. An LSU is defined as a distinct area that channels runoff into a specific reach, which can be further segmented into floodplain and upslope zones based on floodplain raster data. The SWAT+ model created 280 Landscape Spatial Units (LSUs) for the parameterization of hydrological processes using the automated SWAT+ routine (Figure 4.6(e)).

Each LSU is delineated as a unique polygon. Within an LSU, Hydrologic Response Units (HRUs) are identified as groups of pixels with homogeneous land use, soil characteristics, and slope categories. These HRUs facilitate a summarized view of water movement, offering a unified depiction of hydrologic activity across each spatially distinct unit, as discussed by Srinivasan & George (2018). This study employed the LSU to visualize hydrological fluxes within the basin as it provides a better visual representation of sub-basins compared to the HRUS.

Figure 4.6(f) shows the locations of 'climate stations,' or climate grid points, spaced at 0.5° intervals, where climatic data was distributed across the basin. Climate data was sourced from ERA5-Land and the CORDEX model ensemble, as described in sections 4.2.2 and 4.2.3.

SWAT+ is capable of modelling and integrating groundwater processes; however, this feature was not implemented in the scope of the research due to limited documentation, implementation guidelines and data references available for groundwater modelling. Additionally, the approach for incorporating groundwater is complex and resource-intensive, making it challenging to implement within the constraints of this study. As a result, groundwater dynamics were excluded from the model's configuration.

4.3.2.6 Development of river network and sub-catchment structure

In this study, the Rufiji Basin was divided into six sub-basins, an increase from the historical four. This adjustment was achieved by subdividing the Great Ruaha into three parts: the Upper Great Ruaha, Lower Great Ruaha, and Little Ruaha (Figure 4.6). The Upper Great Ruaha and Little Ruaha sub-basins each contain distinct rivers that discharge into the Mtera Reservoir, while the Lower Great Ruaha includes the basin area encompassing the reservoir's outflow and its downstream regions.

The SWAT+ model was calibrated at Channel 19 in the Lower Rufiji Basin (Figure 4.6), specifically at the Stiegler Gorge gauge, which is the most downstream station with reliable and continuous streamflow data. Additionally, five other gauging points were delineated across the catchment to capture outflows from the sub-basins. These outflow points include channel 40 for the Upper Great Ruaha sub-basin, channel 32 for the Little Ruaha sub-basin, channel 22 for the entirety of the Great Ruaha (Lower Great Ruaha), channel 124 for the Kilombero sub-basin, and channel 133 for the Luwegu sub-basin.

These designated points serve as pivotal gauging locations for the Streamflow Drought Index Analysis, capturing essential outflows from distinct segments of the Rufiji Catchment. Due to the absence of observed recorded flow data at these points for comparison, future Streamflow Drought Index (SDI) values were benchmarked against the model's outputs from the historical period of 1991-2020.The Kilombero Wetland was identified and designated as a reservoir within the SWAT+ model to regulate and attenuate streamflow’s. This approach helped create delayed stream flows in the hydrograph, providing a more accurate representation of simulated versus observed flows (Figure 5.1).

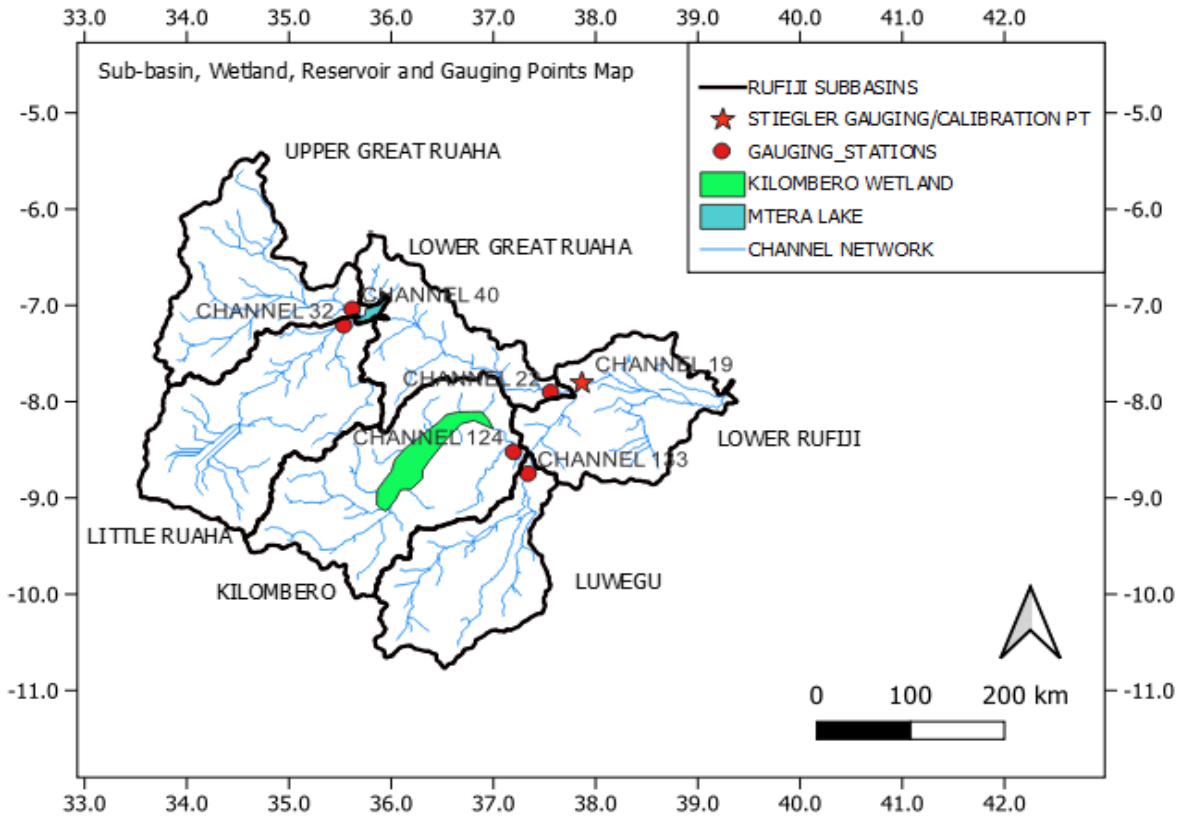

Figure 4.6: Map delineating the sub-basins used in the study, the Kilombero wetland, lakes, and the calibration and gauging points within the Rufiji Basin

4.3.3 Preparation of climate input files for setting up model calibration and simulations

After setting up the initial model structure, the next phase involved preparing model inputs, such as climate files, for the calibration process. The climate dataset used for model calibration consisted of historical climate data sourced from ERA5-Land. This dataset included five climate variables—precipitation, temperature, humidity, wind speed, and solar radiation—provided at a regular grid spacing of 0.5° (Figure 4.6(f)). Each data point was treated as a weather station, facilitating the seamless integration of data into the SWAT software. The data from each station were converted from the NetCDF format to the SWAT format, resulting in an array of 80 “pseudo-stations” (Figure 4.6(f)).

Similarly, bias-corrected climate projection data from the CORDEX ensemble for each of the 13 available RCM-GCM combinations, provided in gridded format, were converted into SWAT station data. Each combination was simulated as an independently to. assess the potential variations in future hydrological conditions

This allowed implementation of the model as follows:

- over the 1960 to 1980 period for the purpose of calibration and validation of the SWAT+ model using the ERA5-Land data. In this simulation model outputs were compared against the available hydrological observations.
- over the period of 1987-2020 forced by ERA5-Land data for the purpose of establishing historical observational reference conditions (SDI) (as seen in chapter 5.3.1).
- over the period from 1987 to 2099, forced by bias-corrected CORDEX climate data, to facilitate the comparison of future hydrological conditions with historical ones.

A 3-year warm up period was used in each set of simulations.

4.3.4 SWAT+ Calibration and Validation

The calibration of the hydrological model was performed using the SWAT+ Toolbox (Version 1.0.1). This process involved systematically adjusting model parameter values to improve the model's alignment with observed data, thus enhancing its predictive accuracy. Using the objective function as a metric for comparison, model outputs were evaluated against target values. Seven parameters were identified as particularly sensitive and were selected for calibration, guided by established recommendations from prior studies (Gyamfi et al., 2016; Thavhana et al., 2018) and further supported by insights from the broader SWAT calibration literature (Abbaspour et al., 2017). The selection and tuning of these parameters were crucial for refining the model's performance and ensuring its suitability for accurately simulating hydrological conditions within the study area.

The parameters calibrated included the Curve Number (CN), Available Water Capacity (AWC), Soil Conductivity (K), Soil Water Factor for CN3 (CN3_SWF), Lateral Flow Coefficient (LATQ_CO), Lateral Flow Time (LATT_TIME) and the Percolation Coefficient (PERCO) (see table 5.1).

A manual calibration approach was selected to provide a thorough understanding of the parameters involved in the calibration process. The type of parameter adjustments followed the recommendations of Abbaspour (2017). Each parameter was individually calibrated to assess sensitivity, and a combination of the most sensitive parameters was then tested collectively in an ensemble-like approach. This was aimed at improving Nash Sutcliffe Efficiency (NSE) values, shifting the hydrograph to enhance baseflows, reducing peak flows and simulate a 1-month lag in the hydrograph. Adjustments to parameters within SWAT+ were made in the following ways:

a. Percentage changes to the original SWAT+ Figure, i.e., +/- 30%.

b. Relative value changes, where the original value is modified by a specified amount.

c. Direct replacement of the Figure with a new inputted value.

Further details on the types and values of parameter adjustments implemented during calibration are provided in Table 5.1.

The initial calibration steps involved defining the warm-up and simulation periods. The simulation period was set as the 1972-1978 period, which encompassed a 3-year warm-up phase (1972-1974) and a subsequent 4-year calibration period (1975-1978). For validation purposes, a separate simulation was conducted for the period 1968-1974, again with a 3-year warm-up period and a subsequent 4-year validation period (1971-1974).

Nash Sutcliffe Efficiency (NSE) was used as calibration objective function. The Nash Sutcliffe Efficiency (NSE), a normalized statistic introduced by Nash and Sutcliffe (1970), measures the relative magnitude of the residual variance compared to the variance in measured data over the modelling period. It serves as a tool to assess the effectiveness of hydrological models in simulating streamflow. The NSE is a unitless metric that ranges from negative infinity to 1, where an NSE of 1 indicates optimal performance, reflecting a perfect alignment between observed and simulated streamflow.

In accordance with the classification proposed by Moriasi et al. (2007), NSE values in the range of 0.75 < NSE ≥ 1 are considered very good, indicating highly accurate model results. Values falling within 0.65 < NSE ≥ 0.75 suggest good model performance, while the range of 0.5 < NSE ≥ 0.65 indicates satisfactory results. On the other hand, an NSE below 0.5 implies unsatisfactory model performance. When NSE is ≤ 0, it signifies that the observed average serves as a more reliable predictor than the model simulation. The governing equation for NSE is provided below:

$$NSE = 1 - \frac{\sum_{i=1}^{n}(Q_{sim(i)} - Q_{Obs(i)})^2}{\sum_{i=1}^{n}(Q_{Obs(i)} - \overline{Q_{Obs(i)}})^2}$$

Where: $QObs$ represents the observation record, $Qsim$ represents the simulated modelling response, $\overline{QObs}$ is the average observation record at time step i, n is the total number of time steps for the simulation.

4.3.5 Spatial Analysis of projected changes in hydrological fluxes

The final stage of the methodology involved visualizing the impacts of climate change on hydrological processes across the Rufiji Basin in a spatial format. This was accomplished using the Visualizer option within the QSWAT+ plug-in (Step 4), enabling a clear, spatially distributed representation of hydrological changes across the basin. Each CORDEX model was loaded as a distinct scenario, and specific time periods (i.e., 1991-2020, 2031-2060, and 2071-2100) were conFigured to produce output.

Thereafter, maps detailing changes in variables such as precipitation, actual evapotranspiration, lateral flow, and soil moisture at the Land Scape Unit (LSU) level were generated. Lateral flow was selected

to represent water movement throughout the basin, rather than surface runoff, as it is better suited to the LSU (Landscape Unit) framework compared to surface flow, which appears in smaller, more pixelated segments in HRU (Hydrologic Response Unit) visualizations. During calibration, lateral flow was also identified as a sensitive parameter, contributing to the creation of a lag in the hydrograph, and was chosen for its close alignment with soil moisture dynamics.

Maps representing the minimum, maximum, and mean of the CORDEX model ensemble were displayed to illustrate the 'driest,' 'wettest,' and average projections of each variable across the ensemble. These were determined by calculating an average for each model over the specified time period, with the models having the highest and lowest averages across all Landscape Units (LSUs) selected as the 'wettest' and 'driest' projections, respectively. The ensemble average was calculated and used as the 'mean-ensemble model.

CHAPTER 5: RESULTS & ANALYSIS

5.1 Results of hydrological model calibration

The table below shows the parameter changes made during calibration of the SWAT+ mode:

Table 5.1: SWAT+ Parameters used for Calibration

Parameters	**Input File**	**Description**	**Change Type**	**Change Value**
CN	.HRU	Curve number	Percentage	-40
AWC	.SOL	Available Water Capacity (mm_H_20/mm)	Relative	0.255
K	.SOL	Soil conductivity (mm/hr)	Relative	1.162
CN3_SWF	.HRU	Soil Water Factor for CN3	Replace	0.965
LATQ_CO	.HRU	Lateral Flow Coefficient	Replace	0.136
LATT_TIME	.HRU	Lateral Flow Time (days)	Replace	106.216
PERCO	.HRU	Percolation Coefficient (fraction)	Replace	0.742

The calibration process followed the recommendations of Abbaspour (2017) in determining the necessary adjustments for each parameter, specifying whether an increase or decrease was required. Percentage changes were primarily applied to the curve number, while relative changes were used for some variable parameters across the basin, such as soil characteristics. Parameters that remain constant across the basin were updated by directly replacing them with newly inputted values. These parameters were adjusted until a good NSE value was achieved, while ensuring that base flows increased, peak flows were reduced, and a one-month lag on peak flows could be established. This varied approach facilitated a thorough exploration of the parameter space and contributed to refining the model's performance.

Before commencing the model calibration, it was observed that SWAT+'s initial simulated streamflow's exhibited discrepancies when compared to the observed streamflow's. These discrepancies were characterized by excessively high and premature peak flows, as well as instances where base flows reached zero values (Figure 5.1(a)). Additionally, there was no noticeable delay in the flow, further highlighting the need for calibration adjustments. This deviation from the characteristic streamflow of

the calibration point, which represents a perennial river with flows around 250 m^3/s during dry months, guided the primary objective of the calibration process. The aim was to address these issues by reducing peak flows, moderating the flow rate, and enhancing the representation of base flows.

Reducing the curve number (CN2) significantly reduced peak flows, while increasing the available soil moisture and conductivity (AWC, CN3_SWF, and K) helped sustain base flows even during drier months. It was also found that the hydrograph was particularly sensitive to lateral flow parameters (LATQ_CO and LATQ_TIME) during calibration, which allowed for a realistic delay in simulated flows, closely matching real-life scenarios and aiding in the representation of increased base flows during drier periods. Additionally, the creation of the Kilombero reservoir during the model setup contributed to the delayed streamflow's, further enhancing the realism of the hydrograph.

The calibration efforts proved successful, as demonstrated by a controlled increase in base flows, decreased peak flows, delayed flows, and the attainment of an NSE value of 0.70, which is indicative of good model performance, as outlined by Moriasi et al. (2017). However, the validation period yielded a slightly less favourable outcome, with an NSE value of 0.30. This lower value is likely due to a significant disparity during the 1973/74 season, which may be attributed to errors in either the modelled rainfall data or the observed river discharge data. The magnitude of this discrepancy suggests that it is more likely due to data errors rather than miscalibration of the model. The streamflow graphs for both the calibration and validation periods are presented below:

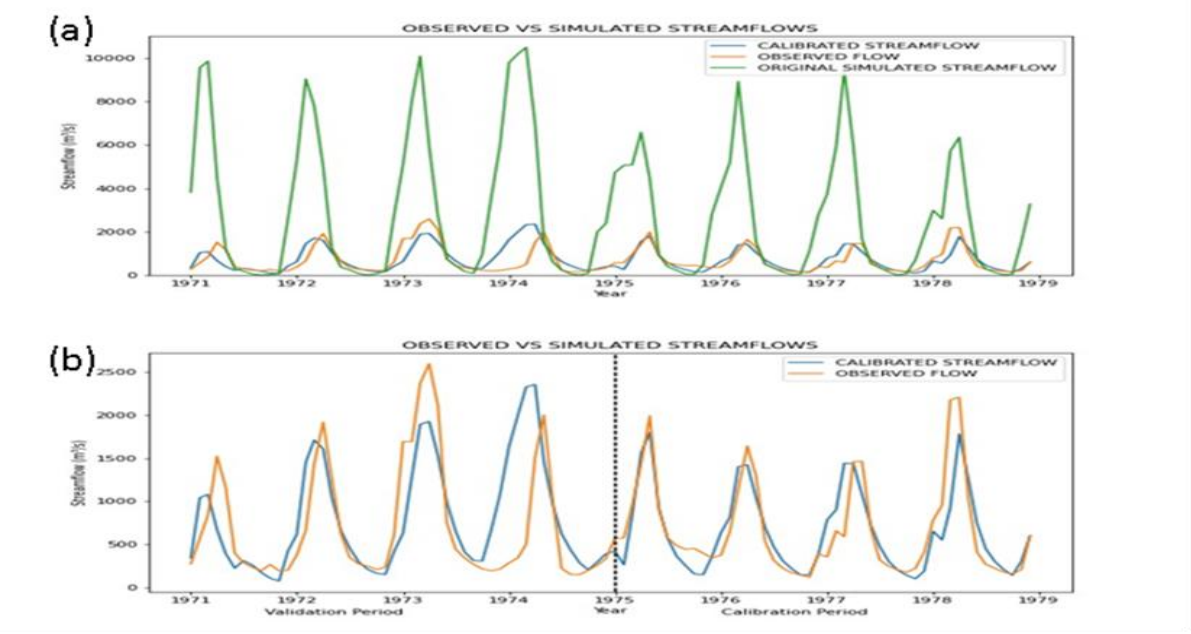

Figure 5.1: (a) Hydrograph of Stiegler Gorge (Observed flow – orange) vs SWAT+ simulation before calibration (green), (b) Simulated hydrograph after calibration (blue) vs Observed flow at Stiegler Gorge (orange) (shows validation and calibration periods).

5.2 Historical drought

Occurrence of the 3 different types of droughts within the 1991-2020 period were analysed at the sub-basin scale, i.e. using climate data (rainfall, temperatures and the derived potential evapotranspiration) averaged over each of the sub-basins (for SPI and SPEI), and streamflow data generated by the calibrated hydrological model (for SDI).

Figures 5.2 presents the frequency and intensity of the three considered drought indices in each of the sub-basins for severe droughts (SPI/SPEI/SDI < -1.5).

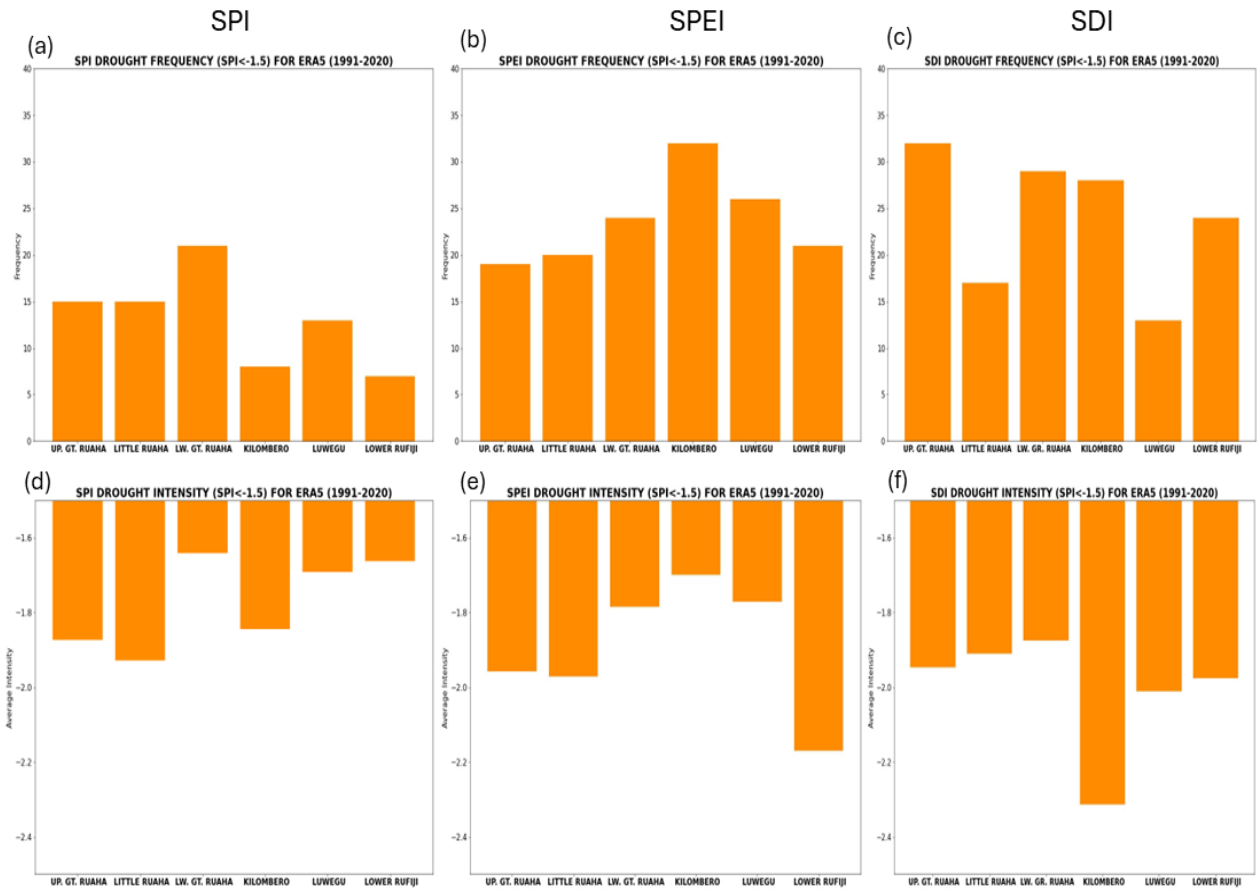

Figure 5.2: Comparative Analysis of Drought Frequency (a), (b), (c) and Drought Intensity (d), (e), (f) Across Different Indices Using ERA5-Land Data (1991-2020) for severe droughts (<-1.5).

Figure 5.2 reveals that, from 1991 to 2020, the Lower Great Ruaha sub-basin experienced the highest frequency of SPI-indexed severe meteorological droughts across the basin, with a total of 22 drought months. This was followed by the Upper Great Ruaha, Little Ruaha, and Luwegu sub-basins, which recorded relatively high climate modelled drought frequencies of about 15 months each. In contrast, the

Kilombero and Lower Rufiji sub-basins exhibited the fewest occurrences of severe drought, with only 7 and 6 SPI-indexed drought months, respectively, over the same period.

Regarding drought intensity, although the Lower Great Ruaha exhibits a high frequency of climate modelled droughts, the intensity of the droughts are relatively mild compared to other areas within the basin, with an average intensity of -1.6 on the SPI scale for droughts greater than -1.5. In contrast, both the Upper and Little Ruaha sub-basins are characterized by higher identified drought intensities, averaging around -1.9 for SPI-indexed droughts. The Kilombero sub-basin also shows significant vulnerability to drought intensity, with an average SPI value just above -1.8. Meanwhile, the Luwegu and Lower Rufiji sub-basins report historically lower drought intensities, with average SPI values around -1.7 for droughts greater than -1.5.

These findings suggest that, on average, the Upper and Little Ruaha regions are the most vulnerable to droughts driven by rainfall anomalies, historically experiencing both high frequency and intensity of such events. Although the Kilombero sub-basin has a lower frequency of SPI-indexed climate modelled droughts, likely due to its mountainous terrain, it still faces moderate drought intensities when droughts occur. The Lower Great Ruaha, while experiencing the highest frequency of SPI-indexed droughts, endures events of lower intensity compared to those in its upstream areas. In contrast, the Luwegu and Lower Rufiji sub-basins show moderate to low drought frequencies and intensities, likely influenced by their proximity to rainfall from the Indian Ocean.

The SPEI Figures (Figure 5.2(b) and (e)) reveal that incorporating Potential Evapotranspiration (PET) into the calculation of meteorological drought increases the frequency of climatically modelled drought events across all sub-basins, with each experiencing around 20 or more months of severe SPEI-indexed drought during the 1991–2020 period. Notably, the Kilombero, Luwegu, and Lower Great Ruaha sub-basins display the highest identified frequencies, with 33, 25, and 24 drought months, respectively. The rest of the sub-basins show slightly lower frequencies of SPEI-indexed drought events, with 21, 20, and 19 drought months recorded for the Lower Rufiji, Little Ruaha, and Upper Great Ruaha, respectively.

Interestingly, when examining average SPEI-indexed drought intensities across the sub-basins, a contrasting pattern emerges - basins with lower drought frequencies exhibit the highest intensities. This trend is most pronounced in the Lower Rufiji, which shows an average SPEI-indexed drought intensity approaching -2.2 for droughts exceeding the -1.5 threshold. Similarly, the Upper Great Ruaha and Little Ruaha basins display average drought intensities of approximately -2. In contrast, basins with the highest drought frequencies, such as Kilombero and Lower Great Ruaha, report lower average intensities, generally above -1.8.

This indicates that the Lower Rufiji, along with the Upper and Little Ruaha, are the most vulnerable to climate modelled SPEI-indexed droughts, characterized by both high intensity and a moderately high frequency of such events.

An examination of the SDI Figures (Figure 5.2(c)) reveals that the Upper and Lower Great Ruaha, along with the Kilombero and Lower Rufiji sub-basins, are the most susceptible to streamflow-indexed droughts, each recording close to or exceeding 25 drought months during the 1991–2020 period. In contrast, the Little Ruaha and Luwegu sub-basins exhibit the lowest frequencies of SDI-indexed droughts, with 16 and 13 drought months, respectively.

In terms of SDI-indexed drought intensity (for droughts < -1.5), the Kilombero sub-basin stands out as the most vulnerable, with an average intensity of approximately -2.2, despite its relatively low drought intensity in SPEI terms. The intensities for other sub-basins are also notable, ranging from -1.9 to -2 on the SDI scale, indicating substantial drought impacts across the basin.

The graphs illustrate that SDI-indexed drought frequency is notably high in the Upper Great Ruaha, despite a comparatively lower frequency of SPI- and SPEI-indexed droughts, potentially reflecting the river's ephemeral nature. The Kilombero and Luwegu sub-basins also exhibit high SDI drought intensities, likely due to the impact of frequent SPEI-indexed meteorological droughts on streamflow levels, combined with the influence of wetlands within these areas.

The SDI results for the Lower Great Ruaha and Lower Rufiji sub-basins cannot be directly compared to their SPI or SPEI counterparts due to differences in methodology. While SPI and SPEI were based only on basin area, SDI was calculated using measurements from basin outflows, incorporating hydrological inputs from upstream areas for a broader view of the basin's water dynamics.

5.3 Projected changes in LSU-level hydrological fluxes

5.3.1 Historical Period

An analysis of hydrological fluxes within the Landscape Units (LSUs) of the Rufiji Basin, derived from SWAT model simulations and ERA5-Land data for the 1991-2020 period (Figure 5.3), uncovers distinct spatial patterns across the basin's sub-basins. The Kilombero basin receives the highest annual rainfall within the studied area, with a significant portion of the region experiencing precipitation exceeding 1000 mm annually. This correlates with the basin's low frequency of SPI-indexed droughts, as shown in Figure 5.2. Similarly, the Little Ruaha sub-basin, particularly in its elevated and mountainous areas that encompass the Kipengere Mpanga Game Reserve, also registers high annual rainfall, reflecting similar hydrological characteristics to those observed in Kilombero.

In contrast, the regions encompassing the lower reaches of the Little Ruaha, Upper Great Ruaha, and the upper segments of the Lower Great Ruaha experience relatively lower rainfall, ranging from 200 mm to 700 mm annually. On the other hand, the Lower Great Ruaha, Luwegu, and Lower Rufiji sub-basins show varying precipitation patterns, with the Lower Rufiji standing out for notably high rainfall

levels (900-1100), especially in its low-lying sections, which contributes to its distinct hydrological characteristics within the basin.

Historical Actual Evapotranspiration (AET) (Figure 5.3(b)) rates as estimated by SWAT+ align closely with precipitation patterns, wherein regions with higher rainfall exhibit elevated predicted AET rates exceeding >1300mm. Analogous to precipitation, the Kilombero sub-basin had the highest AET rates, while other areas of the basin display moderate to lower rates. This illustrates that the actual AET at a catchment level reflects water availability in that catchment.

The Kilombero sub-basin features the highest modelleda annual average rates of lateral flow (>100) (Figure 5.3(c)), originating from the Udzungwa Mountains and the vicinity of the Kibasira Wetland. These high lateral flow rates extend into portions of the Lower Great Ruaha sub-basin and the upper mountainous regions of the Little Ruaha sub-basin. The Luwegu sub-basin exhibits moderate modelled lateral flow rates (25-50mm), while the remainder of the Rufiji basin demonstrates low lateral flow (0-10mm).

In terms of soil moisture, moderate to high levels are modelled in the Kilombero, Luwegu, Lower Rufiji, and parts of the Lower Great Ruaha sub-basins (>100mm annual average) (Figure 5.3(d)). Conversely, areas surrounding the Mtera reservoir exhibit low predicted soil moisture, aligning with the patterns observed in the lateral flow map (<100mm annual average).

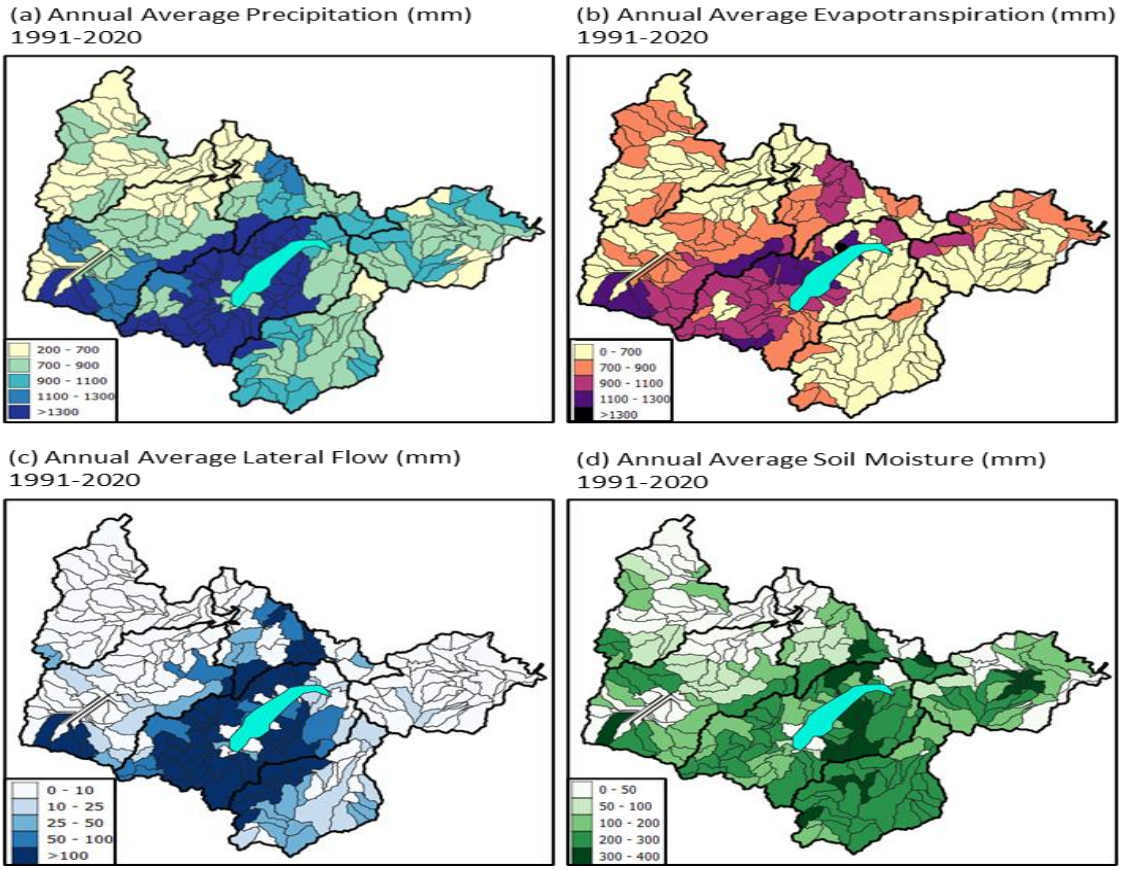

Figure 5.3: Historical LSU maps showing the (a) Annual Average Precipitation, (b) Annual Average Evapotranspiration, (c) Annual Average Lateral flow, (d) Annual Average Soil Moisture in mm for the 1991-2020 period over the Rufiji Basin, derived from SWAT+ and ERA5-Land climate data.

5.3.2 Hydrological fluxes under RCP 4.5 projections

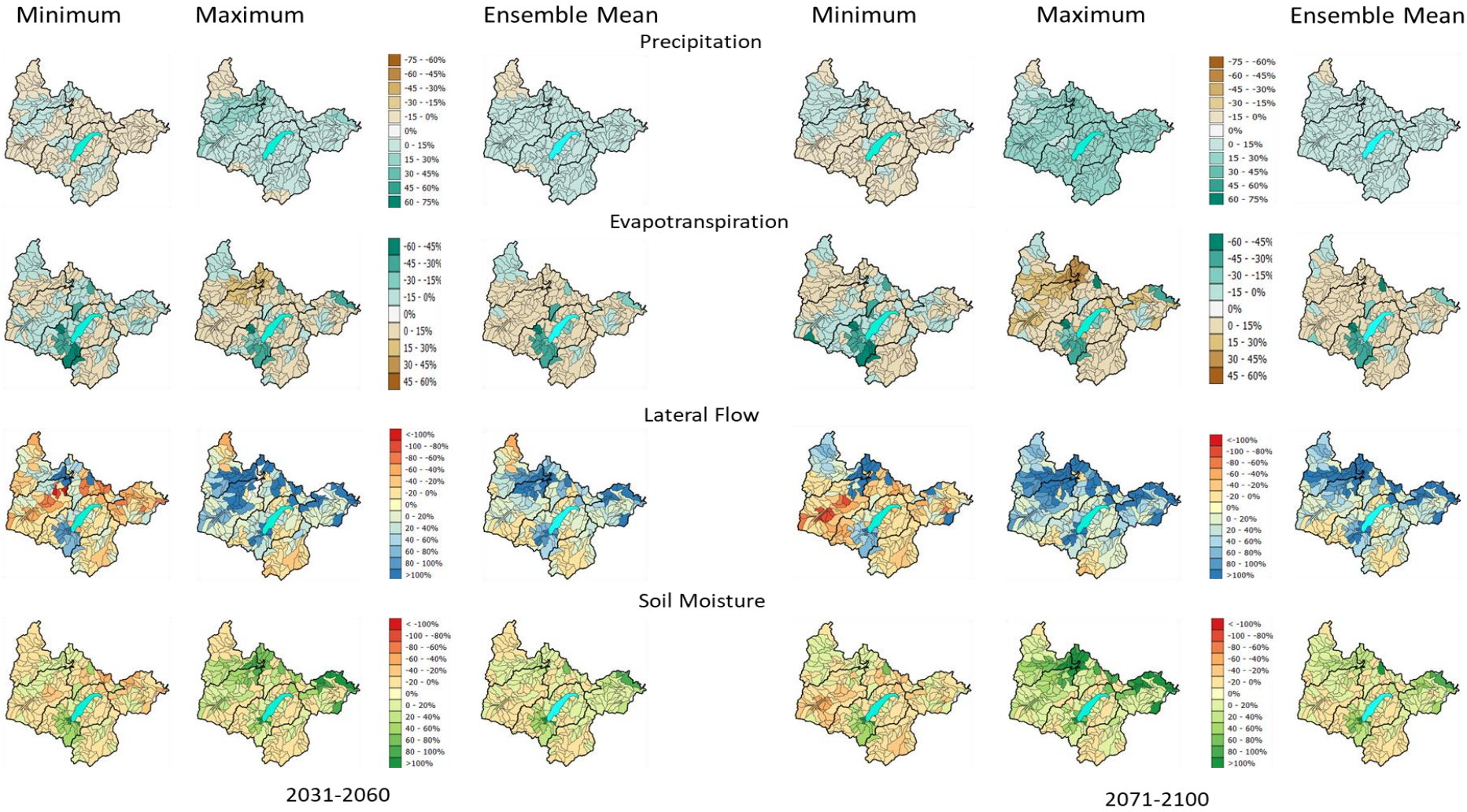

Figure 5.4: Spatial Maps displaying the Minimum, Maximum, and Ensemble Mean changes in values for Precipitation, Evapotranspiration, Lateral Flow, and Soil Moisture under RCP 4.5 scenario for the two time periods: 2031-2060 and 2071-2100, compared to 1991-2020

5.3.3 Hydrological fluxes under RCP 8.5 projections

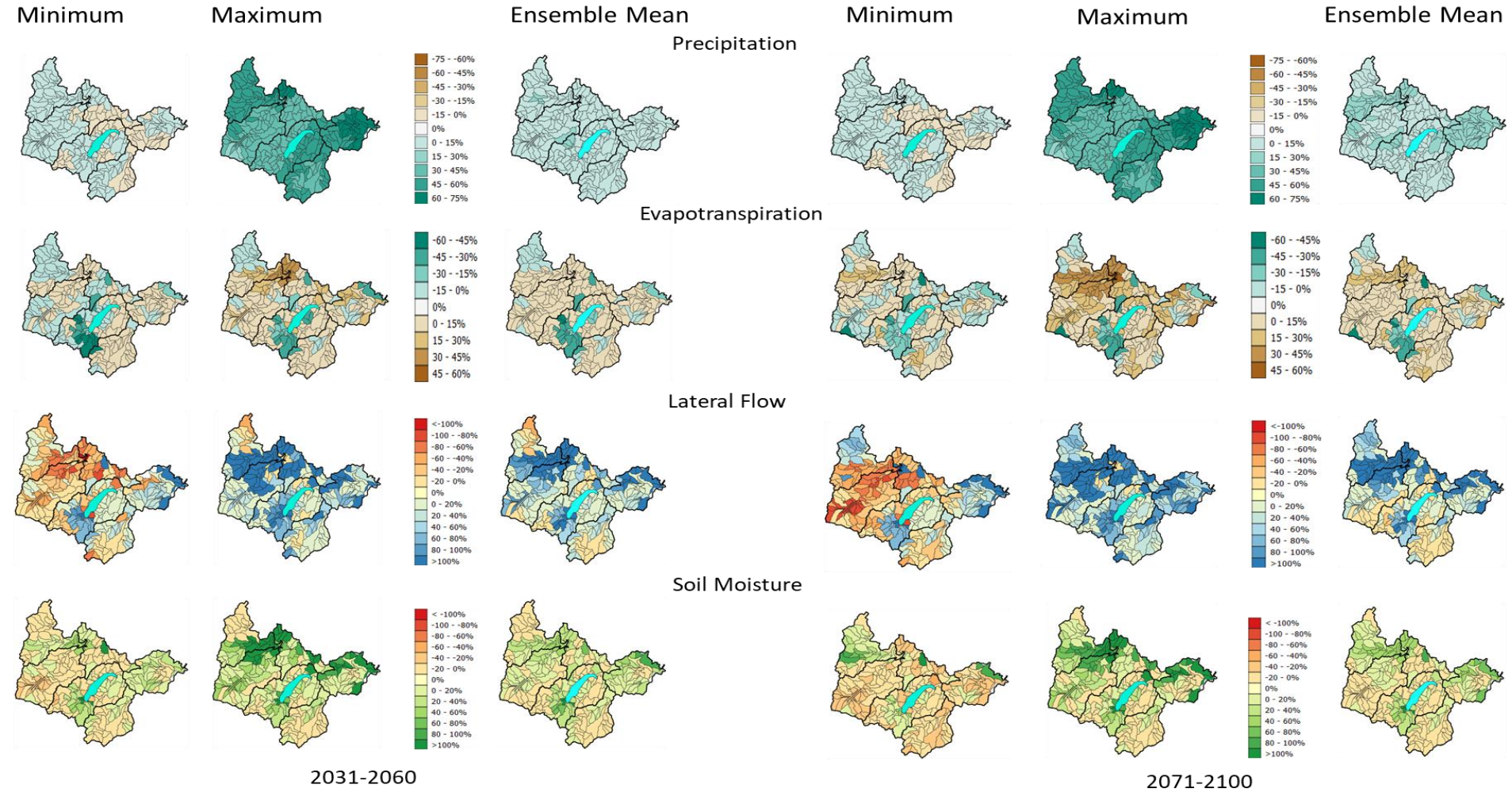

Figure 5.5: Spatial Maps displaying the Minimum, Maximum, and Ensemble Mean changes in values for Precipitation, Evapotranspiration, Lateral Flow, and Soil Moisture under RCP 4.5 scenario for the two time periods: 2031-2060 and 2071-2100, compared to 1991-2020

5.3.3.1 Changes in rainfall

Under the RCP 4.5 scenario (Figure 5.4) for 2031–2060, projections indicate increased rainfall around the Mtera Reservoir. This trend is consistent across both the driest and wettest model scenarios. The ensemble mean suggests that most of the basin will experience wetter conditions, with rainfall increases of 0–15%. However, the upper regions of the Upper Great Ruaha stand out, showing consistent reductions in rainfall across the driest, wettest, and average scenarios.

In the far future (2071–2100) under RCP 4.5 (Figure 5.4), precipitation trends are similar to those projected for 2031–2060. The driest models predict widespread drying across the sub-basin, except for areas near the Mtera Reservoir, where rainfall increases. Conversely, the wettest models project a 15–30% rise in average annual precipitation across most of the basin, with the upper regions of the Upper Great Ruaha continuing to experience reductions. The ensemble mean suggests precipitation rates comparable to those of the 2031–2060 period across the basin.

Precipitation projections under the RCP 8.5 scenario (Figure 5.5) indicate an overall increase in rainfall across the basin. The driest model scenarios show only a few sub-basin areas with reduced rainfall, suggesting a broader trend of increased precipitation. The wettest models project significant rainfall increases, particularly around the Mtera Reservoir and the Lower Rufiji, with rises ranging from 60–75%. The ensemble mean reflects a consistent basin-wide increase in rainfall, predominantly in the 15–30% range. Toward the century's end, these patterns persist, with widespread higher rainfall anticipated across the basin.

5.3.3.2 Changes in AET

Analysis of the percentage change in modelled Actual Evapotranspiration (AET) under the RCP 4.5 scenario (Figure 5.4) for the 2031–2060 period reveals a general increase in AET in areas projected to experience higher rainfall. Most of the basin shows an AET increase within the 0–15% range, while regions surrounding the Mtera Reservoir exhibit slightly higher increases of 15–30%, likely reflecting the elevated rainfall projections for this area. In contrast, the upper regions of the Kilombero sub-basin and the Upper Great Ruaha display a decline in AET, consistent with the anticipated decrease in rainfall.

Modeled Actual Evapotranspiration (AET) rates under the RCP 8.5 scenario (Figure 5.5) closely align with those of the RCP 4.5 scenario, showing notable increases around the Mtera Reservoir, particularly in the wettest and ensemble mean projections. Consistent with the RCP 4.5 scenario, most of the basin is expected to experience rising AET rates, while areas within the Kilombero, Upper Great Ruaha, and Lower Rufiji sub-basins exhibit localized decreases. In the far future, these trends persist, with an overall increase in AET rates, especially around the Mtera Reservoir. The wettest projections indicate

pronounced increases in evapotranspiration in regions such as the Little Ruaha, Upper Great Ruaha, and the Luwegu sub-basins.

5.3.3.3 Changes in lateral flow

Changes in lateral flow correspond to projections of increased precipitation or reduced evapotranspiration in many regions within the Rufiji Basin. Figure 5.4 illustrates an expansion of areas with increased lateral flow around the Mtera Reservoir in the far future, compared to the modeled historical average (Figure 5.3). However, a persistent decrease in lateral flow is observed in the Little Ruaha, with reductions reaching the -20% to -40% range in the extreme driest case. The Luwegu sub-basin also shows a consistent decline in flow rates across the driest and mean scenarios.

In the Kilombero basin, the projected rise in lateral flow may result from the anticipated decrease in evapotranspiration in the near future. Around the Mtera Reservoir, higher lateral flow rates are likely driven by the projected increase in rainfall. Additionally, the Lower Rufiji region is expected to experience increases in lateral flow. However, the driest model projections suggest that the Little Ruaha could face adverse impacts, leading to further reductions in flow rates. The Luwegu sub-basin shows a consistent decreasing trend in lateral flow across the driest, wettest, and ensemble mean projections.

In Figure 5.5, the driest model projections indicate a decrease in lateral flow around the Mtera Reservoir in the near future under RCP 8.5, with this area of reduced flow expanding as the century progresses. Conversely, the wettest model projections suggest that this region is likely to experience increased lateral flows. The ensemble mean for both timescales indicates a general rise in lateral flows in the area, with the extent of this increase expanding over time.

Most parts of the Kilombero and Lower Rufiji sub-basins are projected to experience elevated lateral flows under both dry and wet model scenarios. However, the Little Ruaha shows varying outcomes depending on the scenario. Under the driest conditions, lateral flows are projected to decline significantly, while the wettest projections indicate increased flows. On average, the model ensemble mean suggests a mix of reduced and increased flows, ranging from -20% to 20% in the upper regions of the basin. Similar to the Little Ruaha, the Luwegu sub-basin shows divergent outcomes, with lateral flow changes ranging from -20% to 20% across scenarios. However, the ensemble mean indicates a drying trend for lateral flows across most of the basin.

5.3.3.4 Changes in soil moisture

For the period of 2031-2060, soil moisture across most of the basin fall within the -20% to 20% range (Figures 5.4 and 5.5). Areas projected to experience a slightly higher elevation in soil moisture rates include the regions around the Mtera Reservoir, parts of the Kilombero Basin, and the Lower Rufiji.

Conversely, almost the entire Luwegu, Little Ruaha, and Upper Great Ruaha are projected to witness a decrease in soil moisture (Figures 5.4 and 5.5). Similar trends persist in the far future, with the same areas exhibiting comparable conditions. There is a slight increase in both the area and rates around the Mtera Reservoir in the far future

Soil moisture rates within the basin display patterns similar to lateral flow rates, where areas with higher lateral flows also exhibit higher soil moisture rates. The most significant percentage increases in soil moisture are anticipated to be concentrated around the Mtera Reservoir, with similar occurrences in the Kilombero and Lower Rufiji Basins. The remaining portions of the basin are projected to have lower rates of soil moisture, with Figures falling into the 0 to -20 percentage range. The areas that may be most affected include the Luwegu Basin, parts of the Little Ruaha Basin, and the Upper Great Ruaha.

5.4 Future meteorological and hydrological drought

5.4.1 Projected changes in frequency of meteorological and hydrological Drought

Evaluation of future drought conditions are based on the climate data from the multi-model CORDEX ensemble, and on streamflow's simulated by the calibrated hydrological model when forced with the climate model data.

As outlined in the methodology section the evaluation focuses on comparison of two future periods 2031-2060 and 2071-2100 with the historical period 1991-2020. Figure 5.6 and 5.7 show model ranges of frequency for occurrence of severe droughts (< -1.5) indexed by SPI, SPEI and SDI for both the RCP 4.5 and RCP 8.5 scenarios respectively.

The SDI results of the Lower Great Ruaha and the Lower Rufiji sub-basins cannot be directly aligned with their SPI or SPEI counterparts. This discrepancy arises from differences in the methodologies used for these indices. While their SPI and SPEI calculations were based solely on basin area and did not consider contributions from upperstream sub-basins, the SDI calculations were derived from measurements taken at the basin outflows (culmination of upstream rivers). Consequently, the SDI results inherently incorporate hydrological inputs from upstream areas, providing a broader representation of the basin's water dynamics compared to the more localized focus of SPI and SPEI.

5.4.1.1 RCP 4.5

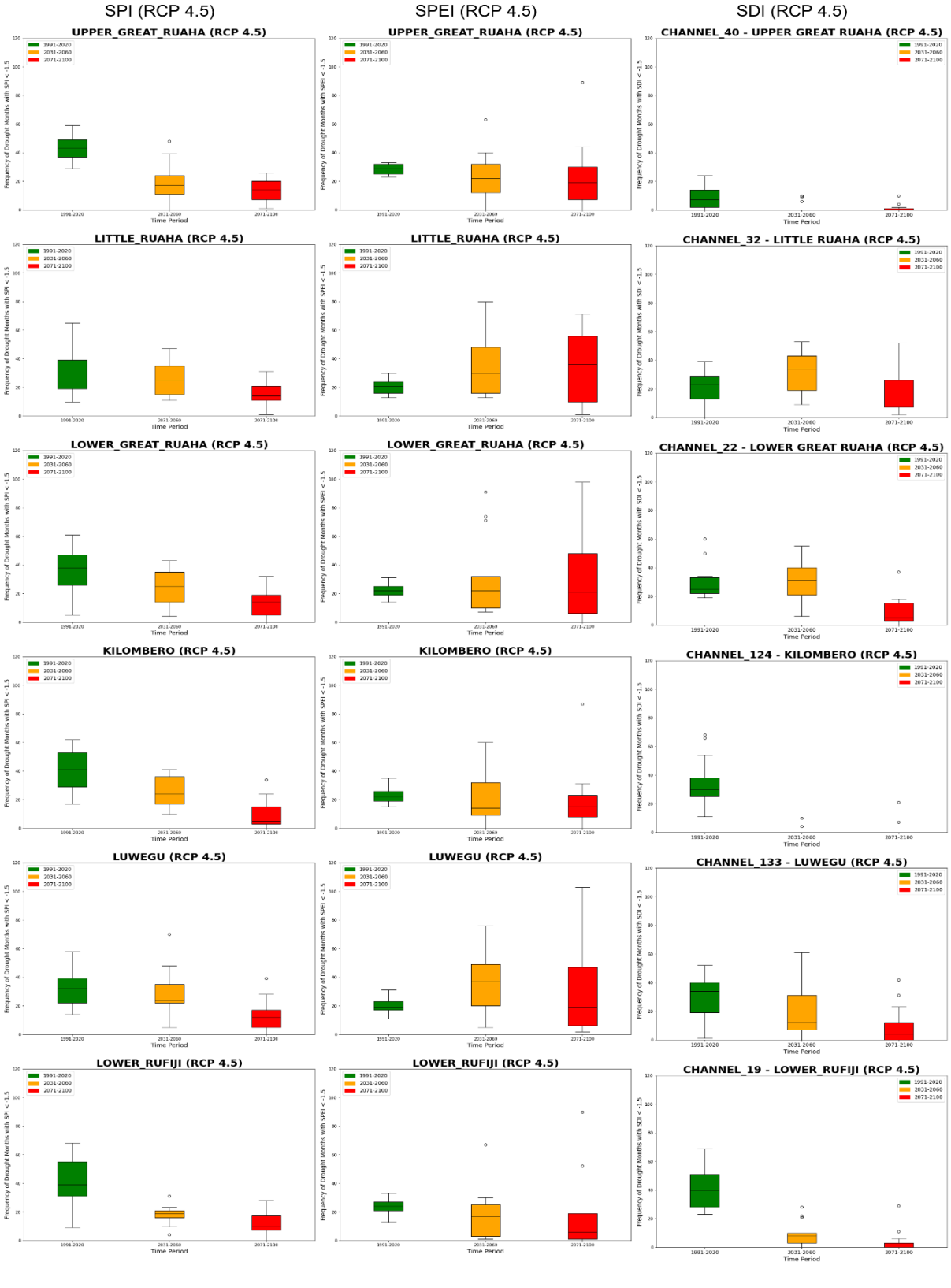

Figure 5.6: Boxplots of Frequencies of Drought Months with SPI/SPEI/SDI < -1.5 over various time periods for the RCP 4.5 scenario

The SPI boxplot presented above highlights a significant projected decline in the frequency of meteorological drought across all sub-basins within the Rufiji Basin over time. This trend suggests a decreasing occurrence of SPI-indexed drought events as the century progresses, with the lowest frequencies observed towards its end. This reduction is likely attributed to the generally increasing rainfall projected across the Rufiji Basin in future climate scenarios.

Analysis of the projected frequency of SPEI-indexed droughts reveals that considering PET as a driver of drought has a discernible impact on predictions across various sub-basins. The Upper Great Ruaha sub-basin however shows no noticeable projected change in the frequency of drought occurrences for the RCP 4.5 scenario, with the mean frequency in the near and far future being similar to historical conditions. The Little Ruaha and Luwegu are projected to experience increases in frequency of SPEI-indexed drought in both the near and distant future.

In the Lower Great Ruaha, the mean frequncy of SPEI-indexed drought is projected to reduce slightly over the course of the century. Nevertheless, projections for the far future are characterized by a strong uncertainty, with some models projecting heightened frequency of SPEI-indexed drought reaching nearly 100 months within a 30-year timeframe towards the close of the century, compared to the ensemble mean of about 20 months/30 years.

The Kilombero exhibits a decline in the mean frequencies of SPEI indexed droughts within the sub-basin in both the near and far future. It is important to note, however, that some models show that there could however be a possibility of an increase in the number of drought months in the near future.

The Luwegu demonstrates an increaseing likelihood of SPEI-indexed meteorological drought months as the century advances. Towards the end of the century, values exceed the 100-month mark for the 30-year climatic time period, i.e. representing approx. 30% of the time. Interestingly, the mean of the near future surpasses that of the far future, indicating high labels of decadeal scale variability.

In the furthest downstream basin, the Lower Rufiji, there is a reduction of frequency of SPEI-drought months in both the near and far future.

The SDI plots generally suggest a reduction in the frequency of projected hydrological drought in the Upper Great Ruaha, Kilombero, Lower Rufiji, and Luwegu sub-basins as time progresses. However, certain extreme models indicate the potential for a slight increase in the frequency of SDI-drought months in the Luwegu sub-basin during the near future.

Both the Little Ruaha and Lower Great Ruaha exhibit a higher frequency of SDI-drought in the near future when compared to the historical period. Moreover, within the Little Ruaha, some models show a comparable maximum amount of drought months in the far future when compared to the near future, albeit with the mean model ensemble being lower.

5.4.1.2 RCP 8.5

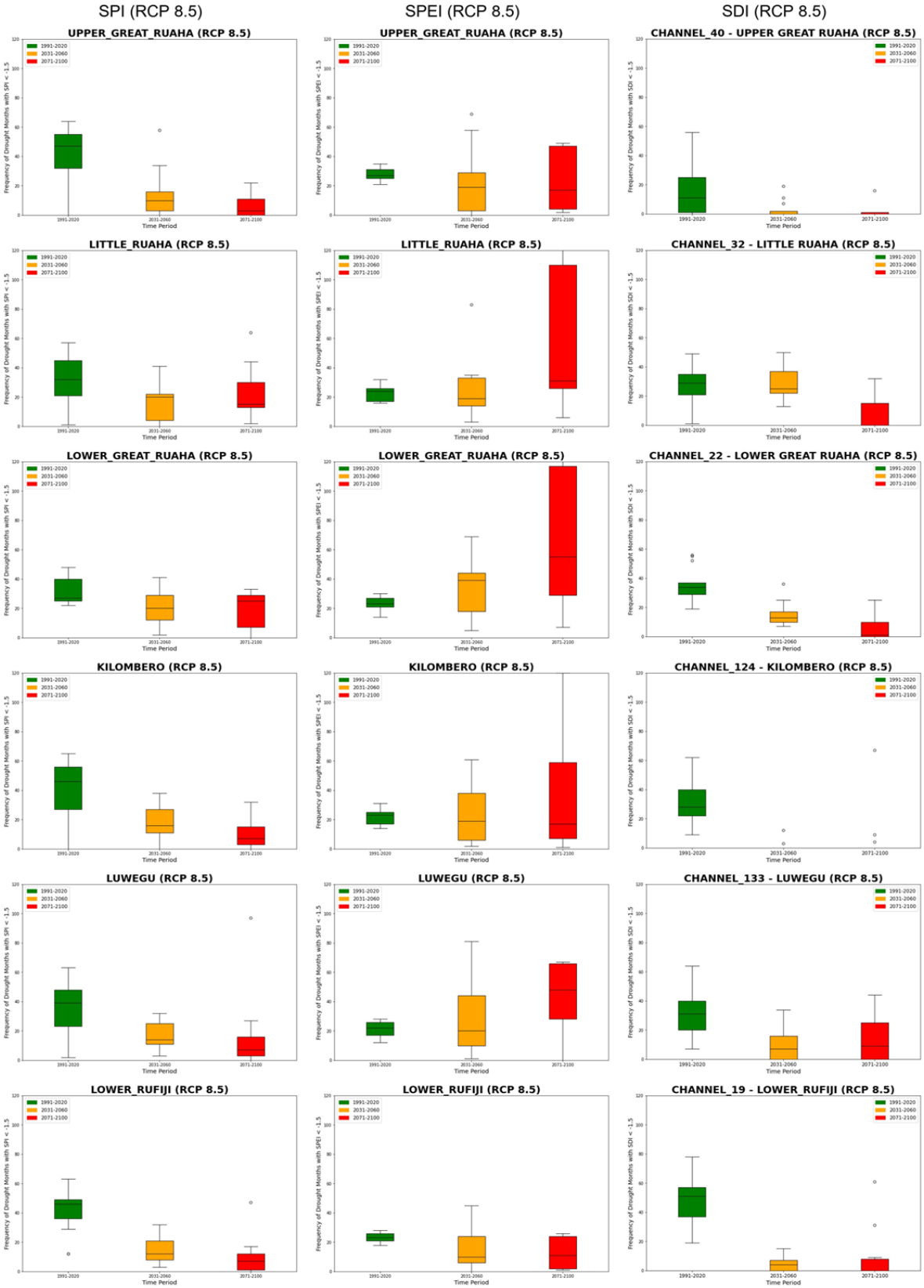

Figure 5.7: Boxplots of Frequencies of Drought Months with SPI/SPEI/SDI < -1.5 over various time periods for the RCP 8.5 scenario

Much like the RCP 4.5 scenario, the drought frequency box plots for SPI droughts reveals a downward trend in droughts as the century progresses under the RCP 8.5 scenario. Notably, only the Little Ruaha sub-basin displays a comparable sustained drought frequency projection when comparing the near and far future.

Similar to the RCP 4.5 scenario, the SPEI graphs for RCP 8.5 indicate an increase in the frequency of meteorological drought across most sub-basins as the century progresses, driven by the inclusion of the PET factor. For the near future (2031–2060), the RCP 8.5 SPEI graphs show a significantly higher magnitude of drought frequency compared to the RCP 4.5 graphs, except in the Little Ruaha sub-basin, where the trend is less pronounced.

Towards the close of the century, the frequency of droughts in three basins—specifically, the Little Ruaha, Lower Great Ruaha, and Kilombero—undergoes a strong increase. Each of these basins surpasses the 120-month mark/30-year period, signifying the potential for a period of over 10 years within the 30-year timeframe experiencing SPEI-indexed severe meteorological drought conditions (Figure 5.7). For comparison, the frequency of such droughts during the 1991–2020 period (Figure 5.2) ranged between 20–40 months, historically accounting for approximately 10% of the time. The ensemble mean values also show substantial increases for the Little Ruaha and Lower Great Ruaha sub-basins. In contrast, the Upper Great Ruaha and Luwegu catchments exhibit similar drought frequencies in the far future compared to the near future. Notably, the Lower Rufiji sub-basin is projected to experience a decline in SPEI-indexed drought frequency towards the end of the century.

The SDI trends under the RCP 8.5 scenario closely mirror those observed in the RCP 4.5 scenario, showing a consistent decline in the frequency of hydrological droughts throughout the century. Notable exceptions include the Little Ruaha in the near future, where drought frequency remains comparable to historical levels, and the Luwegu, where some model projections indicate a slight increase in drought frequency in the far future compared to the near future. Despite these variations, the ensemble mean projections for both scenarios remain largely similar.

Overall, the frequencies of SDI-indexed hydrological droughts at the basin outlets and calibration points appear to be minimally influenced by the intensification of global warming conditions.

.

5.4.2 Projected changes in intensity of meteorological and hydrological Drought

Evaluation of future drought conditions are based on the climate data from the multi-model CORDEX ensemble, and on streamflows simulated by the calibrated hydrological model when forced with climate model data.

As outlined in the methods section, this evaluation focuses on comparison of two future periods 2031-2060 and 2071-2100 with the historical period 1991-2020. Figures 5.6 and 5.7 show ranges of intensities of occurrence of severe droughts (< -1.5) indexed by SPI, SPEI and SDI for both the RCP 4.5 and RCP 8.5 scenarios respectively.

5.4.2.1 RCP 4.5

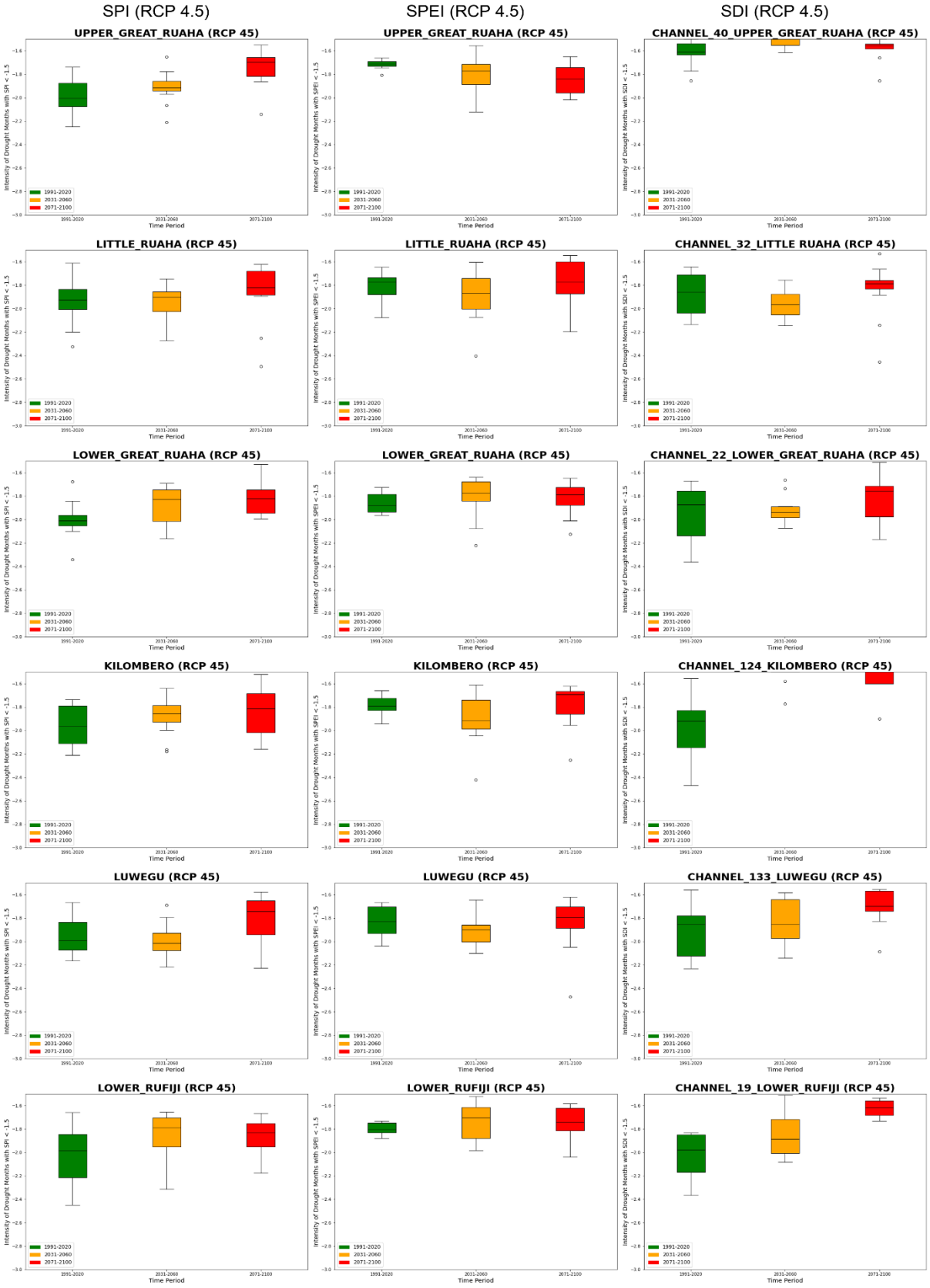

Figure 5.8: Boxplots of Intensities of Drought Months with SPI/SPEI/SDI < -1.5 over various time periods for the RCP 4.5 scenario

Unlike the steadily decreasing SPI-indexed drought frequency, SPI intensity shows greater variability, particularly in the near future, indicating fluctuating drought severity despite reduced frequency.

The RCP 4.5 SPI intensity plot (Figure 5.8) reveals that certain models project a modest increase in drought intensity in the near future across the Little Ruaha, Lower Great Ruaha, and Luwegu sub-basins. However, the mean intensities across these models remain constant or exhibit a decrease when compared to the historical period within these sub-basins. In contrast, both the mean and potential drought intensities are projected to decline in the Upper Great Ruaha, Kilombero, and Lower Rufiji sub-basins. In the far future, a consistent reduction in SPI-drought intensity is observed across all sub-basins, with the exception of the Luwegu and Kilombero sub-basins. In these two regions, while the maximum projected intensities remain comparable, the ensemble mean values are lower than those observed during the historical period.

The influence of PET on drought intensities demonstrates a clear trend of increasing drought severity as the century progresses, particularly in the near future, as illustrated by the SPEI intensity graphs (Figure 5.8). The Upper Great Ruaha, Lower Great Ruaha, Lower Rufiji, Kilombero, and Luwegu sub-basins show an increase in drought intensity in the near future relative to the historical period. In contrast, the Little Ruaha sub-basin exhibits comparable drought intensities, albeit with a lower negative mean compared to the historical period.

Towards the end of the century, drought intensities indexed by the SPEI exhibit similar values to those observed in the mid-century across most sub-basins. However, some models indicate a slight increase in the potential intensity of droughts in the Lower Great Ruaha and Kilombero sub-basins. The Luwegu basin maintains intensity probabilities comparable to the near future, albeit with a reduction in the mean intensity. In the Lower Rufiji, some models project an increase in drought intensities in the far future compared to both the near future and historical periods. Notably, model projections for the Little Ruaha basin suggest the most significant changes in drought intensity in the far future, with one model forecasting an average SPEI drought intensity that exceeds the < -2.2 threshold.

The SDI intensity plots (Figure 5.8) show that there is a general decreasing trend in intensity of hydrological drought across almost all basins as the century progresses. The Little Ruaha exhibits similar maximum intensities in the near future compared to the historical period with an increase in the mean. The Luwegu, Lower Rufiji, and Lower Great Ruaha show decreased intensities compared to the historical period, while the Kilombero and Upper Great Ruaha show little impact of intensive hydrological droughts.

Interestingly, comparisons across SPEI and SDI reveal a similar mean intensity of meteorological and hydrological drought in the near future for the Little Ruaha, Lower Great Ruaha, Luwegu and Lower Rufiji sub-basins.

5.4.2.2 RCP 8.5

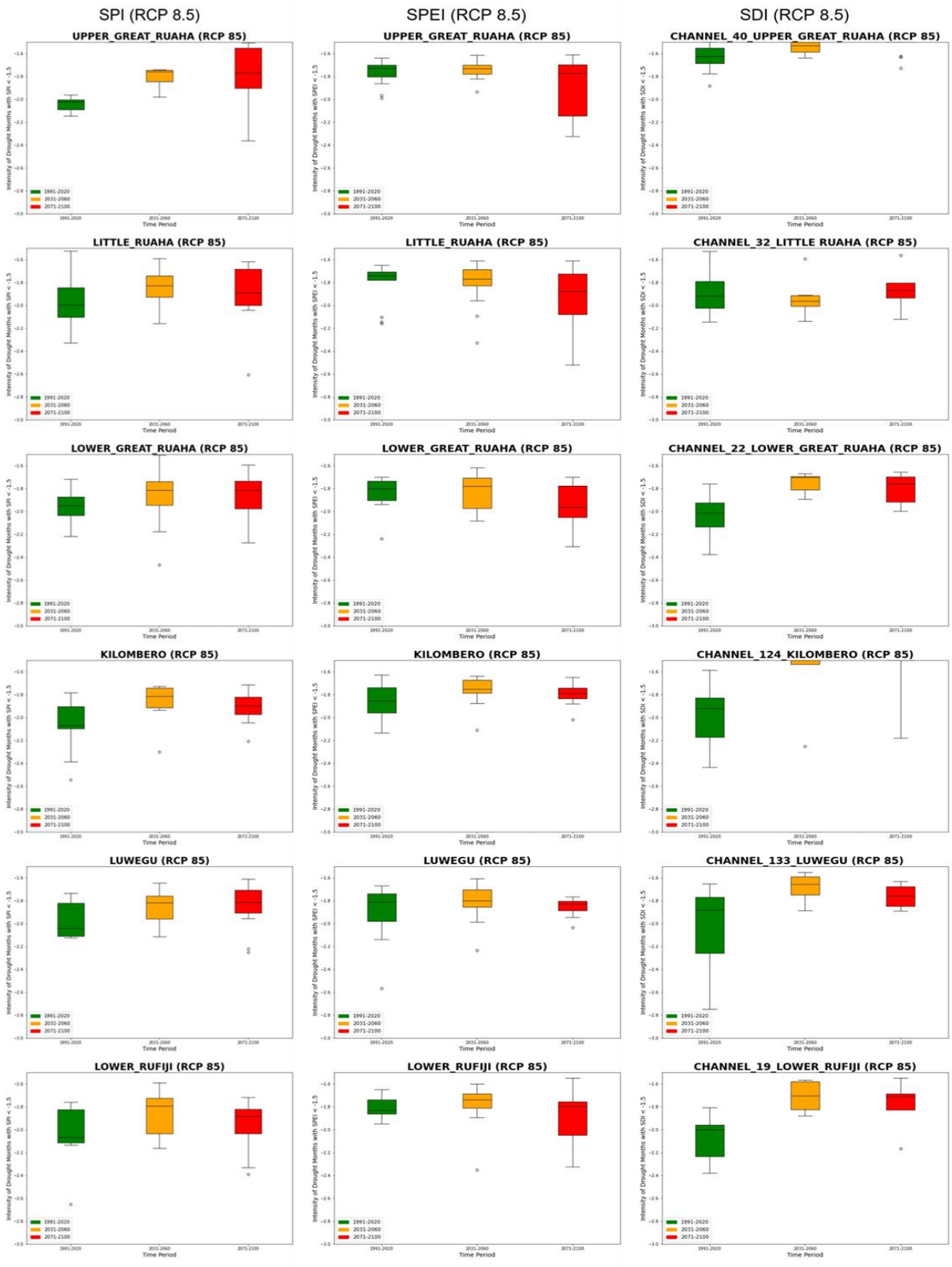

Figure 5.9: Boxplots of Intensities of Drought Months with SPI/SPEI/SDI < -1.5 over various time periods for the RCP 8.5 scenario

The RCP 8.5 SPI intensity graph (Figure 5.9) reveals variable drought intensities especially in the latter part of the century when compared to the near future. In the near future, the Upper Great Ruaha and Kilombero sub-basins most model projections exhibit intensities similar to the historical period, with a reduction in SPI-indexed drought intensity events. Model projections for the latter part of the century suggest that the Upper Great Ruaha, Lower Great Ruaha, and Lower Rufiji sub-basins may experience an increased potential for SPI-indexed drought intensity, surpassing the SPI < -2.4 threshold. However, this is accompanied by a reduction in the overall mean values.

The SPEI graphs (Figure 5.9) illustrate decreases of drought intensites in the near future when compared to the historical except for the Little Ruaha and the Lower Great Ruaha. A heightened propensity for intensified SPEI-indexed meteorological drought is anticipated in the distant future across all sub-basins, with the exception of Kilombero and Luwegu, where magnitudes are anticipated to remain consistent with mid-century levels. The susceptibility to meteorological drought, as ascertained through the Standardized Precipitation Evapotranspiration Index (SPEI), is notably elevated, with values produced by some models approaching -2.4. Specifically, the mean intensity of severe meteorological drought in the Little Ruaha and Lower Great Ruaha is projected to approximate > -2.0.

As we transition from SPI to SPEI graphs, it becomes apparent that the inclusion of the PET variable consistently stabilizes or increases the likelihood of more intense meteorological droughts in the Upper Great Ruaha, Little Ruaha, Lower Great Ruaha, and Lower Rufiji sub-basins, particularly in the far future. Furthermore, the impact of increased global warming, as reflected in the comparison between RCP 4.5 and RCP 8.5 scenarios, similarly elevates the likelihood of more intense droughts in these four basins, while slightly reducing the probability of such events in the Kilombero and Luwegu sub-basins.

The SDI plot (Figure 5.9) shows a decrease in hydrological drought intensity for all basins in the near future under the RCP 8.5 scenario, except for the Little Ruaha sub-basin, which exhibits similar intensities to the historical period. As the century progresses, increased warming rates influence the hydrology of all basins, with all sub-basins maintaining consistent intensities between the near and far future— a trend less evident in the RCP 4.5 scenario. The Lower Great Ruaha shows an increase in both mean and potential SDI-indexed drought intensity in the far future compared to the near future. The Lower Rufiji, Luwegu, and Little Ruaha show similar lower bound thresholds in the far future. Kilombero's lower bound exceeds the -2.2 mark, while the Upper Great Ruaha has two outliers surpassing the near future values. When comparing across scenarios, the RCP 8.5 scenario exacerbates drought intensities in the Little Ruaha, Luwegu, and Lower Rufiji sub-basins during the latter part of the century, with more extreme intensities than in the RCP 4.5 scenario.

CHAPTER 6: DISCUSSION

The primary objective of this study was to evaluate potential drought occurrences within the study area, with a focus on both meteorological and hydrological droughts. The analysis emphasized assessing hydrological fluxes alongside the frequency and intensity of drought events, employing specific drought indicators. As stated by Nikulin et al. (2018), there is a notable lack of detailed studies on the potential effects of future global warming scenarios, such as 1.5°C, 2°C, or higher, on regional climates in Africa. This gap is particularly evident in the East African region, where research on drought and climate change remains limited. Most existing studies rely on coarse-resolution global models, which fail to capture the complexities of regional climate dynamics.

For meteorological drought analysis, the study utilized two key indicators: the Standardized Precipitation Index (SPI) and the Standardized Precipitation Evapotranspiration Index (SPEI). SPI was applied to assess potential variations in rainfall patterns within the basin, while SPEI accounted for the combined effects of rainfall and evapotranspiration on meteorological drought conditions. For hydrological drought evaluation, the Streamflow Drought Index (SDI) was employed to detect and quantify hydrological drought occurrences within the basin.

To gain a better understanding of the basin's hydrological dynamics, the study incorporated hydrological modeling using the SWAT+ model. This approach enabled the simulation of streamflow during historical periods and projections under future climate scenarios, providing insights into both current and anticipated hydrological behaviors. Additionally, changes to hydrological fluxes, encompassing hydrological parameters such as precipitation, evapotranspiration, lateral flow, and soil moisture, was included to discern the areas or extents of basins affected by projected changes. This spatial analysis was conducted across different time slices for both the RCP 4.5 and RCP 8.5 scenarios focusing on the driest, wettest and mean model output, contributing valuable insights into the projected changes in spatial distribution of these critical variables and their potential impact on the basin.

The results indicate a projected decrease in the frequency of SPI-drought events across all sub-basins as the century progresses, suggesting an overall increase in rainfall within the basin. However, an increase in the intensity of SPI-droughts is observed in certain sub-basins, highlighting that while drought events may become less frequent, their severity could intensify.

Climate change and increased warming are generally associated with heightened evapotranspiration, which can exacerbate drought frequency and severity (Naumann et al., 2018). By incorporating potential evapotranspiration (PET) into the calculation of meteorological drought, the projections offer a more nuanced and realistic representation of future drought occurrences. The analysis reveals an

increase in drought frequency across almost all sub-basins in both the near and far future, particularly under the RCP 8.5 scenario. However, there is variability in the intensity of these droughts, with some basins demonstrating greater vulnerability to more severe conditions.

The Great Ruaha Basin, particularly the Little Ruaha sub-basin, is highly vulnerable to the impacts of climate change and water resource challenges. Historically, the basin has been the subject of numerous studies due to its issues with precipitation deficits and water scarcity (Pauline et al., 2017; Mtahiko et al., 2006; Sokile et al., 1993; Mwakalila, 2013). However, much of the existing research has focused primarily on past trends, with few studies offering projections for future climate scenarios. Pauline et al. (2017) highlight the vulnerability of the Upper Great Ruaha and Little Ruaha catchments to SPI-induced drought, utilizing data from three gauging stations, and demonstrate an increased risk of severe droughts in the later years of their study. Similarly, Mtahiko et al. (2006) and Mwakalila (2013) underscore the sensitivity of the Little Ruaha sub-basin to historical changes in precipitation and temperature, and their effects on water resources.

This study confirms that the Little Ruaha is particularly at risk, with projections suggesting reduced rainfall and increased evapotranspiration if drier climate scenarios are followed (Figures 5.4 and 5.5). Such changes could have significant negative impacts on lateral flow and soil moisture storage within the sub-basin (Figure 5.5). Even though the SPI analysis (Figures 5.6 to 5.9) shows a decline in both the frequency and intensity of SPI-indexed droughts, with the near future under the RCP 4.5 scenario showing drought intensities comparable to those observed historically, the SPEI analysis reveals an increase in drought frequency under both scenarios (Figures 5.6 and 5.7). While the intensity of SPEI-induced droughts is expected to remain stable in the near future, an increase is projected for the far future under the RCP 4.5 scenario (Figure 5.8). The RCP 8.5 scenario on the other hand predicts a consistent upward trend in drought intensity throughout the course of the century (Figure 5.9).

Moreover, the frequency of SDI droughts is projected to rise in the near future under both scenarios, with this trend continuing into the far future under the RCP 4.5 scenario (Figure 5.6). SDI drought intensities are expected to remain consistent with historical patterns in both the near and far future under both scenarios (Figures 5.8 and 5.9). These projected changes in drought conditions could have substantial negative consequences for both the agricultural and hydrological sectors, particularly for farmers who rely on soil moisture and water availability for crop production. Furthermore, the region's wetlands and wildlife, which are essential components of local ecosystems, may be severely threatened as a result of these projected climate changes.

The Upper Great Ruaha, which has been relatively understudied due to its predominant coverage by game reserves, is projected to experience wetter conditions on average, particularly in areas surrounding the Mtera Reservoir. Hydrological flux maps (Figures 5.4 and 5.5) suggest that most models predict increased wetting in this region, which historically received some of the lowest rainfall levels within

the basin (Figure 5.3). Additionally, projections indicate an increase in lateral flow and soil moisture under the wettest or mean ensemble model trajectories, further highlighting potential improvements in hydrological conditions in these areas.

SPI-indexed drought conditions in the Upper Great Ruaha show a decline in frequency and intensity under both RCP 4.5 and 8.5 scenarios, with the exception of far-future conditions under the RCP 8.5 scenario, where intensities are projected to rise. However, dry model simulations suggest that this area could still be highly susceptible to drought in the far future under RCP 8.5 due to increased evapotranspiration, leading to reductions in lateral flow and soil moisture (Figures 5.4 and 5.5). SPEI projections portray slight increases in the frequency of meteorological droughts in both the near and far future under RCP 4.5 (Figures 5.6 and 5.8), albeit with lower intensities. Conversely, the RCP 8.5 scenario (Figures 5.7 and 5.9) predicts increased frequency and intensity of droughts in the far future.

Interestingly, these meteorological drought conditions are not reflected in hydrological drought trends. SDI-indexed drought conditions show a decline in both frequency and intensity for both scenarios and across both future time periods. This divergence may be attributed to its arid landscape and the perennial nature of the Upper Great Ruaha River system and its historical propensity to dry up under specific thresholds for baseflow measurements. Consequently, lower thresholds for calculating future flows could explain the projected decline in hydrological drought frequency and intensity despite the meteorological drought trends.

The Lower Great Ruaha region acts as an extension of the Upper Great and Little Ruaha rivers, receiving significant contributions from the outflows of the Mtera Reservoir. Historically, this sub-basin has experienced moderately high rainfall levels, supporting substantial lateral flow and soil moisture storage (Figure 5.3). However, it is also characterized by elevated evapotranspiration rates, which influence its hydrological balance (Figure 5.3). Hydrological flux maps (Figures 5.4 and 5.5) project considerable variability in the sub-basin's future hydrological conditions, contingent on the chosen climate model trajectory. Depending on these projections, the sub-basin could experience either increases or decreases in lateral flow rates and soil moisture levels.

SPI analysis over the Lower Great Ruaha reveals a decline in precipitation-induced drought conditions, while SPEI results highlight the significant influence of potential evapotranspiration (PET), resulting in an increased frequency of SPEI-indexed droughts within the basin. The intensity of SPI-droughts is projected to remain similar to, or slightly higher than, historical levels under most scenarios, with the exception of the far future under the RCP 4.5 scenario, where a reduction in intensity is projected.

SDI projections indicate an increase in the frequency of hydrological droughts in the near future under the RCP 4.5 scenario, followed by a decline in the far future (Figure 5.6). Conversely, the RCP 8.5 scenario predicts a reduction in SDI-drought frequency (Figure 5.8). The intensities of SDI-droughts are also expected to be lower than historical levels, likely due to the combined contributions from the

Upper Great Ruaha River and the regulated flows from the Mtera Reservoir. However, it is important to note that SDI is not a precise measure of the hydrological susceptibility of this sub-basin due to its downstream nature.

Additionally, SPI and SPEI cannot be directly compared to SDI values because of differences in their calculation methods. While SPI and SPEI were derived for the sub-basin's bounding area without considering upstream contributions, SDI calculations account for cumulative flows from upstream regions, as discussed in Chapter 5.4.1. This distinction underscores the complexity of interpreting and comparing drought indices across spatial and hydrological contexts within the basin.

The Kilombero Basin provides the bulk of the water to the Greater Rufiji Basin. As highlighted by Naschen et al. (2018, 2019), this sub-basin plays a vital role in the hydrology of the region, but it is hindered by limited availability of hydrological data, a challenge similarly observed in this study. Naschen et al. (2018) emphasize that their study was the first to provide distributed information on the water balance within the Kilombero Catchment, marking a significant contribution to understanding the basin's hydrology.

Their initial study focused on calibrating the SWAT model to analyze the effects of land use changes on water balance components. This study provided a foundational understanding of the sub-basin's hydrological dynamics. The follow-up research by Naschen et al. (2019) shifted focus to assessing the impacts of climate change over the 2010–2060 period under RCP 4.5 and RCP 8.5 scenarios. Using a subset of CORDEX ensemble RCM-GCM pairs integrated with the SWAT model, they projected monthly changes in precipitation and temperature, offering critical insights into future hydrological trends within the Kilombero Basin.

Similar to this study, Naschen et al. (2018, 2019) utilized older hydrological data from the 1958–1970 period to validate and calibrate the SWAT model with satisfactory results. Their model calibration demonstrated accurate discharge patterns during both calibration and validation periods, achieving good to very good statistical performance, which aligns closely with the findings of this study. The observed reductions in statistical performance metrics, such as the Nash-Sutcliffe Efficiency (NSE), were attributed to overestimations of discharge during certain years and challenges in simulating discharge peaks—issues also noted in this study.

However, a notable divergence in findings relates to the sensitivity of model parameters. Naschen et al. identified five of the seven most sensitive parameters as being related to groundwater, whereas this study, which modeled the entire Rufiji Basin without incorporating a groundwater component, found its most sensitive parameters to be linked to soil characteristics. Interestingly, preliminary model setups in this study revealed that including a reservoir to simulate the Kilombero wetland successfully introduced a one-month delay, enabling the model to align better with observed data.

Naschen et al. (2018) also observed that the discharge peak, crucial for flood recession agriculture in the floodplain, is likely to shift from April to May starting in the 2020s. This underscores the importance of this study's critical calibration of the model to reflect lags in peak flows (Figure 5.1), as this could be vital for future hydrological and agricultural assessments of the Greater Rufiji Basin

Naschen et al. (2019) highlighted that precipitation is the primary driver of hydrological processes within the Kilombero Basin, largely due to its location at the base of the Udzungwa Mountains. Their study emphasized a pronounced trend towards wetter conditions in the future, particularly for the catchment. Similarly, this study found that the Kilombero sub-basin is projected to experience wetter conditions under both RCP 4.5 and RCP 8.5 scenarios, as shown in Figures 5.4 and 5.5, aligning with its historical status as the region receiving the most rainfall within the Rufiji Basin (Figure 5.3). Projections also indicate a decrease in evaporation rates in the upper parts of the basin, which is expected to result in increased lateral flow rates and soil moisture storage (Figure 5.4). Naschen et al. similarly observed spatial variations in evaporation rates across the sub-basin, reinforcing these findings.

Moreover, their study revealed that annual averages of water yield and surface runoff could increase by up to 61.6% and 67.8%, respectively, under bias-corrected climate simulations compared to historical conditions. These increases are within a comparable range to this study's projected enhancements in lateral flows for similar time periods and climate scenarios (Figures 5.4 and 5.5). These parallels underscore the consistent hydrological responses projected for the Kilombero sub-basin under wetter future climate scenarios.

The Luwegu Basin, characterized by low population density and its location within a conservation area, has limited research available for direct comparisons. Historically, the basin received moderate rainfall, high soil moisture, and low evapotranspiration rates but is projected to face increasing drought risks. Hydrological flux maps (Figures 5.4 and 5.5) indicate higher evapotranspiration rates, leading to reduced lateral flow and soil moisture storage. SPEI projections show increased drought frequency under both future periods and scenarios, with intensities remaining stable under RCP 4.5 but decreasing under RCP 8.5 (Figures 5.7 and 5.9).

SDI projections suggest a rise in hydrological drought frequency in the near future under RCP 4.5, followed by a decline in the far future, while RCP 8.5 predicts reduced drought frequency overall. SDI drought intensities are expected to decrease across both time periods and scenarios, with near-future conditions under RCP 4.5 showing intensities comparable to historical levels.

These changes could adversely impact the basin's wetlands and water resources, particularly within the Julius Nyerere National Park. Enhanced conservation measures may be needed, especially under the near-future RCP 4.5 scenario, to mitigate the effects of these projected changes.

The Lower Rufiji is projected to experience regions with increased precipitation in future decades under both scenarios, likely due to its proximity to rainfall from the Indian Ocean. Lateral flow rates and soil moisture storage are generally expected to rise, particularly around the Stiegler Gorge and Rufiji Delta areas, as depicted in Figures 5.4 and 5.5. This could mean better prospects for agriculture in the area.

SPI and SPEI analyses indicate a general decrease in the frequency of meteorological droughts in both the near- and long-term future under both scenarios. A slight increase in SPEI-indexed drought frequency is observed in one model under the RCP 8.5 scenario for the near future (Figure 5.7). SPEI drought intensities however show slight increases under the RCP 4.5 scenario over the course of the century (Figure 5.8), with the RCP 8.5 scenario (Figure 5.9) projecting the highest drought intensities in the far future for the sub-basin.

The SDI charts (Figures 5.6 to 5.9) indicate a decline in both the frequency and intensity of hydrological drought conditions under both scenarios and time periods. However, these results may be influenced by biases, as the basin is situated downstream and thus receives the accumulated streamflow. The SDI charts also suggest a reduction in both the occurrence and severity of hydrological droughts in the Lower Rufiji Basin, which is a positive development, particularly considering its proximity to Stiegler Gorge. This reduction could benefit farming communities in the lower regions, which might otherwise face water shortages due to water retention, as well as communities in the delta areas. However, the region could also remain vulnerable to potential future flooding, as highlighted by Duvail and Hamerlynck (2007), Hamerlynck et al. (2007), and Andrea and Kangalawe (2018).

All in all, the Streamflow Drought Index (SDI) employed to assess hydrological droughts and proved to be an acceptable indicator of drought conditions under unrestricted flow scenarios. However, the SWAT+ model's omission of critical factors such as agricultural and domestic water abstractions and dam management operations resulted in an oversimplified representation of hydrological realities. Consequently, while the SDI effectively identified potential vulnerabilities within the basin, it did not accurately reflect the full complexity of the region’s water resource dynamics.

This limitation also contributed to the observed divergence between SDI and the Standardized Precipitation-Evapotranspiration Index (SPEI). Whereas SPEI analysis projected heightened frequencies and intensities of meteorological droughts under future scenarios, these trends were not consistently mirrored by the SDI. The discrepancy highlights the importance of integrating anthropogenic and management influences into hydrological models to improve the reliability of drought assessments and better inform adaptive strategies.

6.1 Summary

- CORDEX models predominantly project an increase in precipitation across the entire basin in both the near- and far-future scenarios. This trend has significant implications for future drought conditions, with projected reductions in SPI-indexed drought frequency. However, under the driest scenarios, particularly the RCP 4.5 scenario, precipitation levels are expected to decline across much of the basin. Even under the RCP 8.5 scenario, reductions in precipitation remain evident in regions such as the Luwegu, parts of the Lower Rufiji, and sections of the Lower Great Ruaha.
- The findings from the SPEI analysis underscore the significant role of evapotranspiration in meteorological drought, indicating heightened frequencies and intensities of meteorological droughts across all basins, particularly in the far future.
- In the near future under the RCP 4.5 scenario, only the Little Ruaha exhibits little or no change in intensity of hydrological drought, while all other basins show decreasing drought intensities as the century progresses.
- When comparing the RCP 4.5 and RCP 8.5 scenarios, the near future is characterized by more intense hydrological droughts under the RCP 4.5 scenario, while the RCP 8.5 scenario projects more severe droughts in the far future.
- Areas that historically received less rainfall, such as those around the Mtera Reservoir, are projected to experience more wetting in the future.
- Soil moisture and lateral flow rates show similarities and indicate a decrease in historically wetter areas such as the Luwegu and Little Ruaha, both in the near and far future under both scenarios.
- There is a high likelihood of an increase in soil moisture storage and lateral flow rates around the Mtera Reservoir area. However, there could also be detrimental effects on soil moisture if the minimum model projections are followed, especially under the RCP 8.5 scenario.
- The Luwegu and the Little Ruaha are more influenced by higher evaporation rates, resulting in predicted lower lateral flows and soil moisture storages in drier model projections. In contrast, the Kilombero, Lower Rufiji, and the areas surrounding the Mtera Reservoir are more responsive to changes in precipitation.

6.2 Limitations

The utilization of the configured Soil and Water Assessment Tool (SWAT) model in the Rufiji Basin analysis presents several limitations that warrant consideration:

- Generic Model Configuration: The SWAT model employed is based on a generic framework that utilizes global soil and land cover data, alongside climate data derived from reanalysis climate models rather than direct station data. The gridded climate data used in the model is relatively coarse, potentially limiting the precision of the model's representation of actual hydrological conditions within the Rufiji Basin. While designed to encapsulate the principal characteristics of the basin and highlight distinctions among its six sub-basins, the model's generic nature may not fully capture the specific hydrological dynamics of the area.
- Static Land Use Representation: The SWAT model employs static land use data, relying on outdated land use maps to simulate historical flows. This static approach does not reflect potential changes in land use over time, which could affect the basin's hydrology.
- Hydrological Processes Focus: The model is exclusively focused on hydrological processes, omitting considerations of water management practices such as water offtakes, dam storage and releases, and irrigation schedules. This approach means that the model evaluates only the influence of climate and natural hydrological processes on water resources, without accounting for the impacts of human water management activities on upstream-downstream linkages.
- The SWAT+ model did not account for groundwater which may have resulted in inaccurate SDI levels.
- Obtaining recent flow data is challenging due to restrictions on data availability for educational purposes and the lack of major gauging stations on the main tributaries, further complicating efforts to accurately calibrate the model.
- The model's threshold was set based on the 1970s, whereas population, agriculture, and industries have significantly increased since then, leading to not entirely robust results.
- By nature of available data and resources (time) the study is regional and a “first-order” in nature.

These limitations highlight the challenges of using the SWAT model for detailed hydrological analysis in the Rufiji Basin. While useful for understanding fundamental hydrological patterns, the model lacks the capacity to fully capture complex water management dynamics and precise regional conditions.

CHAPTER 7: SUMMARY AND CONCLUSIONS

This chapter encapsulates the outcomes derived from the analyses conducted throughout the study. It serves as a synthesis of the key findings and offers concluding remarks.

The motivation for this study arises from the critical need to investigate the dynamics of drought occurrences within the Rufiji Basin, taking into account both historical trends and projected climatic scenarios. The severity of droughts poses a significant threat to the lives and developmental prospects of the region's inhabitants. Both meteorological and hydrological droughts loom large over the Rufiji Basin, necessitating a comprehensive investigation. This study employs three drought indices—namely, the Standardized Precipitation Index (SPI), the Standardized Precipitation-Evapotranspiration Index (SPEI), and a hydrological drought indicator, the Streamflow Drought Index (SDI)—to delineate 12-month drought occurrences across the Rufiji Basin. It unfolds the temporal and spatial nuances of various drought characteristics, encompassing factors such as frequency, intensity, and the spatial distribution of meteorological and hydrological variables, including precipitation, evapotranspiration, lateral flow, and soil moisture.

The study divided the Rufiji River into six primary sub-basins: the Upper Great Ruaha, the Little Ruaha, the Lower Great Ruaha, the Kilombero, the Luwegu, and the Lower Rufiji. The investigation focused on understanding drought characteristics specific to each basin. A diverse array of methodologies was employed to scrutinize various indices. Python programming, along with the SPEI package in RStudio, facilitated the SPI and SPEI analyses.

The Streamflow Drought Index (SDI) analysis was conducted using the hydrological model SWAT+ and the DRINC SDI calculator. The successful calibration of the SWAT+ model, achieving a Nash-Sutcliffe Efficiency (NSE) of 0.70, produced streamflow simulations closely aligned with observed data. This calibration resulted in attenuated peak flow estimates and improved representation of base flows compared to the initial SWAT+ simulation output using default parameters for the input of landuse, vegetation, soils, and other catchment characteristics. Incorporating the Kilombero wetland as a reservoir effectively delayed the occurrence of peak flows at the calibration point, introducing a lag of approximately one month.

Historical climate data was sourced from ERA5 Land, while simulated projected climate data was acquired from 13 Coordinated Regional Climate Downscaling Experiment (CORDEX) Regional Climate Models (RCMs). The results of the study can be summarised as follows:

- The successfully calibrated SWAT+ model offers a valuable resource for studying the spatial extent and characteristics of hydrological variables within the Rufiji River basin and their likely responses to projected changes in climate.

- The use of the CORDEX ensemble is deemed reasonable for projecting future climates, given its ability to replicate historical climates closely in comparison to observed data.
- The CORDEX models consistently project a warmer climate in the Rufiji Basin, indicating an increase in both minimum and maximum temperatures. Under the RCP 4.5 scenario, there is an approximate 3°C rise in temperatures towards the end of the century compared to the historical. In contrast, the RCP 8.5 scenario suggests a more substantial change, with an almost average 5°C increase in temperatures by the end of the century. These projections highlight the potential impact of climate change on the temperature regime in the Rufiji Basin.
- The CORDEX models, especially under the RCP 8.5 scenario, suggest a marginal rise in precipitation as the century advances. This is evident in plots, where a reduction in troughs and an increase in peaks towards the end of the century imply a potential trend of heightened precipitation events in the basin. This observation aligns with the SPI and its anticipated impact on precipitation patterns in the Rufiji Basin.
- The SPI-indexed drought is projected to decrease drought frequency in the basin under both scenarios but intensities are expected to vary, with the far future under the RCP 8.5 exhibiting higher drought intensities in some sub-basins.
- The SPI is, however, not a comprehensive indicator for meteorological drought, as it does not account for the influence of global warming. Its limitations include an underestimation of meteorological drought, making it suitable primarily for assessing projected rainfall amounts rather than providing a holistic view of meteorological drought conditions.
- The SPEI analysis revealed that both RCP 4.5 and RCP 8.5 scenarios project an escalation in the intensity and frequency of meteorological droughts across nearly all sub-basins, both in the near and far future. Notably, far-future projections indicate markedly amplified impacts, characterized by a pronounced exponential trend.
- The Streamflow Drought Index (SDI) was utilized as a measure of hydrological drought, demonstrating its utility in indicating drought conditions under unrestricted flow scenarios. However, the SWAT+ model's inability to account for abstractions related to agricultural and domestic water use, as well as dam management practices, limited its capacity to represent realistic hydrological conditions. Despite this limitation, the SDI analysis provided insights into potential areas of vulnerability within the basin.
- The lack of congruence between the SDI and the Standardized Precipitation-Evapotranspiration Index (SPEI) was attributed to the SWAT+ model's limitations. While SPEI highlighted increases in the frequency and intensity of drought events under future scenarios, such trends

were not consistently reflected in the SDI, underscoring the model's constraints in capturing anthropogenic and management-related influences on hydrology.

- The frequency of hydrological drought as indexed by SDI is anticipated to rise in the near future under the RCP 4.5 scenario particularly in the Little Ruaha, Luwegu, and Lower Rufiji sub-basins.
- The Kilombero and Lower Rufiji, along with the regions surrounding the Mtera Reservoir, exhibit trends indicating increased wetting, primarily influenced by precipitation. However, these areas might face challenges such as reduced soil moisture and lateral flow if minimum model projections are realized. On the other hand, the Luwegu and Little Ruaha appear more susceptible to variations in evapotranspiration and rising temperatures.
- Based on the results and analysis, the Luwegu and Little Ruaha basins, and to some extent, the Lower Great Ruaha, appear to be the most impacted. These areas exhibit increases in both meteorological and hydrological drought frequencies and intensities. Additionally, projections suggest a decrease in soil moisture and lateral flow in both the near and far future.
- The potential impacts on these basins could have significant consequences for the ecosystems and activities in the affected areas. For instance, in the Luwegu, where the Nyerere National Park is located, changes in drought conditions may affect wildlife and the overall flora and fauna. In the Little Ruaha, where wetlands are present, agricultural and forestry practices reliant on these ecosystems could face challenges due to decreased soil moisture and lateral flow. This emphasizes the importance of considering the broader environmental and socioeconomic implications of changing drought patterns in the region.
- The potential impacts on these basins could be further exacerbated by human activities, including detrimental land-use changes such as unsustainable agricultural practices, excessive water extraction, and deforestation. These anthropogenic factors, coupled with meteorological events like prolonged droughts, may contribute to heightened vulnerabilities in the affected ecosystems. Therefore, it becomes imperative to address not only climatic influences but also human-induced stressors to foster sustainable management and resilience in the face of changing environmental conditions

The anticipated rise in both intensity and frequency of agricultural and hydrological droughts poses significant threats to various economic activities, including agriculture, industrial water supply, and tourism. Such changes may exert adverse impacts on regional development, especially in the context of a growing population that places additional demands on the already water-stressed Rufiji Basin. Developing strategies to address these challenges and ensure sustainable water management becomes imperative for the future well-being of the region.The findings underscore the limitations of relying

solely on meteorological drought indices (SPEI and SPI) for assessing the impact of global warming on hydrological droughts. Since SPI may underestimate drought severity while SPEI may overstate it, effective climate change mitigation and adaptation strategies should be informed by projections from hydrological drought indices rather than relying solely on meteorological drought projections.

To enhance the accuracy and relevance of studies, it is crucial for governments and water management authorities in the area to make data, particularly streamflows and weather data, publicly accessible to the academic community. The reliance on outdated data hampers the development and calibration of models based on recent information, hindering the ability to connect computational projections to model simulations effectively. Establishing streamflow gauging stations at strategic locations along key rivers within the basin (as done with the generic gauging stations in this study), both downstream and upstream, would provide valuable insights. This approach would enable the study of individual sub-basins, facilitating more robust results through improved calibration and understanding of hydrological dynamics.

Future research efforts should focus on exploring the effects of land-use changes within the most vulnerable basins and their implications for hydrological flows and related variables. Investigating the intricate interactions of groundwater systems and wetland processes, particularly within critical basins such as the Kilombero, would offer valuable insights into the complex dynamics of the Rufiji River system. These studies could significantly enhance our understanding of the factors influencing the river's sustainability. Furthermore, future modeling endeavors should prioritize the integration of groundwater dynamics, abstraction practices, and dam operations to establish a more realistic and comprehensive linkage between meteorological and hydrological droughts, thereby improving the accuracy and applicability of drought assessment.

REFERENCES

Abbaspour, K.C., Vaghefi, S.A. and Srinivasan, R., 2018. A guideline for successful calibration and uncertainty analysis for soil and water assessment: a review of papers from the 2016 international SWAT conference.

Abbott, M.B., Bathurst, J.C., Cunge, J.A., O'Connell, P.E. and Rasmussen, J., 1986. An introduction to the European Hydrological System−Systeme Hydrologique Europeen, "SHE", 1: History and philosophy of a physically based, distributed modelling system. *Journal of hydrology*, *87*(1-2), pp.45-59.

Allen, R., Pereira, L., Raes, D. & Smith, M. (1998) Crop evapotranspiration. FAO irrigation and drainage paper 56. FAO, Rome, Italy, 10.

Alley, W.M., 1984. The Palmer drought severity index: limitations and assumptions. *Journal of Applied Meteorology and Climatology*, *23*(7), pp.1100-1109.

Andrea, J.M. and Kangalawe, R.Y., 2018. Analysing Vulnerabilities of local communities to flood disasters in the Lower Rufiji Floodplain, Tanzania. *Journal of the Geographical Association of Tanzania*, *39*(1).

Anyah, R.O. and Qiu, W., 2012. Characteristic 20th and 21st century precipitation and temperature patterns and changes over the Greater Horn of Africa. *International Journal of Climatology*, *32*(3), pp.347-363.

Arnold, J.G., Srinivasan, R., Muttiah, R.S. and Williams, J.R., 1998. Large area hydrologic modeling and assessment part I: model development 1. *JAWRA Journal of the American Water Resources Association*, *34*(1), pp.73-89.

Arnold, J.G., Moriasi, D.N., Gassman, P.W., Abbaspour, K.C., White, M.J., Srinivasan, R., Santhi, C., Harmel, R.D., Van Griensven, A., Van Liew, M.W. and Kannan, N., 2012. SWAT: Model use, calibration, and validation. *Transactions of the ASABE*, *55*(4), pp.1491-1508.

Ayana, E.K., Ceccato, P., Fisher, J.R. and DeFries, R., 2016. Examining the relationship between environmental factors and conflict in pastoralist areas of East Africa. *Science of the Total Environment*, *557*, pp.601-611.

Ayugi, B.O. and Tan, G., 2019. Recent trends of surface air temperatures over Kenya from 1971 to 2010. *Meteorology and Atmospheric Physics*, *131*, pp.1401-1413.

Ayugi, B., Zhihong, J., Zhu, H., Ngoma, H., Babaousmail, H., Rizwan, K. and Dike, V., 2021. Comparison of CMIP6 and CMIP5 models in simulating mean and extreme precipitation over East Africa. *International Journal of Climatology*, *41*(15), pp.6474-6496.

Barrios, S., Bertinelli, L. and Strobl, E., TRENDS IN RAINFALL AND ECONOMIC GROWTH IN AFRICA. *European Commission, Directorate General Joint Research center Institute for Prospective technological studies*.

Belayneh, A., Adamowski, J., Khalil, B. and Ozga-Zielinski, B.J.J.O.H., 2014. Long-term SPI drought forecasting in the Awash River Basin in Ethiopia using wavelet neural network and wavelet support vector regression models. *Journal of Hydrology*, *508*, pp.418-429.

Bergström, S. (1992). The HBV Model -Its Structure and Applications. *Swedish Meteorological and Hydrological Institute, 4*.

Beguería, S., Vicente-Serrano, S.M., Reig, F. and Latorre, B., 2014. Standardized precipitation evapotranspiration index (SPEI) revisited: Parameter fitting, evapotranspiration models, tools, datasets and drought monitoring. *International Journal of Climatology*, 34(10), pp.3001–3023. http://hdl.handle.net/10261/128892

Beguería, S., Vicente-Serrano, S.M. and Beguería, M.S., 2017. Package 'spei'. *Calculation of the Standardised Precipitation-Evapotranspiration Index, CRAN [Package]*.

Bernard, B., Vincent, K., Frank, M. and Anthony, E., 2013. Comparison of extreme weather events and streamflow from drought indices and a hydrological model in River Malaba, Eastern Uganda. *International journal of environmental studies*, *70*(6), pp.940-951.

Beven, K.J. and Kirkby, M.J., 1979. A physically based, variable contributing area model of basin hydrology/Un modèle à base physique de zone d'appel variable de l'hydrologie du bassin versant. *Hydrological Sciences Journal*, *24*(1), pp.43-69.

Beven,2012: Beven, K.J., 2011. *Rainfall-runoff modelling: the primer*. John Wiley & Sons. -report

Beven, K., 2012. Causal models as multiple working hypotheses about environmental processes. *Comptes rendus geoscience*, *344*(2), pp.77-88.

Bhalme, H.N. and Mooley, D.A., 1979. On the performance of modified Palmer index. *Archives for Meteorology Geophysics and Bioclimatology Series B Theoretical and Applied Climatology*, *27*(4), pp.281-295.

Bouimetarhan, I., Dupont, L., Kuhlmann, H., Pätzold, J., Prange, M., Schefuß, E. and Zonneveld, K., 2015. Northern Hemisphere control of deglacial vegetation changes in the Rufiji uplands (Tanzania). *Climate of the Past*, *11*(5), pp.751-764.

Brown, C., Meeks, R., Hunu, K. and Yu, W., 2011. Hydroclimate risk to economic growth in sub-Saharan Africa. *Climatic Change*, *106*(4), pp.621-647.

Calzi DL (2013): Dams, Drought and Energy-Water Interdependencies.178pp, Nova Publishers. New York.

Camberlin, P., 2018. Climate of eastern Africa. In *Oxford research encyclopedia of climate science*.

Cannon, A.J., Sobie, S.R. and Murdock, T.Q., 2015. Bias correction of GCM precipitation by quantile mapping: how well do methods preserve changes in quantiles and extremes? *Journal of Climate*, *28*(17), pp.6938-6959.

Ceccherini, G., Russo, S., Ameztoy, I., Marchese, A.F. and Carmona-Moreno, C., 2017. Heat waves in Africa 1981–2015, observations and reanalysis. *Natural Hazards and Earth System Sciences*, *17*(1), pp.115-125.

Chang, T.J., Stenson, J.R., 1990. Is it realistic to define a 100-year drought for water management? Water Resour. Bull. 26 (5), 823–829.

Chang'a, L.B., Kijazi, A.L., Luhunga, P.M., Ng'ongolo, H.K. and Mtongori, H.I., 2017. Spatial and temporal analysis of rainfall and temperature extreme indices in Tanzania.

Conway, D., Dalin, C., Landman, W.A. and Osborn, T.J., 2017. Hydropower plans in eastern and southern Africa increase risk of concurrent climate-related electricity supply disruption. *Nature Energy*, *2*(12), pp.946-953.

Conway, D., Curran, P.G.K.E. and Gannon, K., 2018. Policy Brief: Climate Risks to Hydro-Power Supply in Easte rn and Southern Africa. *Grantham Research Institute on Climate Change and Environment: London, UK*.

Cook, K.H. and Vizy, E.K., 2013. Projected changes in East African rainy seasons. *Journal of Climate*, *26*(16), pp.5931-5948.

CMIP6; The CMIP6 landscape. *Nat. Clim. Chang.* **9**, 727 (2019). https://doi.org/10.1038/s41558-019-0599-1. Accessed 29/01/2024

Dai, A., 2011. Drought under global warming: a review. *Wiley Interdisciplinary Reviews: Climate Change*, *2*(1), pp.45-65.

Degefu, M.A. and Bewket, W., 2014. Variability and trends in rainfall amount and extreme event indices in the Omo-Ghibe River Basin, Ethiopia. *Regional environmental change*, *14*, pp.799-810.

Devia, G.K., Ganasri, B.P. and Dwarakish, G.S., 2015. A review on hydrological models. *Aquatic procedia*, *4*, pp.1001-1007.

Dosio, A. and Panitz, H.J., 2016. Climate change projections for CORDEX-Africa with COSMOCLM regional climate model and differences with the driving global climate models. *Climate Dynamics*, *46*(5), pp.1599-1625.

Dosio, A., 2017. Projection of temperature and heat waves for Africa with an ensemble of CORDEX Regional Climate Models. *Climate Dynamics*, *49*(1-2), pp.493-519.

Dracup, J.A., Lee, K.S. and Paulson Jr, E.G., 1980. On the definition of droughts. *Water resources research*, *16*(2), pp.297-302

Duvail, S. and Hamerlynck, O., 2007. The Rufiji River flood: plague or blessing?. *International journal of biometeorology*, *52*, pp.33-42.

Dye, B., 2019. Stiegler's Gorge Dam, Tanzania.

Dye, B., 2021. What does Tanzania's new government mean for the controversial Julius Nyerere mega-dam?.

ECMWF, 2023. Fact Sheet: Reanalysis. [online] Available at: https://www.ecmwf.int/sites/default/files/2023-08/Fact%20sheet%20-%20Reanalysis%20-v3_1.pdf [Accessed 30 November 2023].

Endris, H.S., Omondi, P., Jain, S., Lennard, C., Hewitson, B., Chang'a, L., Awange, J.L., Dosio, A., Ketiem, P., Nikulin, G. and Panitz, H.J., 2013. Assessment of the performance of CORDEX regional climate models in simulating East African rainfall. *Journal of Climate*, *26*(21), pp.8453-8475.

Endris, H.S., Lennard, C., Hewitson, B., Dosio, A., Nikulin, G. and Panitz, H.J., 2015. Teleconnection responses in multi-GCM driven CORDEX RCMs over Eastern Africa. *Climate Dynamics*, 46(9-10), pp.2821–2846.

Engelbrecht, F., Adegoke, J., Bopape, M.J., Naidoo, M., Garland, R., Thatcher, M., McGregor, J., Katzfey, J., Werner, M., Ichoku, C. and Gatebe, C., 2015. Projections of rapidly rising surface temperatures over Africa under low mitigation. Environmental Research Letters, 10(8), p.085004.

Elton JF (1879) Travels and research among lakes and mountains of eastern and central Africa. Murray, London

England, M.I., Dougill, A.J., Stringer, L.C., Vincent, K.E., Pardoe, J., Kalaba, F.K., Mkwambisi, D.D., Namaganda, E. and Afionis, S., 2018. Climate change adaptation and cross-sectoral policy coherence in southern Africa. *Regional Environmental Change*, *18*, pp.2059-2071.

ESA. Land Cover CCI Product User Guide Version 2. Tech. Rep. (2017). Available at: maps.elie.ucl.ac.be/CCI/viewer/download/ESACCI-LC-Ph2-PUGv2_2.0.pdf [Accessed on 25th April 2022]

Eyring, V., Bony, S., Meehl, G.A., Senior, C.A., Stevens, B., Stouffer, R.J. and Taylor, K.E., 2016. Overview of the Coupled Model Intercomparison Project Phase 6 (CMIP6) experimental design and organization. *Geoscientific Model Development*, *9*(5), pp.1937-1958.

FAO, 1983. World Food Security: A Reappraisal of the Concepts and Approaches. Director General's Report.
FAO (Food and Agriculture Organization). 2005. Local Climate Estimator. Environment and Natural Resources, Working paper No. 20. http://www.fao.org/nr/climpag/

Finney, D.L., Marsham, J.H., Rowell, D.P., Kendon, E.J., Tucker, S.O., Stratton, R.A. and Jackson, L.S., 2020. Effects of explicit convection on future projections of mesoscale circulations, rainfall, and rainfall extremes over Eastern Africa. *Journal of Climate*, *33*(7), pp.2701-2718.

Gannon, K.E., Conway, D., Pardoe, J., Ndiyoi, M., Batisani, N., Odada, E., Olago, D., Opere, A., Kgosietsile, S., Nyambe, M. and Omukuti, J., 2018. Business experience of floods and drought-related water and electricity supply disruption in three cities in sub-Saharan Africa during the 2015/2016 El Niño. *Global Sustainability*, *1*, p.e14.

Gassman, P.W., Reyes, M.R., Green, C.H. and Arnold, J.G., 2007. The soil and water assessment tool: historical development, applications, and future research directions. *Transactions of the ASABE*, *50*(4), pp.1211-1250.

Gebrechorkos, S.H., Hülsmann, S. and Bernhofer, C., 2019. Changes in temperature and precipitation extremes in Ethiopia, Kenya, and Tanzania. *International Journal of Climatology*, *39*(1), pp.18-30.

General, U.S., 1994. United Nations convention to combat drought and desertification in countries experiencing serious droughts and/or desertification, particularly in Africa. *Particularly in Africa*.

Geressu, R., Siderius, C., Harou, J.J., Kashaigili, J., Pettinotti, L. and Conway, D., 2020. Assessing river basin development given water-energy-food-environment interdependencies. *Earth's Future*, *8*(8), p.e2019EF001464.

Giannini, A., Saravanan, R. and Chang, P., 2003. Oceanic forcing of Sahel rainfall on interannual to interdecadal time scales. *Science*, *302*(5647), pp.1027-1030.

Gibbs, W.J., 1975. Drought-its definition, delineation and effects. *Drought. Lectures presented at the twenty-sixth session of the WMO Executive Committee.*, pp.1-39.

Giorgi, F. and Mearns, L.O., 1999. Introduction to special section: Regional climate modeling revisited. *Journal of Geophysical Research: Atmospheres*, *104*(D6), pp.6335-6352.

Gleixner, S., Demissie, T. and Diro, G.T., 2020. Did ERA5 improve temperature and precipitation reanalysis over East Africa?. *Atmosphere*, *11*(9), p.996.

Government of Tanzania (2016). National Five Year Development Plan, 2016/17-2020/21.

GRDC - The Global Runoff Data Centre, D - 56002 Koblenz, Germany (citation)

Grey, D. and Sadoff, C.W., 2007. Sink or swim? Water security for growth and development. *Water policy*, *9*(6), pp.545-571.

Gutierrez, J. M. et al., 2021: Atlas [Masson-Delmotte, V., P. Zhai, A. Pirani, S. L. Connors, C. Pean, S. Berger, N. Caud, Y. Chen, L. Goldfarb, M. I. Gomis, M. Huang, K. Leitzell, E. Lonnoy, J. B. R. Matthews, T. K. Maycock, T. Waterfield, O. Yelekci, R. Yu and B. Zhou (ed.)]. Climate Change 2021: The Physical Science Basis. Contribution of Working Group I to the Sixth Assessment Report of the Intergovernmental Panel on Climate Change In Press, Cambridge University Press. Available at: https://www.ipcc.ch/report/ar6/wg1/downloads/report/IPCC_AR6_WGI_Atlas.pdf.

Guttman, N.B., 1991. A sensitivity analysis of the palmer hydrologic drought index 1. *Jawra Journal of the American Water Resources Association*, *27*(5), pp.797-807.

Guttman, N.B., Wallis, J.R. and Hosking, J.R.M., 1992. Spatial comparability OF the palmer drought severity index 1. *JAWRA Journal of the American Water Resources Association*, *28*(6), pp.1111-1119.

Guttman, N.B., 1999. Accepting the standardized precipitation index: a calculation algorithm 1. *JAWRA Journal of the American Water Resources Association*, *35*(2), pp.311-322.

Gyamfi, C., Ndambuki, J.M. and Salim, R.W., 2016. Application of SWAT model to the Olifants Basin: calibration, validation and uncertainty analysis. *Journal of Water Resource and Protection*, *8*(03), p.397.

Haensler, A., Saeed, F. and Jacob, D., 2013. Assessing the robustness of projected precipitation changes over central Africa on the basis of a multitude of global and regional climate projections.

Climatic Change, *121*(2), pp.349-363.

Hall, J.W., Grey, D., Garrick, D., Fung, F., Brown, C., Dadson, S.J. and Sadoff, C.W., 2014. Coping with the curse of freshwater variability. *Science*, *346*(6208), pp.429-430.

Haile, M., 2005. Weather patterns, food security and humanitarian response in sub-Saharan Africa. *Philosophical Transactions of the Royal Society B: Biological Sciences*, *360*(1463), pp.2169-2182.

Haile, G.G., Tang, Q., Sun, S., Huang, Z., Zhang, X. and Liu, X., 2019. Droughts in East Africa: Causes, impacts and resilience. *Earth-science reviews*, *193*, pp.146-161.

Hamerlynck, O., Duvail, S., Vandepitte, L., Kindinda, K., Nyingi, D.W., Paul, J.L., Yanda, P.Z., Mwakalinga, A.B., Mgaya, Y.D. and Snoeks, J., 2011. To connect or not to connect? Floods, fisheries and livelihoods in the Lower Rufiji floodplain lakes, Tanzania. *Hydrological Sciences Journal*, *56*(8), pp.1436-1451.

Hamisi, R., 2013. Simulations of water balance conditions and cli-mate variability for Sustainable Agriculture and Energy in the Lower Rufiji Basin.

Hargreaves, G. H. & Samani, Z. A. (1985) Reference crop evapotranspiration from ambient air temperature. American Society of Agricultural Engineers, 96–99.

Hartmann, J., 2019. Economic Feasibility of the Stiegler's Gorge Hydropower Project, Tanzania. OECD Watch, Amsterdam, Netherlands < https://www. oecdwatch. org/2019/02/14/the-true-cost-of-the-stieglers-gorge-hydropower-project-in-tanzania, 79, pp.946-953.

Hastenrath, S., Nicklis, A. and Greischar, L., 1993. Atmospheric-hydrospheric mechanisms of climate anomalies in the western equatorial Indian Ocean. *Journal of Geophysical Research: Oceans*, *98*(C11), pp.20219-20235.

Hastenrath, S., 2001. Variations of East African climate during the past two centuries. *Climatic change*, *50*(1-2), pp.209-217.

Hausfather, Z., 2019. Explainer: The high emissions 'RCP8.5' global warming scenario. [Online] Available at: https://www.carbonbrief.org/explainer-the-high-emissions-rcp8-5-global-warming-scenario/ [Accessed Date: 25/01/2024].

Hayes, M., Svoboda, M., Wall, N. and Widhalm, M., 2011. The Lincoln declaration on drought indices: universal meteorological drought index recommended. *Bulletin of the American Meteorological Society*, *92*(4), pp.485-488.

Heim Jr, R.R., 2002. A review of twentieth-century drought indices used in the United States. *Bulletin of the American Meteorological Society*, *83*(8), pp.1149-1166.

Herrmann, S.M. and Mohr, K.I., 2011. A continental-scale classification of rainfall seasonality regimes in Africa based on gridded precipitation and land surface temperature products. *Journal of Applied Meteorology and Climatology*, *50*(12), pp.2504-2513.

Hewitson, B., Lennard, C., Jack, C. and Coop, L., 2013, April. Statistical and dynamical downscaling in CORDEX-Africa: differing views on the regional climate. In *EGU General Assembly Conference Abstracts* (pp. EGU2013-11702).

Hoag, H.J., 2003. *Designing the delta: a history of water and development in the Lower Rufiji River Basin, Tanzania, 1945–1985*. Boston University.

Hoag, H.J., 2013. *Developing the rivers of east and west Africa: an environmental history*. A&C Black.

Hoegh-Guldberg, O., Jacob, D., Bindi, M., Brown, S., Camilloni, I., Diedhiou, A., Djalante, R., Ebi, K., Engelbrecht, F., Guiot, J. and Hijioka, Y., 2018. Impacts of 1.5 C global warming on natural and human systems. *Global warming of 1.5° C.*

Hoerling, M., Hurrell, J., Eischeid, J. and Phillips, A., 2006. Detection and attribution of twentieth-century northern and southern African rainfall change. *Journal of climate*, *19*(16), pp.3989-4008.

Hydrotechnik, A.U., 1982. Irrigated agriculture in the lower Rufiji Valley. *Prefeasibility study. Essen, Germany*.

Indeje, M., Semazzi, F.H. and Ogallo, L.J., 2000. ENSO signals in East African rainfall seasons. *International Journal of Climatology: A Journal of the Royal Meteorological Society*, *20*(1), pp.19-46.

IPCC 2007. Climate change 2007 (Intergovernmental Panel on Climate Change) In: Solomon S, Qin D, Manning M, Chen Z, Marquis MC, Averyt KB, Tignor M, Miller HL (eds) The physical science basis. Cambridge University Press, Cambridge.

IPCC 2014. “Africa” Climate change 2014: Impacts, Adaptation, and Vulnerability. Part B: Regional Aspects. Contribution of Working Group II to the 5th Assessment Rep. of the Intergovernmental Panel on Climate Change, Cambridge University Press, Cambridge, 1199–1265.

IPCC, 2022: Trisos, C.H., I.O. Adelekan, E. Totin, A. Ayanlade, J. Efitre, A. Gemeda, K. Kalaba, C. Lennard, C. Masao, Y. Mgaya, G. Ngaruiya, D. Olago, N.P. Simpson, and S. Zakieldeen, 2022: Africa. In: Climate Change 2022: Impacts, Adaptation and Vulnerability. Contribution of Working Group II to the Sixth Assessment Report of the Intergovernmental Panel on Climate Change [H.-O. Pörtner, D.C. Roberts, M. Tignor, E.S. Poloczanska, K. Mintenbeck, A. Alegría, M. Craig, S. Langsdorf, S. Löschke, V. Möller, A. Okem, B. Rama (eds.)]. Cambridge University Press, Cambridge, UK and New York, NY, USA, pp. 1285–1455, doi:10.1017/9781009325844.011.

Isaac, C. and Guyver, P., 2011. Investment framework for SAGCOT—The SAGCOT investment blueprint.

IUSS Working Group WRB. 2015. World Reference Base for Soil Resources 2014, update 2015 International soil classification system for naming soils and creating legends for soil maps. World Soil Resources Reports No. 106. FAO, Rome.

Jain, V.K., Pandey, R.P., Jain, M.K. and Byun, H.R., 2015. Comparison of drought indices for appraisal of drought characteristics in the Ken River Basin. *Weather and Climate Extremes*, *8*, pp.1-11.

Jarvis, A., Reuter, H.I., Nelson, A. and Guevara, E., 2008. Hole-filled SRTM for the globe Version 4. *available from the CGIAR-CSI SRTM 90m Database (http://srtm. csi. cgiar. org)*, *15*(25-54), p.5 [Accessed on 24th April 2022]

Jalowska, A.M. and Yuan, Y., 2019. Evaluation of SWAT impoundment modeling methods in water and sediment simulations. *JAWRA Journal of the American Water Resources Association*, *55*(1), pp.209-227.

JBG Gauff Ingenieure, 2000. Rufiji bridge and its floodplain cross ing. Supplementary hydrological study and evaluation of flood re cords following the 1997-98 El Nino floods. JBG Gauff Ingenieure Gmbh, Frankfurt-Germany, and Dar es Salaam, Tanzania. Final Report.

Jeffrey, S.J., Carter, J.O., Moodie, K.B. and Beswick, A.R., 2001. Using spatial interpolation to construct a comprehensive archive of Australian climate data. *Environmental Modelling & Software*, *16*(4), pp.309-330.

Jones, C., Giorgi, F. and Asrar, G., 2011. The Coordinated Regional Downscaling Experiment: CORDEX‐an international downscaling link to CMIP5. *CLIVAR exchanges*, *16*(2), pp.34-40.

Jury, M.R., 2002. Economic impacts of climate variability in South Africa and development of resource prediction models. *Journal of Applied Meteorology and Climatology*, *41*(1), pp.46-55.

Kendon, E.J., Stratton, R.A., Tucker, S., Marsham, J.H., Berthou, S., Rowell, D.P. and Senior, C.A., 2019. Enhanced future changes in wet and dry extremes over Africa at convection-permitting scale. *Nature communications*, *10*(1), p.1794.

Kent, C., Chadwick, R. and Rowell, D.P., 2015. Understanding uncertainties in future projections of seasonal tropical precipitation. *Journal of Climate*, *28*(11), pp.4390-4413.

Keyantash, John & National Center for Atmospheric Research Staff (Eds). Last modified 2023-08-19 "The Climate Data Guide: Standardized Precipitation Index (SPI)." Retrieved from https://climatedataguide.ucar.edu/climate-data/standardized-precipitation-index-spi on 2023-04-24.

Kijazi, A.L. and Reason, C.J.C., 2005. Relationships between intraseasonal rainfall variability of coastal Tanzania and ENSO. *Theoretical and applied climatology*, *82*, pp.153-176.

Kim, J., Waliser, D.E., Mattmann, C.A., Goodale, C.E., Hart, A.F., Zimdars, P.A., Crichton, D.J., Jones, C., Nikulin, G., Hewitson, B. and Jack, C., 2014. Evaluation of the CORDEX-Africa multi-RCM hindcast: systematic model errors. *Climate dynamics*, *42*(5), pp.1189-1202.

Kinuthia, J.H., 1992. Horizontal and vertical structure of the Lake Turkana jet. *Journal of Applied Meteorology and Climatology*, *31*(11), pp.1248-1274.

Kruger, A.C. and Nxumalo, M.P., 2017. Historical rainfall trends in South Africa: 1921–2015. *Water Sa*, *43*(2), pp.285-297.

Kruger, A.C. and Nxumalo, M., 2017. Surface temperature trends from homogenized time series in South Africa: 1931–2015. *International Journal of Climatology*, *37*(5), pp.2364-2377.

Li, C., Zwiers, F., Zhang, X., Li, G., Sun, Y. and Wehner, M., 2021. Changes in annual extremes of daily temperature and precipitation in CMIP6 models. *Journal of Climate*, *34*(9), pp.3441-3460.

Liebmann, B., Hoerling, M.P., Funk, C., Bladé, I., Dole, R.M., Allured, D., Quan, X., Pegion, P. and Eischeid, J.K., 2014. Understanding recent eastern Horn of Africa rainfall variability and change. *Journal of Climate*, *27*(23), pp.8630-8645.

Liu, W., Sun, F., Lim, W.H., Zhang, J., Wang, H., Shiogama, H. and Zhang, Y., 2018. Global drought and severe drought-affected populations in 1.5 and 2∘ C warmer worlds. *Earth System Dynamics*, *9*(1), pp.267-283.

Lyon, B., Dinku, T., Raman, A. and Thomson, M.C., 2017. Temperature suitability for malaria climbing the Ethiopian Highlands. *Environmental Research Letters*, *12*(6), p.064015.

Lyon, B. and Vigaud, N., 2017. Unraveling East Africa's climate paradox. *Climate extremes: Patterns and mechanisms*, pp.265-281.

Makhanya, N.Z., 2021. *Potential impacts of climate change on hydrological droughts in the Limpopo river basin* (Master's thesis, Faculty of Science).

Manatsa, D. and Behera, S.K., 2013. On the epochal strengthening in the relationship between rainfall of East Africa and IOD. *Journal of Climate*, *26*(15), pp.5655-5673.

Masih, I., Maskey, S., Mussá, F.E.F. and Trambauer, P., 2014. A review of droughts on the African continent: a geospatial and long-term perspective. *Hydrology and Earth System Sciences*, *18*(9), pp.3635-3649.

Mcsweeney, C., New, M., Lizcano, G. and Lu, X., 2010. The UNDP Climate Change Country Profiles: Improving the accessibility of observed and projected climate information for studies of climate change in developing countries. *Bulletin of the American Meteorological society*, *91*(2), pp.157-166.

McKee, T.B., Doesken, N.J. and Kleist, J., 1993, January. The relationship of drought frequency and duration to time scales. In *Proceedings of the 8th Conference on Applied Climatology* (Vol. 17, No. 22, pp. 179-183).

McKee, T.B., 1995. Drought monitoring with multiple time scales. In *Proceedings of 9th Conference on Applied Climatology, Boston, 1995*.

McMahon, T. A., Peel, M. C., Lowe, L., Srikanthan, R. & McVicar, T. R., 2013. Estimating actual, potential, reference crop and pan evaporation using standard meteorological data: a pragmatic synthesis. Hydrol. Earth Syst. Sci. 17, 1331–1363.

Milder, J.C., Buck, L., Hart, A. and Scherr, S., 2012. A green growth investment framework for SAGCOT—The SAGCOT greenprint.

Mishra, A., Froebrich, J. and Gassman, P.W., 2007. Evaluation of the SWAT model for assessing sediment control structures in a small watershed in India. *Transactions of the ASABE*, *50*(2), pp.469-477.

Mishra, A.K. and Singh, V.P., 2010. A review of drought concepts. *Journal of hydrology*,

391(1-2), pp.202-216.

Modarres, R., 2007. Streamflow drought time series forecasting. *Stochastic Environmental Research and Risk Assessment*, *21*, pp.223-233.

Moriasi, D.N., Arnold, J.G., Van Liew, M.W., Bingner, R.L., Harmel, R.D. and Veith, T.L., 2007. Model evaluation guidelines for systematic quantification of accuracy in watershed simulations. *Transactions of the ASABE*, *50*(3), pp.885-900.

Mtahiko, M.G.G., Gereta, E., Kajuni, A.R., Chiombola, E.A.T., Ng'umbi, G.Z., Coppolillo, P. and Wolanski, E., 2006. Towards an ecohydrology-based restoration of the Usangu wetlands and the Great Ruaha River, Tanzania. *Wetlands ecology and management*, *14*, pp.489-503.

Mulyungi, P. (2019). Tanzania to commence construction Stiegler's Gorge hydropower dam. Retrieved from https://constructionreviewonline.com/2019/05/tanzania-to-commence-construction-stieglers-gorge-hydropower-dam

Mutemi, J.N., 2003. *Climate anomalies over eastern Africa associated with various ENSO evolution phases* (Doctoral dissertation).

Muñoz-Sabater, J., Dutra, E., Agustí-Panareda, A., Albergel, C., Arduini, G., Balsamo, G., Boussetta, S., Choulga, M., Harrigan, S., Hersbach, H. and Martens, B., 2021. ERA5-Land: A state-of-the-art global reanalysis dataset for land applications. *Earth system science data*, *13*(9), pp.4349-4383.

Mutayoba, E., Kashaigili, J.J., Kahimba, F.C., Mbungu, W. and Chilagane, N.A., 2018. Assessment of the impacts of climate change on hydrological characteristics of the Mbarali river sub catchment using high resolution climate simulations from CORDEX regional climate models.

Mwakalila, S., 2011. Assessing the hydrological conditions of the Usangu Wetlands in Tanzania.

Mwakalila, S., 2011. Vulnerability of people's livelihoods to water resources availability in semi-arid areas of Tanzania. *Journal of Water Resource and Protection,* pp. 3(9), 678-685.

Mwakalila, S., 2013. Integrated water resource management as climate change adaptation strategy in the Great Ruaha river catchment of Tanzania. *Journal of Environmental Science and Water Resources*, *2*(11), pp.396-402.

Mwalyosi, R.B., 1988. Environmental impacts of the proposed Stiegler's Gorge hydropower project, Tanzania. Environmental conservation, 15(3), pp.250-254.

Mwalyosi, R.B., 1990. Resource potentials of the Rufiji River basin, Tanzania. *Ambio*, pp.16-20.

Nalbantis, I. and Tsakiris, G., 2009. Assessment of hydrological drought revisited. *Water resources management*, *23*, pp.881-897.

Näschen, K., Diekkrüger, B., Leemhuis, C., Steinbach, S., Seregina, L.S., Thonfeld, F. and Van der Linden, R., 2018. Hydrological modeling in data-scarce catchments: The Kilombero floodplain in Tanzania. *Water*, *10*(5), p.599.

Näschen, K., Diekkrüger, B., Leemhuis, C., Seregina, L.S. and van der Linden, R., 2019. Impact of climate change on water resources in the Kilombero Catchment in Tanzania. *Water*, *11*(4), p.859.

Nash, J.E. and Sutcliffe, J.V., 1970. River flow forecasting through conceptual models' part I—A discussion of principles. *Journal of hydrology*, *10*(3), pp.282-290.

Nashwan, M.S. and Shahid, S., 2019. Spatial distribution of unidirectional trends in climate and weather extremes in Nile River basin. *Theoretical and Applied Climatology*, *137*, pp.1181-1199.

Naumann, G., Alfieri, L., Wyser, K., Mentaschi, L., Betts, R.A., Carrao, H., Spinoni, J., Vogt, J. and Feyen, L., 2018. Global changes in drought conditions under different levels of warming. *Geophysical Research Letters*, *45*(7), pp.3285-3296.

Neitsch SL, Arnold JG, Kiniry JR, Williams JR (2005) Soil and water assessment tool theoretical documentation version. Grass Land, Soil and Water Research Laboratory, Agricultural Research Service 808 East Blackland Road, Temple, Texas 76502; Blackland Research Centre, Texas Agricultural Experiment Station 720, East Blackland, Texas USA

Neitsch, S.L., Arnold, J.G., Kiniry, J.R. and Williams, J.R., 2011. *Soil and water assessment tool theoretical documentation version 2009*. Texas Water Resources Institute.

Nicholson, S.E., Kim, J. and Hoopingarner, J., 1988. *Atlas of African rainfall and its interannual variability*. Department of Meteorology, the Florida State University.

Nicholson, S.E. and Kim, J., 1997. The relationship of the El Niño–Southern oscillation to African rainfall. *International Journal of Climatology: A Journal of the Royal Meteorological Society*, *17*(2), pp.117-135.

Nicholson, S.E., 2015. Long-term variability of the East African 'short rains' and its links to large-scale factors. *International Journal of Climatology*, *35*(13), pp.3979-3990.

Nicholson, S.E., 2017. Climate and climatic variability of rainfall over eastern Africa. *Reviews of Geophysics*, *55*(3), pp.590-635.

Nicholson, S.E., 2019. A review of climate dynamics and climate variability in Eastern Africa. *Limnology, Climatology and paleoclimatology of the East African lakes*, pp.25-56.

Nikulin, G., Lennard, C., Dosio, A., Kjellström, E., Chen, Y., Hänsler, A., Kupiainen, M., Laprise, R., Mariotti, L., Maule, C.F. and van Meijgaard, E., 2018. The effects of 1.5 and 2 degrees of global warming on Africa in the CORDEX ensemble. *Environmental Research Letters*, *13*(6), p.065003.

Nguvava, M., Abiodun, B.J. and Otieno, F., 2019. Projecting drought characteristics over East African basins at specific global warming levels. *Atmospheric Research*, *228*, pp.41-54.

Nguvava, M.M., 2020. Understanding the characteristics of droughts over Eastern Africa in past and future climates.

Ntale, H.K. and Gan, T.Y., 2003. Drought indices and their application to East Africa. *International Journal of Climatology: A Journal of the Royal Meteorological Society*, *23*(11), pp.1335-1357.
Nyakwada, W., Ogallo, L.A. and Okoola, R.E., 2009. The Atlantic-Indian Ocean Dipole and its influence on East African seasonal rainfall.

Ogallo, L.J., 1989. The spatial and temporal patterns of the East African seasonal rainfall derived from principal component analysis. *International Journal of Climatology*, *9*(2), pp.145-167.

Ogega, O.M., Koske, J., Kung'u, J.B., Scoccimarro, E., Endris, H.S. and Mistry, M.N., 2020. Heavy precipitation events over East Africa in a changing climate: results from CORDEX RCMs. *Climate Dynamics*, *55*(3-4), pp.993-1009.

Osima, S., Indasi, V.S., Zaroug, M., Endris, H.S., Gudoshava, M., Misiani, H.O., Nimusiima, A., Anyah, R.O., Otieno, G., Ogwang, B.A. and Jain, S., 2018. Projected climate over the Greater Horn of Africa under 1.5 C and 2 C global warming. *Environmental Research Letters*, *13*(6), p.065004.

Otieno, V.O. and Anyah, R.O., 2013. CMIP5 simulated climate conditions of the Greater Horn of Africa (GHA). Part II: Projected climate. *Climate dynamics*, *41*, pp.2099-2113.

Odebrecht, 2013. "Stiegler's Gorge Hydropower Project; Report and Proposal of Development." Grand Cayman:OSEL ODEBRECHT SERVICOS NO EXTERIOR LTD.

Palmer, W.C., 1965. Meteorological drought. US. *Weather Bureau Res. Paper*, *45*, pp.1-58.

Palmer, W.C., 1968. Keeping track of crop moisture conditions, nationwide: the new crop moisture index.

Palmer, P.I., Wainwright, C.M., Dong, B., Maidment, R.I., Wheeler, K.G., Gedney, N., Hickman, J.E., Madani, N., Folwell, S.S., Abdo, G. and Allan, R.P., 2023. Drivers and impacts of Eastern African rainfall variability. *Nature Reviews Earth & Environment*, *4*(4), pp.254-270.

Pardoe, J., Conway, D., Namaganda, E., Vincent, K., Dougill, A.J. and Kashaigili, J.J., 2018. Climate change and the water–energy–food nexus: insights from policy and practice in Tanzania. *Climate Policy*, *18*(7), pp.863-877.

Park, S., Kang, D., Yoo, C., Im, J. and Lee, M.I., 2020. Recent ENSO influence on East African drought during rainy seasons through the synergistic use of satellite and reanalysis data. *ISPRS Journal of Photogrammetry and Remote Sensing*, *162*, pp.17-26.

Paul, H. and Steinbrecher, R., 2013. African agricultural growth corridors and the new alliance for food security and nutrition. *Who benefits, who loses*.

Pauline, N.M., Vogel, C., Grab, S. and Liwenga, E.T., 2017. Smallholder farmers in the Great Ruaha River sub-Basin of Tanzania: coping or adapting to rainfall variability? *Climate and Development*, *9*(3), pp.217-230.

Peck, E.L., 1997. Quality of hydrometeorological data in cold regions. Journal of the American Water Resources Association 33, 125–134.

Pinkeye, S., 1966. Conditional Probabilities of Occurrence of Wet and Dry Years Over a Large Continental Area. Hydrol. Paper 12, Colorado State University, Fort Collins, Colorado

Priestley, C. H. B. & Taylor, R.J. (1972) On the assessment of surface heat flux and evaporation using large-scale parameters. Mon. Weather Rev. 100(2), 81–92.

Refsgaard, J.C. and Knudsen, J., 1996. Operational validation and intercomparison of different types of hydrological models. *Water Resources Research*, *32*(7), pp.2189-2202.

Riahi, K., Rao, S., Krey, V., Cho, C., Chirkov, V., Fischer, G., Kindermann, G., Nakicenovic, N. and Rafaj, P., 2011. RCP 8.5—A scenario of comparatively high greenhouse gas emissions. *Climatic change*, *109*, pp.33-57.

Richardson, C.J., 2007. How much did droughts matter? Linking rainfall and GDP growth in Zimbabwe. *African Affairs*, *106*(424), pp.463-478.

Rojas, O., Vrieling, A. and Rembold, F., 2011. Assessing drought probability for agricultural areas in Africa with coarse resolution remote sensing imagery. *Remote sensing of Environment*, *115*(2),pp.343-352.

Rosnes, O. and Shkaratan, M., 2011. *Africa's power infrastructure: investment, integration, efficiency*. World Bank Publications.

Rowell, D.P., Booth, B.B., Nicholson, S.E. and Good, P., 2015. Reconciling past and future rainfall trends over East Africa. *Journal of Climate*, *28*(24), pp.9768-9788.

Rufiji District Commission statistics: June 2012, http://www.trust.org/item/?map=drought-drives-tanzanian-herders-into-conflict-with-farmers

Russo, S., Marchese, A.F., Sillmann, J. and Immé, G., 2016. When will unusual heat waves become normal in a warming Africa?. *Environmental Research Letters*, *11*(5), p.054016.

SAGCOT. 2013. Environmental and Social Management Framework (ESMF), (August), 1–411.

Saji, N.H., Goswami, B.N., Vinayachandran, P.N. and Yamagata, T., 1999. A dipole mode in the tropical Indian Ocean. *Nature*, *401*(6751), pp.360-363.

Seneviratne, S., 2022. Weather and climate extreme events in a changing climate. In *IPCC Sixth Assessment Report*.

Shafer, B.A. and Dezman, L.E., 1982, January. Development of surface water supply index (SWSI) to assess the severity of drought condition in snowpack runoff areas. PROCEEDING OF THE WESTERN SNOW CONFERENCE.

Shaghude, Y.W., 2016. Estuarine environmental and socio-economic impacts associated with upland agricultural irrigation and hydropower developments: the case of Rufiji and Pangani estuaries, Tanzania. *Estuaries: a lifeline of ecosystem services in the Western Indian Ocean*, pp.169-182.

Shongwe, M.E., Van Oldenborgh, G.J., Van den Hurk, B. and van Aalst, M., 2011. Projected changes in mean and extreme precipitation in Africa under global warming. Part II: East Africa. *Journal of climate*, *24*(14), pp.3718-3733.

Shukla, S. and Wood, A.W., 2008. Use of a standardized runoff index for characterizing hydrologic drought. *Geophysical research letters*, *35*(2).

Siderius, C., Gannon, K.E., Ndiyoi, M., Opere, A., Batisani, N., Olago, D., Pardoe, J. and Conway, D., 2018. Hydrological response and complex impact pathways of the 2015/2016 El Niño in Eastern and Southern Africa. *Earth's Future*, *6*(1), pp.2-22.

Siderius, C., Kolusu, S.R., Todd, M.C., Bhave, A., Dougill, A.J., Reason, C.J., Mkwambisi, D.D., Kashaigili, J.J., Pardoe, J., Harou, J.J. and Vincent, K., 2021. Climate variability affects water-energy-food infrastructure performance in East Africa. *One Earth*, *4*(3), pp.397-410.

Smith, C.D.M., 2016. Environmental flows in Rufiji River Basin assessed from the perspective of planned development in the Kilombero and Lower Rufiji Sub-Basins. *Report to the United States Agency for International Development. 146p. Available for download at: https://dec. usaid. gov/dec/content/search. aspx*, p.4.

Sokile, C.S., van Koppen, B. and Lankford, B., 1993. Ten Years of the drying up of the Great Ruaha River: Institutional and Legal Responses to Water Shortages. *Charles S. Sokile and Barbara van Koppen and Bruce Lankford*.

Spinoni, J., Barbosa, P., Bucchignani, E., Cassano, J., Cavazos, T., Christensen, J.H., Christensen, O.B., Coppola, E., Evans, J., Geyer, B. and Giorgi, F., 2020. Future global meteorological drought hot spots: a study based on CORDEX data. *Journal of Climate*, *33*(9), pp.3635-3661.

Srinivasan, R. and George, C., 2018. *QGIS Interface for SWAT+: QSWAT+ Version 02.0, 2021. Available at: https://swat.tamu.edu/media/116738/qswat3-manual_v16.pdf. Accessed on 01-09-2023*

Refsgaard, J.C. and Knudsen, J., 1996. Operational validation and intercomparison of different types of hydrological models. *Water Resources Research, 32(7), pp.2189-2202.*

Stagge, J.H., Tallaksen, L.M., Xu, C.Y. and Van Lanen, H.A., 2014. Standardized precipitation-evapotranspiration index (SPEI): Sensitivity to potential evapotranspiration model and parameters. In *Hydrology in a changing world* (Vol. 363, pp. 367-373).

Tan, M.L., Juneng, L., Tangang, F.T., Samat, N., Chan, N.W., Yusop, Z. and Ngai, S.T., 2020.SouthEast Asia HydrO-meteorological drought (SEA-HOT) framework: A case study in the Kelantan River Basin, Malaysia. *Atmospheric Research*, *246*, p.105155.

Taylor, K.E., Stouffer, R.J. and Meehl, G.A., 2012. An overview of CMIP5 and the experiment design. *Bulletin of the American meteorological Society*, *93*(4), pp.485-498.

Temple, P.H. and Sundborg, Å., 1972. The Rufiji River, Tanzania hydrology and sediment transport. *Geografiska Annaler: Series A, Physical Geography*, *54*(3-4), pp.345-368.

Thejll, P. and Gleisner, H., 2015. Reanalysis data. *EAS Publication Series. https://www. researchgate. net/publication/311107863_Reanalysis_data*.

Thiery, W., Lange, S., Rogelj, J., Schleussner, C.F., Gudmundsson, L., Seneviratne, S.I., Andrijevic, M., Frieler, K., Emanuel, K., Geiger, T. and Bresch, D.N., 2021. Intergenerational inequities in exposure to climate extremes. *Science*, *374*(6564), pp.158-160.

Thomson, A.M., Calvin, K.V., Smith, S.J., Kyle, G.P., Volke, A., Patel, P., Delgado-Arias, S., Bond-Lamberty, B., Wise, M.A., Clarke, L.E. and Edmonds, J.A., 2011. RCP4. 5: a pathway for stabilization of radiative forcing by 2100. *Climatic change*, *109*, pp.77-94.

Thornthwaite, C. W. (1948). An approach toward a rational classification of climate. Geographical review 38(1), 55–94.

Tigkas, D., Vangelis, H. and Tsakiris, G., 2015. DrinC: a software for drought analysis based on drought indices. *Earth Science Informatics*, *8*, pp.697-709.

Twomlow, S., Mugabe, F.T., Mwale, M., Delve, R., Nanja, D., Carberry, P. and Howden, M., 2008. Building adaptive capacity to cope with increasing vulnerability due to climatic change in Africa–A new approach. *Physics and Chemistry of the Earth, Parts A/B/C*, *33*(8-13), pp.780-787.

Ujeneza, E.L. and Abiodun, B.J., 2015. Drought regimes in Southern Africa and how well GCMs simulate them. *Climate Dynamics*, *44*(5), pp.1595-1609.

UNDRR, 2014. United Nations Office for Disaster Risk Reduction: Drought Risk Reduction Framework and Practices. *International Strategy for Disaster Reduction*.
Available at: https://www.unisdr.org/files/11541_DroughtRiskReduction2009library.pdf (Accessed 01/05/2023)

UNESCO https:/ /whc.unesco.org/ en/ news/ 1920/World Bank (2018). World development indicators DataBank. http://databank.worldbank.org/data/source/world-development-indicators

United Nations convention to Combat desertification (UNCCD). In *The Future of Drylands: International Scientific Conference on Desertification and Drylands Research Tunis, Tunisia, 19-21 June 2006* (pp. 13-16). Dordrecht: Springer Netherlands.

UNISDR, 2009. Drought Risk Reduction Framework and Practices: Contributing to the Implementation of the Hyogo

Framework for Action. United Nations secretariat of the International Strategy for Disaster Reduction (UNISDR), Geneva, Switzerland, 213 pp."

Van Loon, A.F., 2015. Hydrological drought explained. *Wiley Interdisciplinary Reviews: Water*, *2*(4), pp.359-392.

Vaze, J., Jordan, P., Beecham, R., Frost, A., Summerell, G., 2012. Guidelines for rainfall-runoff modelling: Towards best practice model application. pp. 47.

Vicente-Serrano, S.M., Beguería, S. and López-Moreno, J.I., 2010a. A multiscalar drought index sensitive to global warming: The standardized precipitation evapotranspiration index. *Journal of Climate*, 23(7), pp.1696–1718.

Vicente-Serrano, S.M., Beguería, S., López-Moreno, J.I., Angulo, M. and El Kenawy, A., 2010b. A new global 0.5 gridded dataset (1901–2006) of a multiscalar drought index: comparison with current drought index datasets based on the Palmer Drought Severity Index.*Journal of Hydrometeorology*, *11*(4), pp.1033-1043.

Vicente-Serrano, S. M., 2014. Expert Developer Guide: SPEI. (Instituto Pirenaico de Ecología, Spanish National Research Council). Available at: https://climatedataguide.ucar.edu/climate-data/standardized-precipitation-evapotranspiration-index-spei (Accessed on 17/05/2023).

Wainwright, C.M., Marsham, J.H., Keane, R.J., Rowell, D.P., Finney, D.L., Black, E. and Allan, R.P., 2019. 'Eastern African Paradox'rainfall decline due to shorter not less intense Long Rains. *npj Climate and Atmospheric Science*, *2*(1), p.34.

Walter, H. and Lieth, H., 1960. Klimadiagramm-Weltatlas.− Jena. *Gustav Fisher*. Wanders, N. and Wada, Y., 2015. Human and climate impacts on the 21st century hydrological drought. *Journal of Hydrology*, *526*, pp.208-220.

Wang, Y., Leung, L.R., McGREGOR, J.L., Lee, D.K., Wang, W.C., Ding, Y. and Kimura, F., 2004. Regional climate modeling: progress, challenges, and prospects. *Journal of the Meteorological Society of Japan. Ser. II*, *82*(6), pp.1599-1628.

Wang, W., Ertsen, M.W., Svoboda, M.D. and Hafeez, M., 2016. Propagation of drought: from meteorological drought to agricultural and hydrological drought. *Advances in Meteorology*, *2016*.

Watkiss, P., Downing, T., Dyszynski, J., Pye, S., Savage, M., Goodwin, J., Longanecker, M. and Lynn, S., 2011. *The economics of climate change in the United Republic of Tanzania*. Global Climate Adaptation Partnership (GCAP).

Weber, T., Haensler, A., Rechid, D., Pfeifer, S., Eggert, B. and Jacob, D., 2018. Analyzing regional climate change in Africa in a 1.5, 2, and 3 C global warming world. *Earth's Future*, *6*(4), pp.643-655.

Wilhite, D.A., 2000: Drought as a natural hazard: Concepts and definitions. In: Wilhite, D.A. (Ed.), Drought: A Global Assessment, vol. 1. Routledge, New York, pp. 1–18.

Wilhite, D.A. and Glantz, M.H., 1985. Understanding: the drought phenomenon: the role of definitions. *Water international*, *10*(3), pp.111-120.

World Evapotranspiration Web Viewer. 2015. *Mean annual evapotranspiration measured by NASA's Moderate Resolution Imaging Spectroradiometer (MODIS),* URL: http://www.arcgis.com/apps/OnePane/main/index.html?appid=b1a0c03f04994a36b93271b0c39e6c0f, last updated 21 January 2015.

World Meteorological Organization, 2017. Guidelines on the Calculation of Climate Normals (WMO-No. 1203), Geneva.

WREM International Inc. 2012. Rufiji IWRMD Plan: Interim Report. In 3 Volumes: Vol. I, Rufiji River Basin Physical, Socio-economic, and Management Profile; Vol. II, Water Resources Availability Assessment; Vol. III, Current Water Use and Infrastructure Assessment. A Water Sector Development Program (WSDP) report by WREM International Inc. Atlanta, Georgia, USA for the Ministry of Water, URT.

WWF. STIEGLER'S, G.H.D.I., 2017. The true cost of power.

Yang, W., Seager, R., Cane, M.A. and Lyon, B., 2015. The annual cycle of East African precipitation. *Journal of Climate*, *28*(6), pp.2385-2404.

Yevjevich, V.M., 1967. *Objective approach to definitions and investigations of continental hydrologic droughts, An* (Doctoral dissertation, Colorado State University. Libraries).

Yuan, X., Wood, E.F., Chaney, N.W., Sheffield, J., Kam, J., Liang, M. and Guan, K., 2013. Probabilistic seasonal forecasting of African drought by dynamical models. *Journal of Hydrometeorology*, *14*(6), pp.1706-1720.